EXPERIMENTAL AND NUMERICAL STUDY OF DETONATION IN A CLOSED CHAMBER

A THESIS SUBMITTED TO
THE GRADUATE SCHOOL OF NATURAL AND APPLIED SCIENCES
OF
MIDDLE EAST TECHNICAL UNIVERSITY

BY

TUĞBERK İNCEKÜRK

IN PARTIAL FULFILLMENT OF THE REQUIREMENTS
FOR
THE DEGREE OF MASTER OF SCIENCE
IN
MECHANICAL ENGINEERING

JUNE 2016

Approval of the Thesis:

EXPERIMENTAL AND NUMERICAL STUDY OF DETONATION IN A CLOSED CHAMBER

submitted by **TUĞBERK İNCEKÜRK** in partial fulfillment of the requirements for the degree of **Master of Science in Mechanical Engineering Department, Middle East Technical University** by,

Prof. Dr. Gülbin Dural Ünver _____
Dean, Graduate School of **Natural and Applied Sciences**

Prof. Dr. Tuna Balkan _____
Head of Department, **Mechanical Engineering**

Prof. Dr. Abdullah Ulaş _____
Supervisor, **Mechanical Engineering Department, METU**

Examining Committee Members:

Prof. Dr. Hüseyin Vural _____
Mechanical Engineering Dept., METU

Prof. Dr. Abdullah Ulaş _____
Mechanical Engineering Dept., METU

Prof. Dr. Murat Köksal _____
Mechanical Engineering Dept., H.U.

Asst. Prof. Dr. Feyza Kazanç _____
Mechanical Engineering Dept., METU

Asst. Prof. Dr. Halil Işık _____
Mechanical Engineering Dept., TURKISH MILITARY ACADEMY

Date: 16.06.2016

I hereby declare that all information in this document has been obtained and presented in accordance with academic rules and ethical conduct. I also declare that, as required by these rules and conduct, I have fully cited and referenced all material and results that are not original to this work.

Name, Last name : Tuğberk İNCEKÜRK

Signature :

ABSTRACT

EXPERIMENTAL AND NUMERICAL STUDY OF DETONATION IN A CLOSED CHAMBER

İncekürk, Tuğberk

M.S., Department of Mechanical Engineering

Supervisor: Prof. Dr. Abdullah Ulaş

June 2016, 142 pages

The main objective of the thesis is to investigate the performance behavior of high explosive charges in a specific confined space with numerical methods and experiments. Internal blast performances of four different cylindrical high explosive charges in a closed spherical detonation chamber are evaluated and the results are compared with numerical simulations.

For the numerical studies, in order to model explosives, widely used JWL equation of state is used. Numerical simulations are accomplished by commercial hydrocode solver in order for the comparison of the experimental results obtained from detonation chamber experiments. The hydrodynamics of detonation is modeled by 2D Multi-Material Eulerian axisymmetric simulations. The peak over-pressure and time of arrivals obtained from numerical simulations showed very good agreement with the average of experimental results. The variations in the explosive formulation result in variations in blast performance in terms of impulse and peak over-pressure.

Keywords: Closed Detonation Chamber, Internal Detonation, JWL Equation of State, Explosive, Blast Wave.

ÖZ

KAPALI ALANLARDAKİ DETONASYONUN DENEYSEL VE SAYISAL ÇÖZÜMLEMESİ

İncekürk, Tuğberk
Yüksek Lisans, Makina Mühendisliği Bölümü
Tez Yöneticisi: Prof. Dr. Abdullah Ulaş

Haziran 2016, 142 sayfa

Bu tezin amacı yüksek patlayıcıların belirli bir kapalı hacime sahip alandaki performansının deneysel ve sayısal yöntemlerle incelenmesidir. Silindirik dört faklı yüksek patlayıcının kapalı küresel infilak çemberindeki basınç performansları hesaplanmıştır ve sonuçlar sayısal simülasyonlar ile kıyaslanmaktadır.

Sayısal simülasyonlarda, patlayıcıların modellenmesinde sıklıkla kullanılan JWL hal denklemi kullanılmıştır. Kapalı infilak çemberinde elde edilen test sonuçları, sayısal simülasyonlar için geliştirilen ticari hidrokod yazılımından edinilen sonuçlar ile kıyaslanmıştır. İnfilak hidrodinamiği çoklu malzemeli iki boyutlu Euler eksenel simetrik yazılımında modellenmiştir. Sayısal simülasyonlardan elde edilen tepe basıncı ve varma zamanları test sonuçlarının ortalaması ile iyi bir uyumluluk göstermiştir. Kapalı alan infilakına ait sayısal simülasyon sonuçları ile test sonuçlarının birbiri ile güçlü bir uyumluluk sağladığı görülmüştür. Patlayıcı formülasyonundaki farklılıklar darbe ve tepe basıncı açısından patlayıcıların basınç performansında farklılıklar yaratmıştır.

Anahtar Kelimeler: Kapalı İnfilak Çemberi, İçten İnfilak, JWL Hal Denklemi, Patlayıcı, Basınç Dalgası.

To My Family

ACKNOWLEDGEMENTS

First, I thank my supervisor, Prof. Dr. Abdullah Ulaş, for his excellent guidance and providing me a great support and help for this thesis study. His immense knowledge gave me a motivation to prepare this study.

I would like to thank ROKETSAN MISSILES INDUSTRIES INC. for the technical support supplied. I would also like to appreciate my colleagues Mr. İbrahim Can Küçükyılmaz, Mr. Ege Arkın Dileklioğlu, Mr. Melih Yerdelen and Mr. Eshabil Demir for their exertion.

Last but never the least, I would like to express my deepest gratefulness to my family throughout writing this thesis and my life. I dedicate this thesis to my family with special thanks.

TABLE OF CONTENTS

LIST OF TABLES

TABLES

LIST OF FIGURES

FIGURES

NOMENCLATURE

A	JWL equation of state parameter
B	JWL equation of state parameter
$\vec{b}$	acceleration field vector
C	JWL equation of state parameter
C	adiabatic sound speed
c_v	specific heat at constant volume
D	charge Diameter
D_{ij}	rate of deformation tensor
e	specific internal energy
E_o	internal energy
G	shear modulus
k	specific kinetic energy
L	charge Length
L_{ij}	velocity gradient tensor
M	molecular weight
P	pressure
P_{cj}	pressure at the Chapman-Jouguet point
P_u	reference pressure
R_1	JWL equation of state parameter
R_2	JWL equation of state parameter
R_s	specific universal gas constant
R_u	molecular gas constant
S_{ij}	stress deviator tensor
T	temperature
t	time

$\vec{u}$	velocity vector (*U, V, W*)
U	x-component of the velocity
V_d	velocity of detonation
V	y-component of the velocity
v	specific volume ratio
W	y-component of the velocity
W_{ij}	spin tensor
Y	yield strength of a solid material

Greek Symbols:

ρ	density
ω	JWL equation of state parameter
σ_{ij}	Cauchy stress tensor
λ_k	internal state variable
γ	specific heat ratio
λ	burn fraction

ABBREVIATIONS

EOS	Equation of State
JWL	Jones-Wilkins-Lee
EBW	Exploding bridgewire
CCR	Carbon Composition Resistor
TNT	Trinitrotoluene
HMX	Cyclotetramethylenetetranitramine
HNS	Hexanitrostilbene
PETN	Pentaerythritol tetranitrate
RDX	Cyclotrimethylenetrinitramine
TATB	Triaminotrinitrobenzene
Tetryl	Trinitrophenylmethylnitramine
Comp-B	Composition B
C-4	Composition C-4
P-1	Explosive-1
P-2	Explosive-2
P-3	Explosive-3
P-4	Explosive-4
PBX	Polymer-Bonded Explosive
HE	High-Explosive
ALE	Arbitrary-Lagrangian-Eulerian

CHAPTER 1

INTRODUCTION

The main damage mechanism of munitions is called warhead systems which can be defined as “the specific device or part of an armament system that damages a target and renders it incapable of performing its intended function” [1]. Directed energy warheads and omni-directional warheads are the two main classes of conventional warhead systems as shown in Figure 1-1. Directed energy warheads can briefly be categorized into three: shaped charge, hemi charge and explosively formed penetrator. These types of warheads focus the energy with the help of metal liner.

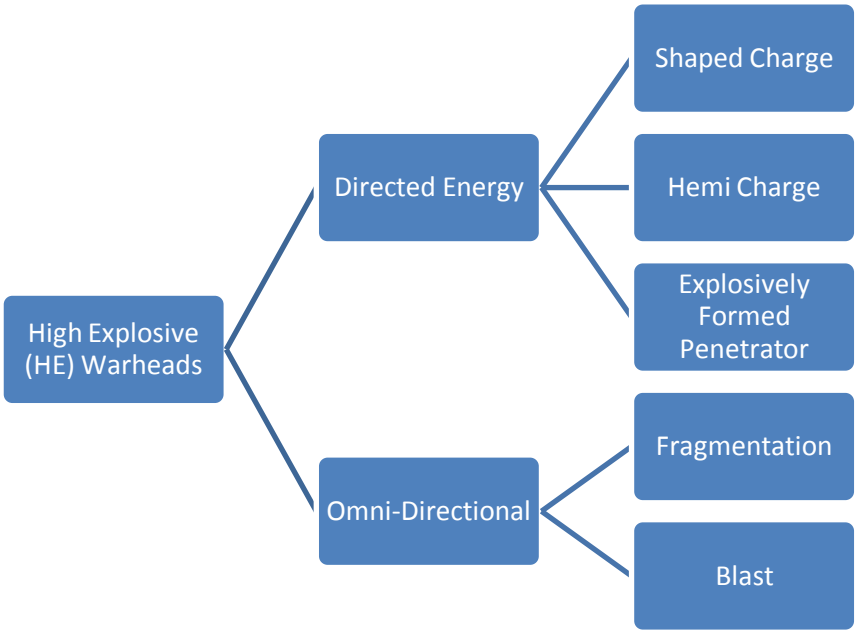

Figure 1-1 Categorization of High Explosive Warheads [1]

Omni-directional warheads can be categorized into two: blast and fragmentation [1]. Blast and fragmentation warheads have damage mechanism in potentially all directions. Target defeat of blast type of warhead primarily depends on blast effect of its high explosive. There is an increasing prominence of blast loading in confined spaces in terms of design of munitions. This blast loading is generated in case of detonation of warhead systems. The internal energy of high explosive is converted to high pressure and temperature within a fraction of a microsecond. With the activation of primary explosive, shock wave moving at supersonic speed throughout the explosive results in decomposition of explosive material. This reaction rate is designated by the velocity of the shock front which depends on the typical properties of explosive [2]. The corresponding detonation pressure and velocity of detonation of commonly used military explosives are listed in Table 1-1 [1].

Table 1-1 Detonation Pressure and Velocity of Detonation of High Explosives [1]

Explosive	**Velocity of Detonation (m/sec)**	**Detonation Pressure (kbars)**
HMX	9110	387
HNS	7000	208
PETN	8310	320
RDX	8950	337.9
TATB	7660	259
Tetryl	7720	226.4
TNT	6950	189.1
Comp-B	8018	264
Cyclotol 75/25	7950	265

Peak pressure and impulse are the two main damage mechanism of blast effect. Peak pressure can be defined as the highest pressure at the shock front of the shock wave, whereas impulse is the area under the pressure-time curve. The measure of the force utilized against a surface by a blast wave can be rendered as peak pressure and impulse is the measure of force multiplied by the duration of blast phase [2]. In order to damage any structure, both peak pressure and impulse must reach threshold values in terms of the strength of the targets. This is described in [2] as "A general rule is that structures that are strong and light in weight, with respect to the area presented to the shock front, require high peak pressure but no great impulse for demolition. Heavy but relatively weak structures require considerable impulse but not such a high peak pressure". This performance comparison can also be evaluated by numerical methods using software packages and compared with experimental results. Numerical methods applied by hydrocodes such as Speed, Autodyn, Ls-Dyna and Dytran enable to identify the effectiveness of warhead systems [1].

In hydrocodes, Jones-Wilkins-Lee equation of state represents the detonation characteristics of energetic materials that undergo detonation process. The general formulation of Jones-Wilkins-Lee equation of state is expressed in following [3].

$$P = A\,exp\,(-R_1 v) + B\,exp\,(-R_2 v) + C v^{(\omega+1)} \tag{1.1}$$

In Equation (1.1), P is the pressure of the detonation products and v is the specific volume ratio of the gaseous detonation products. A, B, C, R_1, R_2 and ω are the parameters which are explosive dependent constants [3].

1.1 Motivation and Objective of the Study

Conventional warhead systems cannot meet the insensitive munition and performance requirements. So-called blast type warheads create significant functionality with regard to peak over-pressure and impulse supposing that destroying the structures and damaging personnel targets are main concerns.

The main objective of this study is to investigate the performance behavior of high explosive charges in a specific confined space so-called detonation chamber with numerical methods. The motivation of the study is to have the capability of analyzing the performance of explosives with numerical methods instead of conducting field experiments.

Also, internal blast performances of four different cylindrical high explosive charges in a fully-confined spherical detonation chamber are evaluated experimentally. In addition to the experiments conducted, the internal hydrodynamics of detonation of specific case study is modeled using 2D Multi-Material Eulerian axisymmetric code called Speed (**S**hock **P**hysics **E**xplicit **E**ulerian **D**ynamics) [4].

In order for modeling in-house developed high explosive compositions in hydrocodes, Jones-Wilkins-Lee parameters obtained in a companion work are used. The experimental and numerical simulation results are compared with each other.

1.2 Outline of the Thesis

Outline of the thesis is as follows:

In Chapter 2, literature survey based on internal detonation and test setup descriptions, related numerical simulations including over-pressure and impulse calculations of high explosives and utilization of JWL equation of state parameters are presented.

In Chapter 3, the experimental method for the specific case study, the design of test setup with the pictures taken before and after test campaigns and the pressure measurement techniques for internal detonation are given.

In Chapter 4, the hydrodynamics of detonations, the numerical model for modeling internal detonation using hydrocodes, validation examples of Speed software and JWL equation of state parameters used for each explosive are presented.

In Chapter 5, numerical results including sensitivity analysis according to mass and distance, effects of uncertainties on the utilized JWL equation of state parameters,

mesh independency studies, pressure contour graphs of Speed, comparison of over-pressure, impulse and time of arrival data obtained from experiment and numerical study and filtering of raw experimental data are presented.

Finally in Chapter 6, summary, conclusion of the current study and the future work are given.

CHAPTER 2

LITERATURE SURVEY

In this chapter, since the aim of the study is to investigate detonation in confined spaces, literature review has been mostly conducted on internal detonation. In addition to the internal detonation characteristics, open area detonation studies are discussed briefly.

2.1 Internal Detonation Studies

Togashi et al. [5] performed experiments in a closed chamber in order to analyze burning particles. The study deals with the heavily aluminized high explosive with reactive multiphase flows modeled into their in-house code, Feflo [5]. The volume of the closed chamber was 26 m^3 and chamber air pressure was one standard atmosphere before the test. The test setup including the gauge locations is shown in Figure 2-1 [5]. The tested explosive sample was cylindrical having an aspect ratio of 0.83 and charge was located in the middle of the chamber and top-detonated.

The experimental data were then compared with the results obtained from the numerical code and presented in Figure 2-2 [5]. The absolute velocities of blast wave at different times are also presented in Figure 2-3 [5]. They concluded that the new burning model used in in-house code showed good conformance with the experimental results.

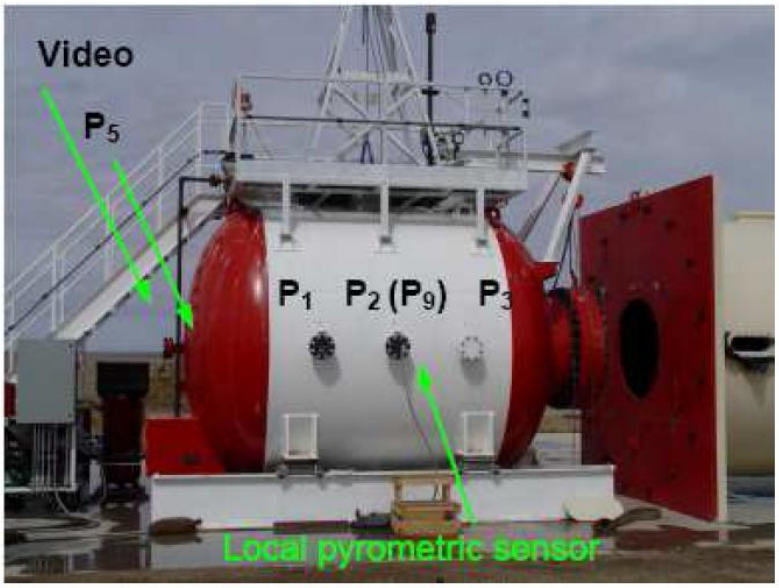

Figure 2-1 Closed Chamber Test Setup and Location of Gauges to Measure the Pressure [5]

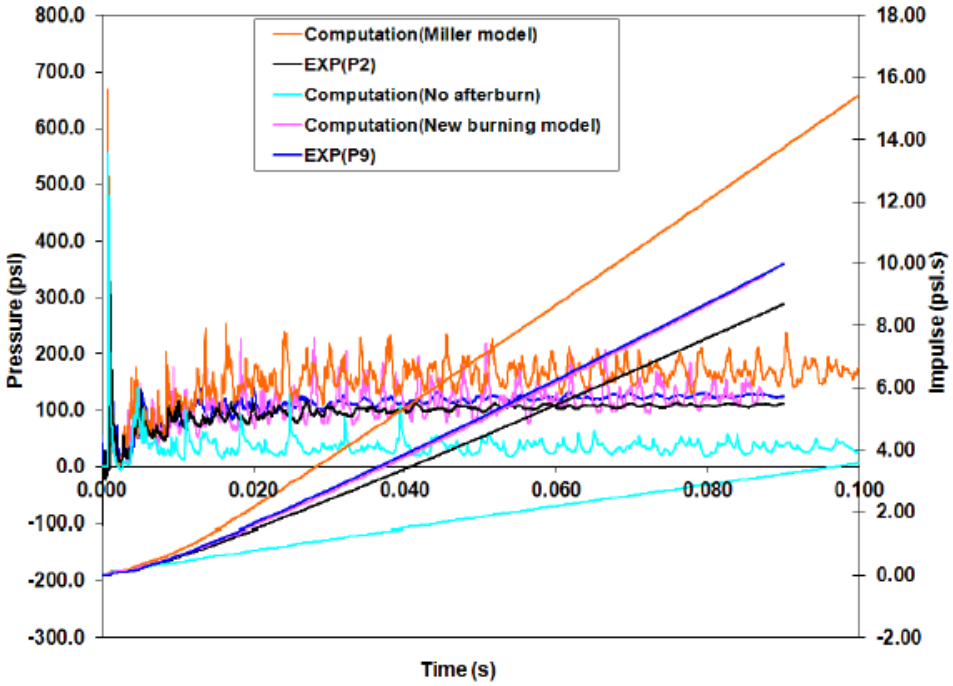

Figure 2-2 Pressure and Impulse Histories obtained from Experiments and Computed Results [5]

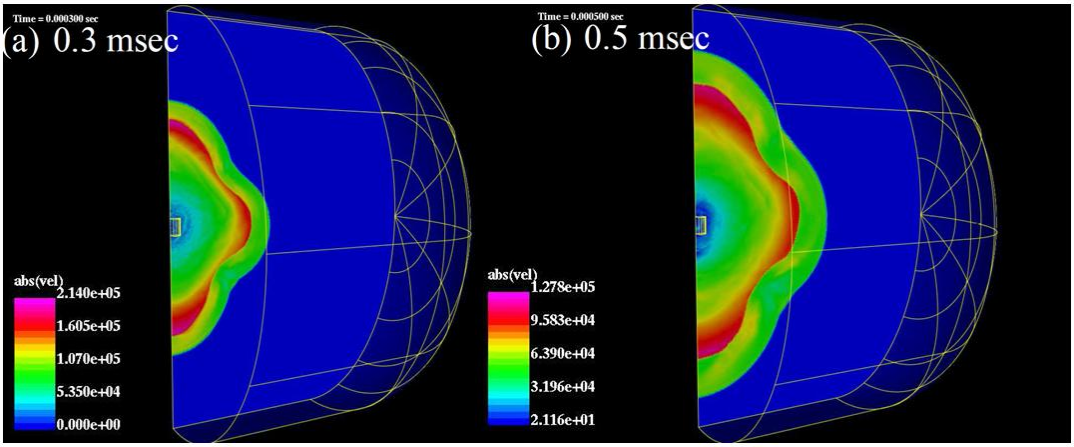

Figure 2-3 Computed Absolute Velocities [5]

Snyman et al. [6] devised research effort at a blast facility hosting 5.4 m long and 5 m diameter submarine section which is presented in Figure 2-4. The intended work involved measurements of reflected pressure, over-pressure and the imparted impulse. The hull section of the semi-confined space was cut in half and sensor ports were attached to the structure as presented in Figure 2-5 [6]. Kulite 375M sensors were used to capture the reflected incident pressure of Comp-B explosive at different masses. They also conducted numerical 2D axisymmetric analysis with Ansys Autodyn and the model is presented in Figure 2-6 [6]. The model was composed of air which was modeled by a multi-material Euler mesh and the cylindrical shell. The cylindrical shell was modeled by Lagrangian elements. JWL equation of state with the additional energy term is used for Comp-B.

They stated that face-on pressure sensors give consistent results for different charge weights and excellent comparison were obtained between experimental and numerical work. In addition, the sensor measuring ports did not lose their integrity during and after the test campaigns [6].

Figure 2-4 Semi-Confined Space to See the Effects of Confinement [6]

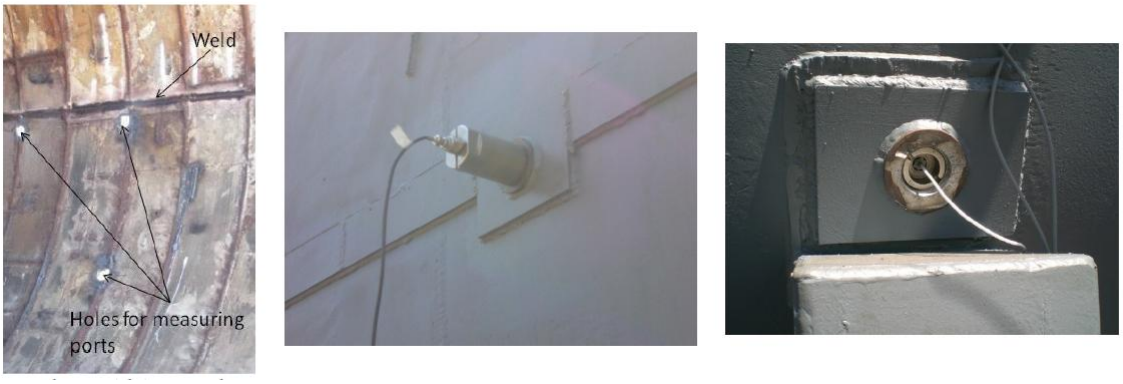

Figure 2-5 Measurement Fixtures to Measure the Pressure [6]

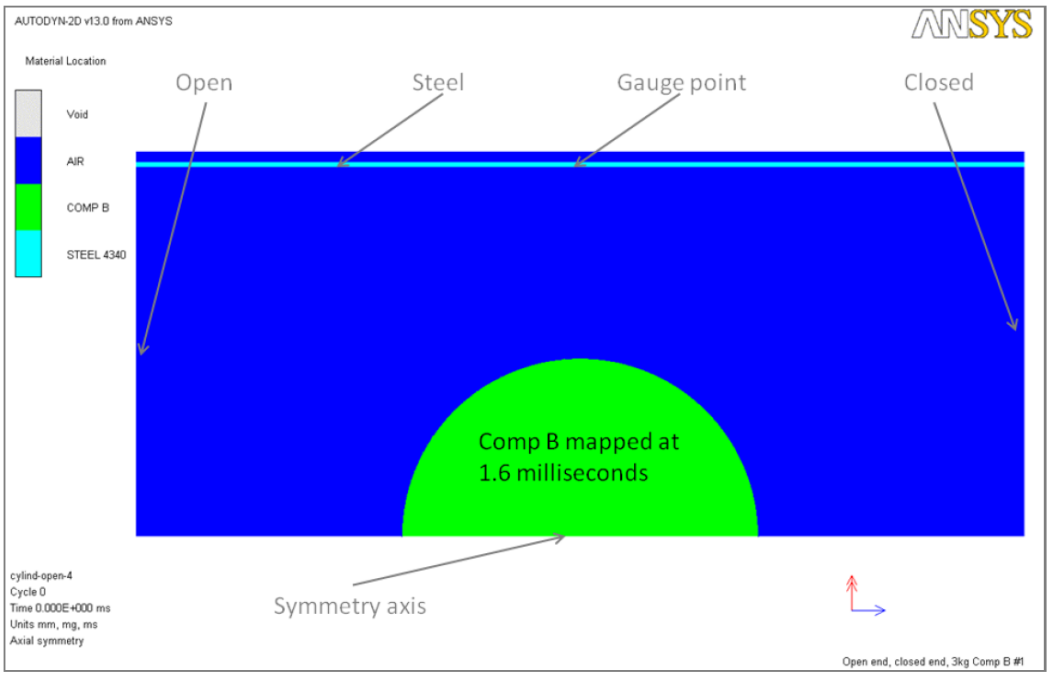

Figure 2-6 2D Axisymmetric Computational Model [6]

Moster et al. [7] carried out series of tests which were based on relative blast output of aluminized explosive charges. The apparatus was designed as semi-confined to provide gathering blast output of charges up to 1 kg mass. The structure is presented in Figure 2-7 [7]. It was made of 30 mm thick rolled cylindrical steel vessel of diameter 1.5 m. In order to strengthen the structure, hoops of 30 mm thick steel with approximately 100 mm spacing between each other was designed. PCB137 probes were located at the wall directly opposite to each other (See Figure 2-8) [7].

They reported that the obtained results with aluminized explosive charges were reliable in terms of variation between similar shots. The over-pressure vs. time plot of test data gathered from oppositely located sensors is given in Figure 2-9 [7].

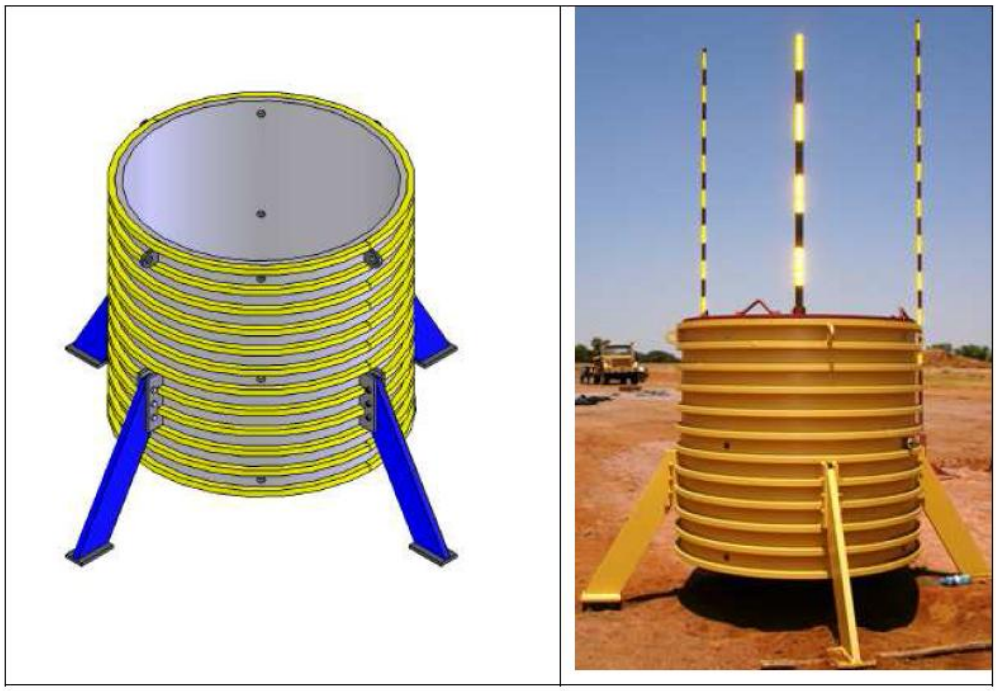

Figure 2-7 Semi-Confined Apparatus to See the Effects of Confinement [7]

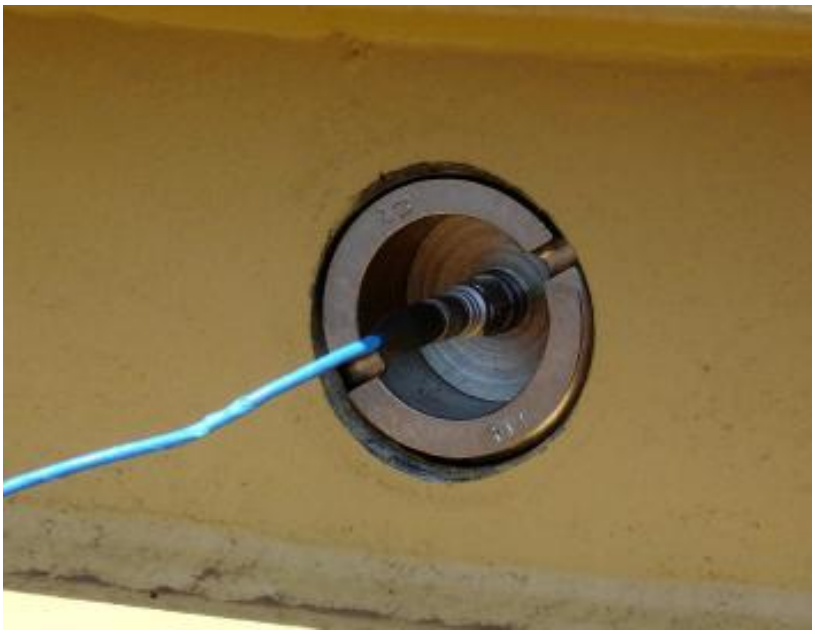

Figure 2-8 Reflected Pressure Sensor to Measure the Pressure [7]

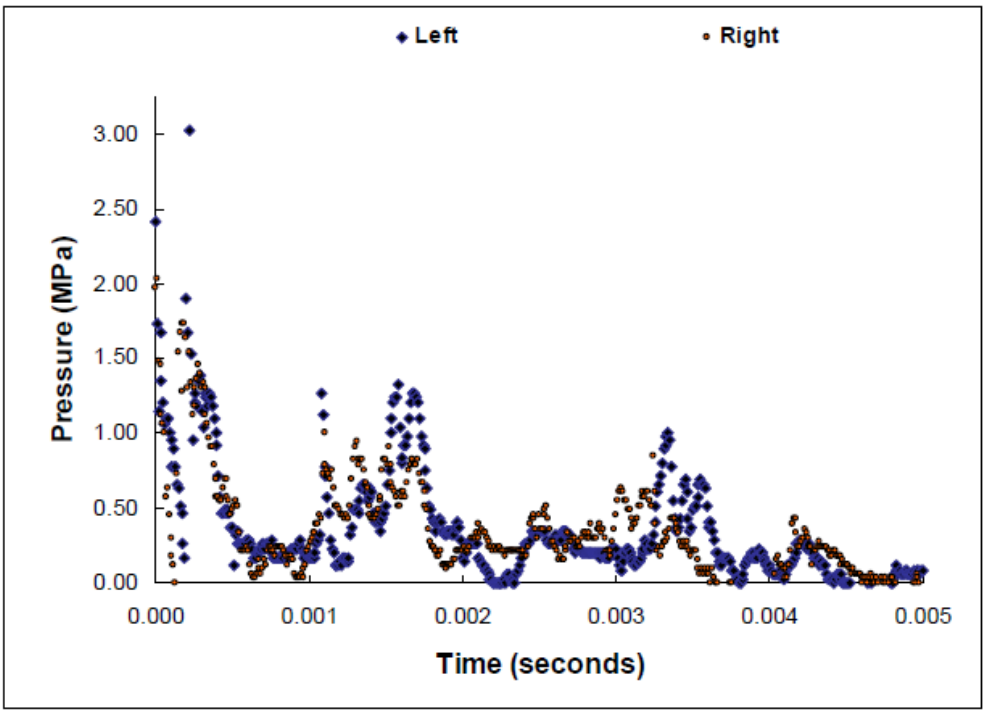

Figure 2-9 Over-Pressure vs. Time Plot of Opposingly Located Sensors [7]

Arnold et al. [8] conducted validation tests in a 45 m^3 bunker with 2 kg of aluminized high explosive charge having diameter 104 mm in order for validation of Eulerian hydrocode called Numhyd. In Figure 2-10, the sketch of the detonation chamber is presented [8]. The simulation was axisymmetric and the walls and floor of the bunker and the platform were modeled by rigid boundaries since the main aim was not the investigation of deformation of the walls and floor. Therefore, this phenomenon could be neglected. The multi-material hydrocode applied the second order advection with the theoretical combustion model [8].

They concluded that in internal detonation applications, the lion's share of quasi-static pressure comes from the combustion of metal particles and under-oxidized detonation products with the available air. According to the results obtained from the experiments and numerical work, the quasi-static curve of the model converged the same asymptotic value with the test curve which was the theoretical equilibrium pressure. It was also concluded that the arrival time of the shock wave and the

produced peak pressure had good conformance which are clearly identified in Figure 2-11. The material location of the detonation products and the temperature generated in the chamber at 25 ms is presented in Figure 2-12 [8].

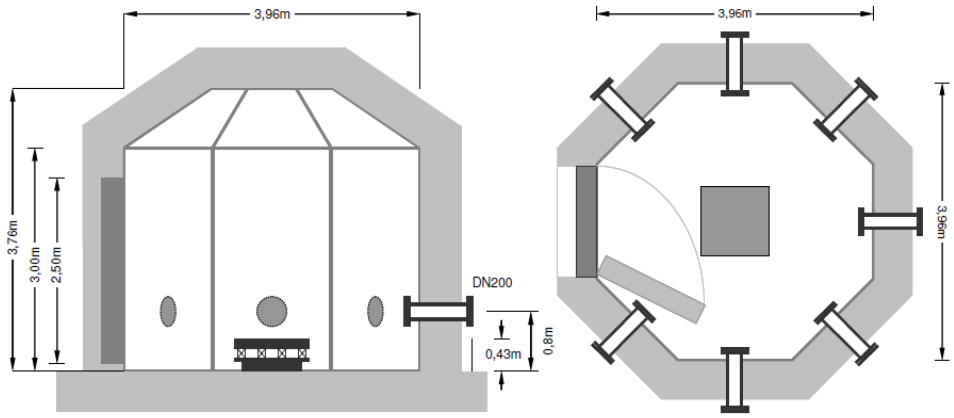

Figure 2-10 Sketch of the Detonation Chamber [8]

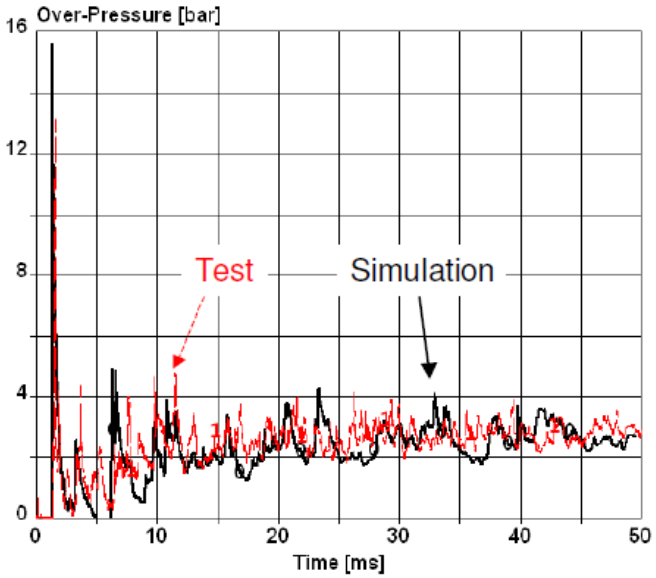

Figure 2-11 Comparison of Over-pressure Calculation and the Test Data [8]

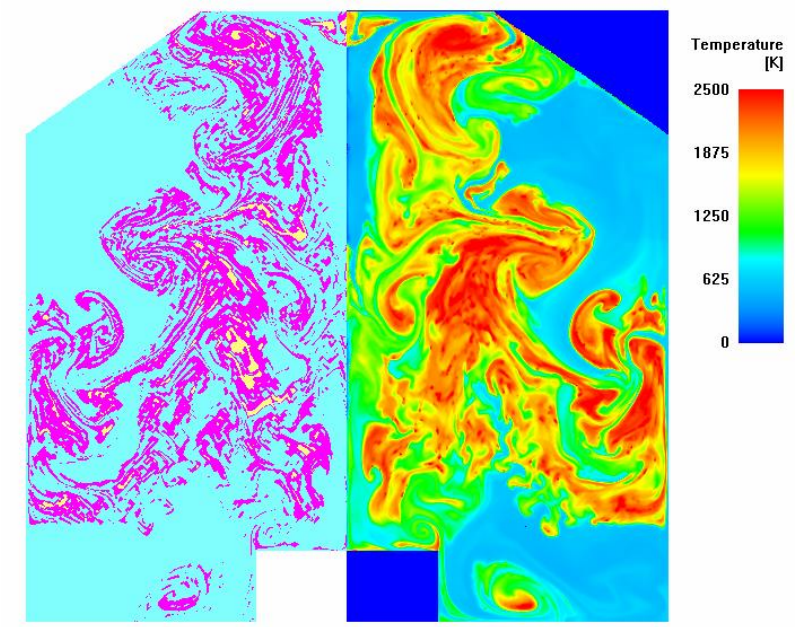

Figure 2-12 Material Location and Temperature Contour Calculated in Simulation [8]

Davison et al. [9] studied the measurement of pressure in two blast chambers by carbon composition resistor gauges. EBW initiator activated the 18 g Primatex 2000 explosive (mostly RDX) in large blast chamber having volume of 11 liters (See Figure 2-13) [9]. In small blast chamber tests, 6 g of RDX explosive was again activated by EBW initiator in 0.46 liters of closed volume. They stated that different experiment results taken from different type of gauges were nearly identical in both large and small blast chamber and the results are shown in Figure 2-14 and Figure 2-15 [9]. It was concluded that the CCR gauges became prevalent due to their low-cost and reliability in blast measurements [9].

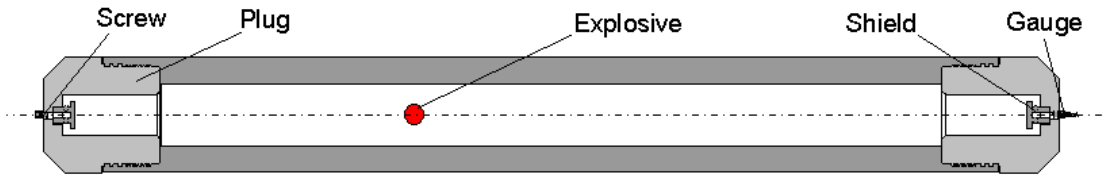

Figure 2-13 Large Blast Chamber [9]

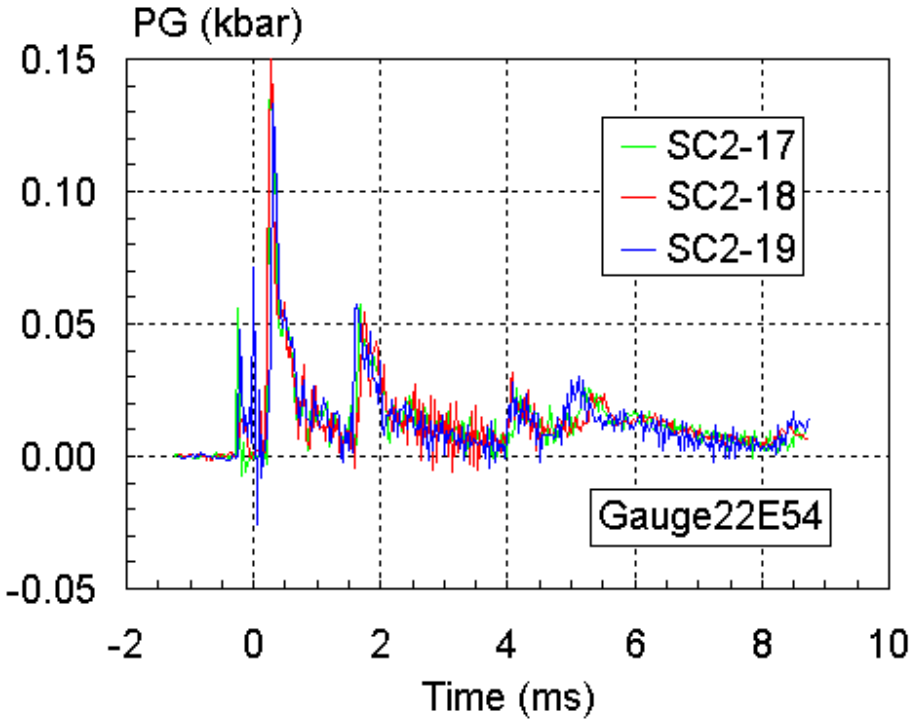

Figure 2-14 Pressure Measurement in Large Blast Chamber [9]

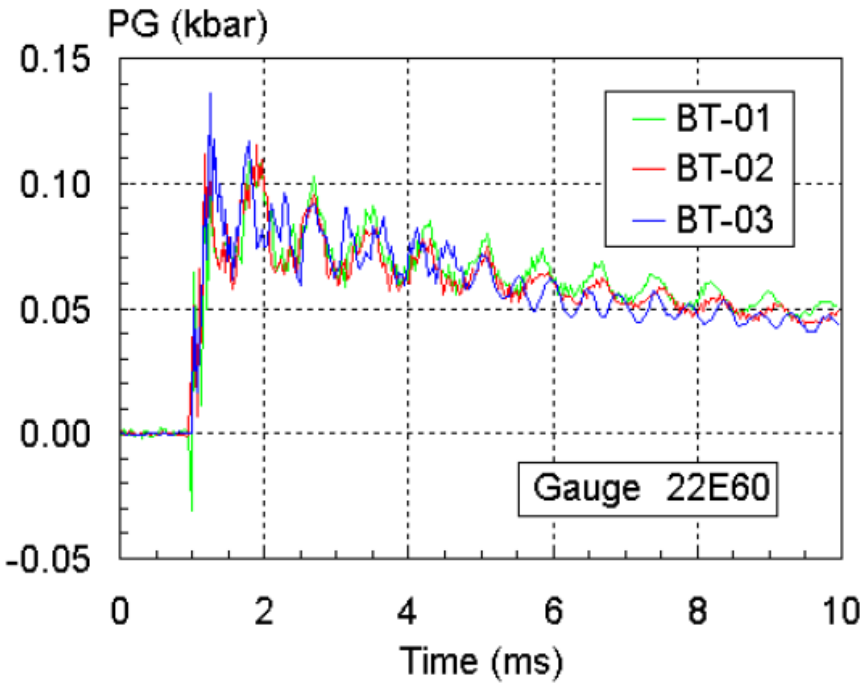

Figure 2-15 Pressure Measurement in Small Blast Chamber [9]

Cullis et al. [10] conducted research to develop an Eulerian hydrocode in order to compare the differences between the simple room explosion and free field blast scenarios. For room explosion, 1 kg of TNT explosive was modeled within a 4 m room. The room was modeled by 4 mm square Eulerian mesh. For free field blast, 1 kg of spherical TNT was modeled in axisymmetrical mesh. The model was run with and without combustion model [10]. The pressure contour result with the reflections of the pressure wave from the interior wall of the room is presented in Figure 2-16 [10]. They also compared the free field blast results with the analytic expressions. The proposed Eulerian code predicted good agreement in terms of positive phase durations in free field blast scenario with combustion model.

They stated that post detonation does not contribute the initial air shock but it significantly enhances the impulse which harms the surrounding structures. It is also concluded that the effect of reflected shocks are important factor when secondary combustion is taken into consideration [10].

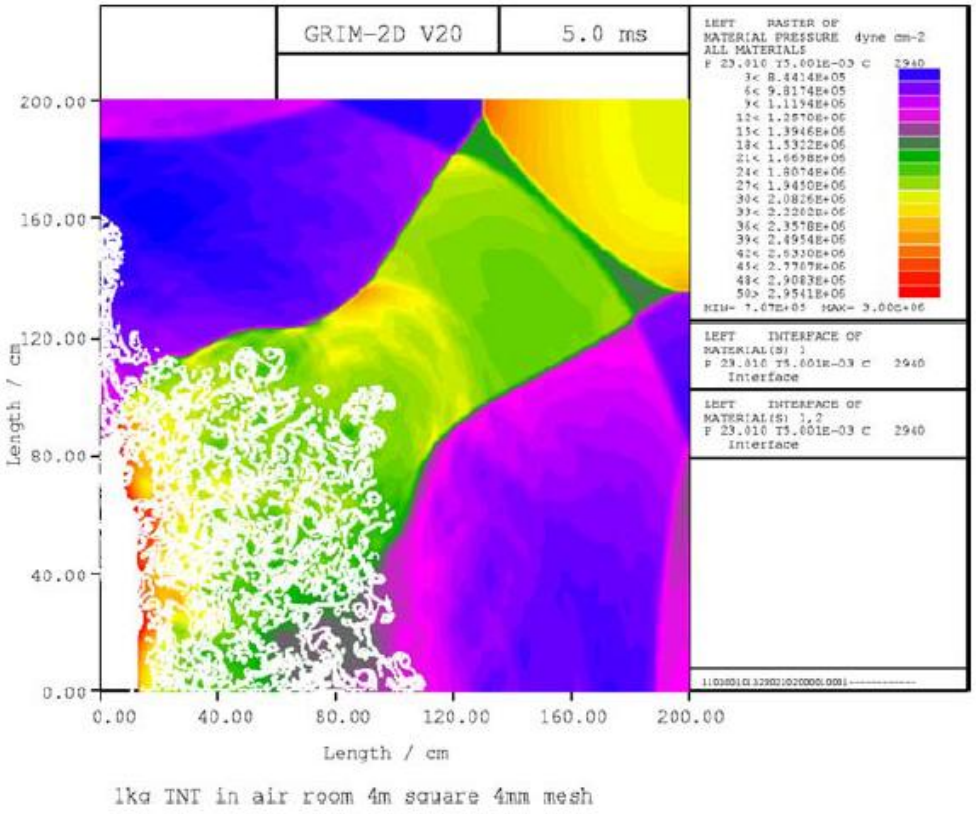

Figure 2-16 Result of Room Explosion [10]

Baum et al. [11] performed research effort to study the quasi-steady behavior of explosives when detonated in confined facilities. 20 lb of C-4 and AFX 757 cylindrical shaped charges were detonated in the center of the testing facility having 5 distinct rooms connected by corridors. In Figure 2-17, locations of pressure gauges are given [11]. Data were collected by total of 10 gauges placed at the room

at which the donation occurred, corridor and ceiling. In addition to testing activities, computational work was also carried out and absolute velocity contours at different times gathered from hydrocode Feflo. The JWL equation of state was used for the explosive modeling. They concluded that the experiment and numerical results when afterburning was included show excellent agreement in terms of total impulse, time of arrival of blast wave and amplitude of peak pressure (See Figure 2-18 and Figure 2-19) [11].

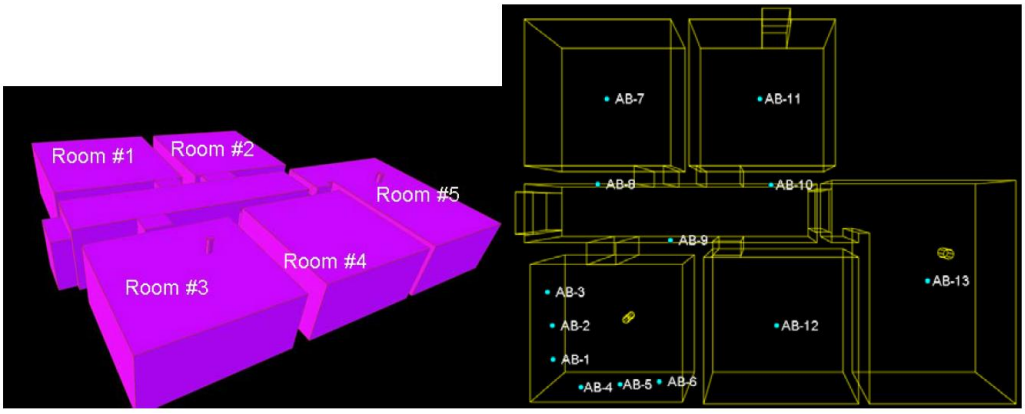

Figure 2-17 Locations of Pressure Gauges to Measure the Blast Wave [11]

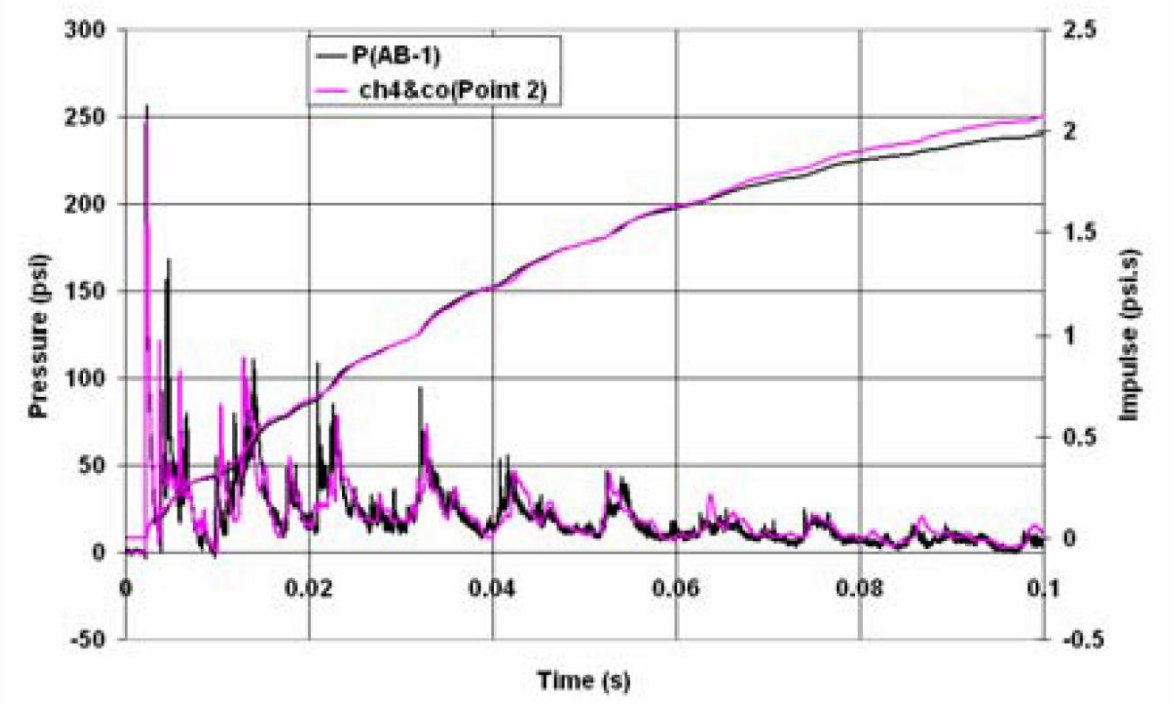

Figure 2-18 Pressure and Impulse vs. Time - C-4 [11]

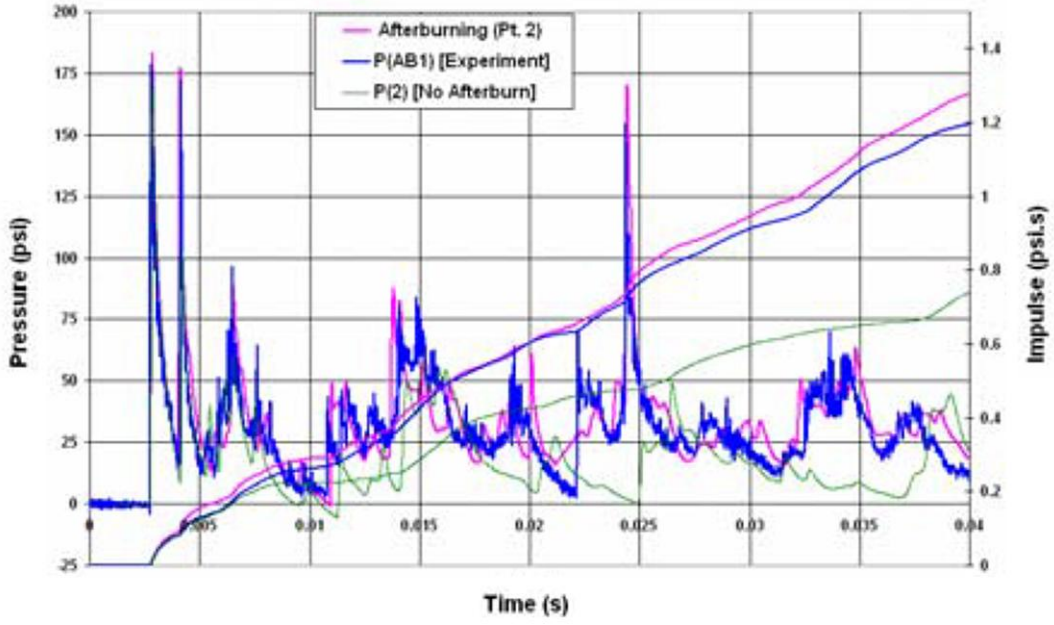

Figure 2-19 Pressure and Impulse vs. Time - AFX 757 [11]

Yu et al. [12] investigated the difference between the effects of gas pressure and blast pressure on the debris velocity. Two different cases were studied in numerical simulations. In the first scenario, 1 kg of hemispherical Pentolite charge and air were modeled using Arbitrary-Lagrangian-Eulerian (ALE) multi-material formulations [12]. JWL EOS was utilized for high explosive, Pentolite. For the beginning scenario, fully constraint quarter chamber was modeled. Quarter model for explosion study is given in Figure 2-20 [12].

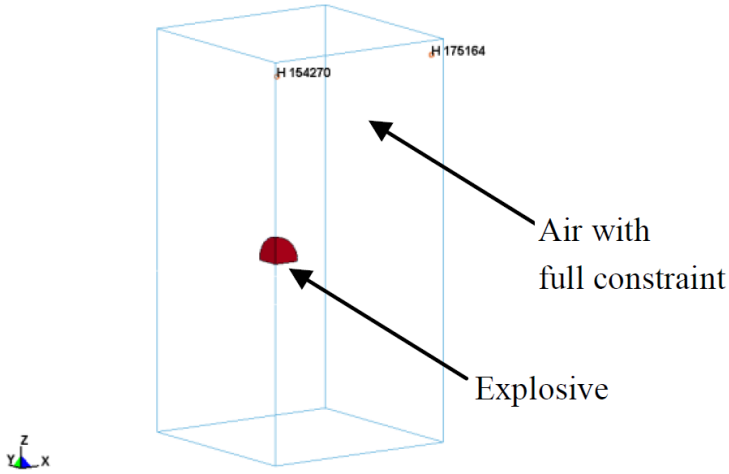

Figure 2-20 Quarter Model for Explosion Study [12]

They expressed that in fully constrained closed volume explosions, extreme peak over-pressure followed by lower peaks occurs and due to face reflections, pressure curve fluctuates about certain value. The corresponding pressure history gathered from numerical simulation is given in Figure 2-21 [12].

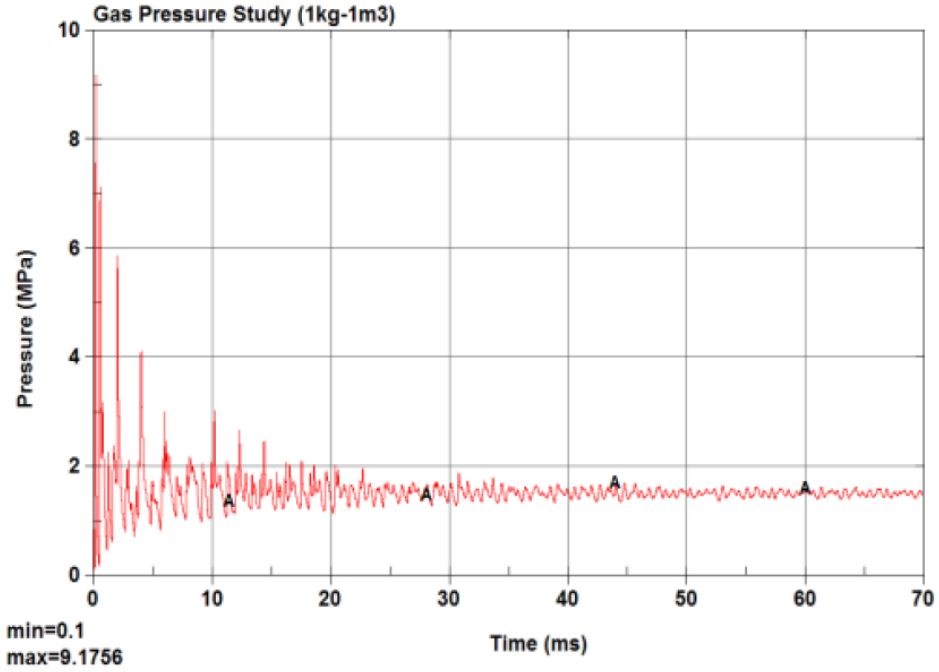

Figure 2-21 Pressure History from Selected Element [12]

The second scenario was conducted in open space to estimate the blast pressure. A top plate was placed and accelerated by blast shock. Rigid boundary conditions to simulate the steel chamber were applied. The blast pressure was amplified by wave reflections from the top plate namely, slab. Five different peaks were observed underneath the slab center resulting from the face reflections. It is concluded that internal pressure arised from initial blast pressure, shock wave reflections and gas pressure built-up [12].

Rodriguez et al. [13] conducted numerical simulation using shock wave physics code, CTH, in which the blast load prediction from high explosive events in a containment vessel was the major aim. In Figure 2-22, the containment vessel is presented. They also compared the results with analytical solutions [13]. The hydrocode was specialized in multi-material and complex multi-dimensional Eulerian method for HE detonation model. 6 feet diameter steel vessel was used to calculate the impulsive load generated from centrally detonated bare and spherical charge of PBX-9501. The Eulerian mesh was composed of 400000 cells and JWL

EOS was utilized for the explosive. In order to evaluate the difference between effects of explosive mass in incident impulse, both 30 and 40 lb. spherical charges were employed in simulation. The numerical results of different explosive masses in terms of pressure are presented in Figure 2-23 [13].

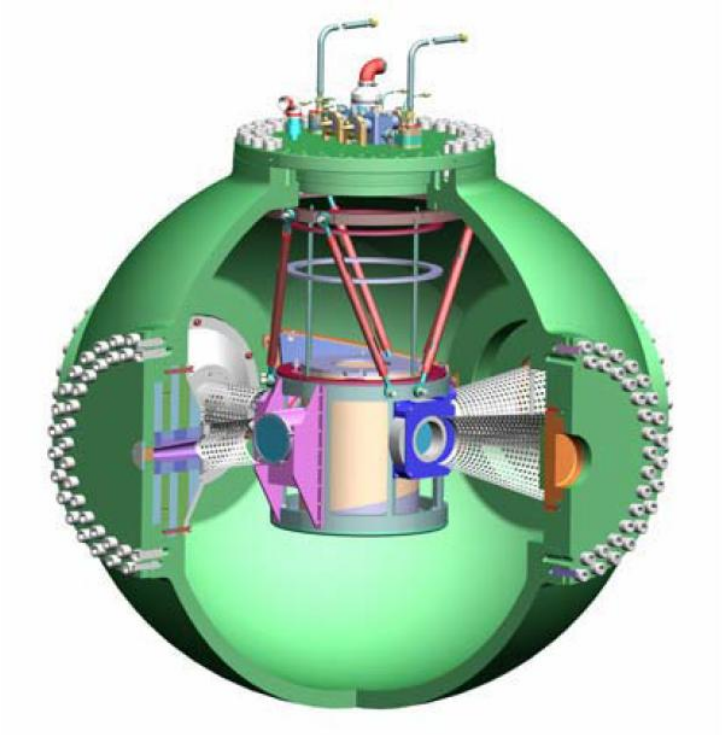

Figure 2-22 Containment Vessel [13]

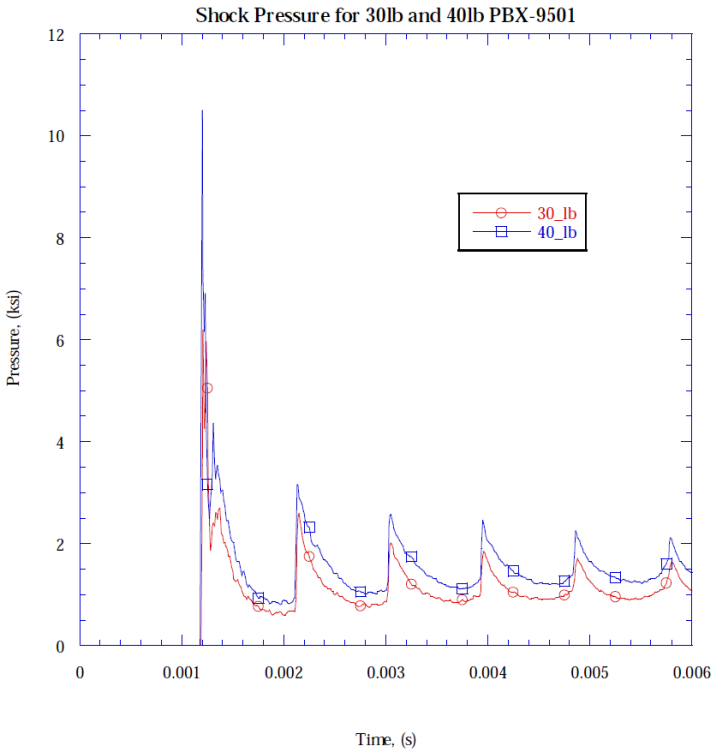

Figure 2-23 Pressure vs. Time History of Spherical PBX-9501 having 30 lb and 40 lb masses [13]

The density distribution of detonation products of HE charge at different times is given in Figure 2-24 [13]. They concluded that increasing the explosive mass by 20%, the reflected impulse will increase about 17%. It is also concluded that the numerical hydrodynamic method is productive to use in prediction of specific impulse and pressures [13].

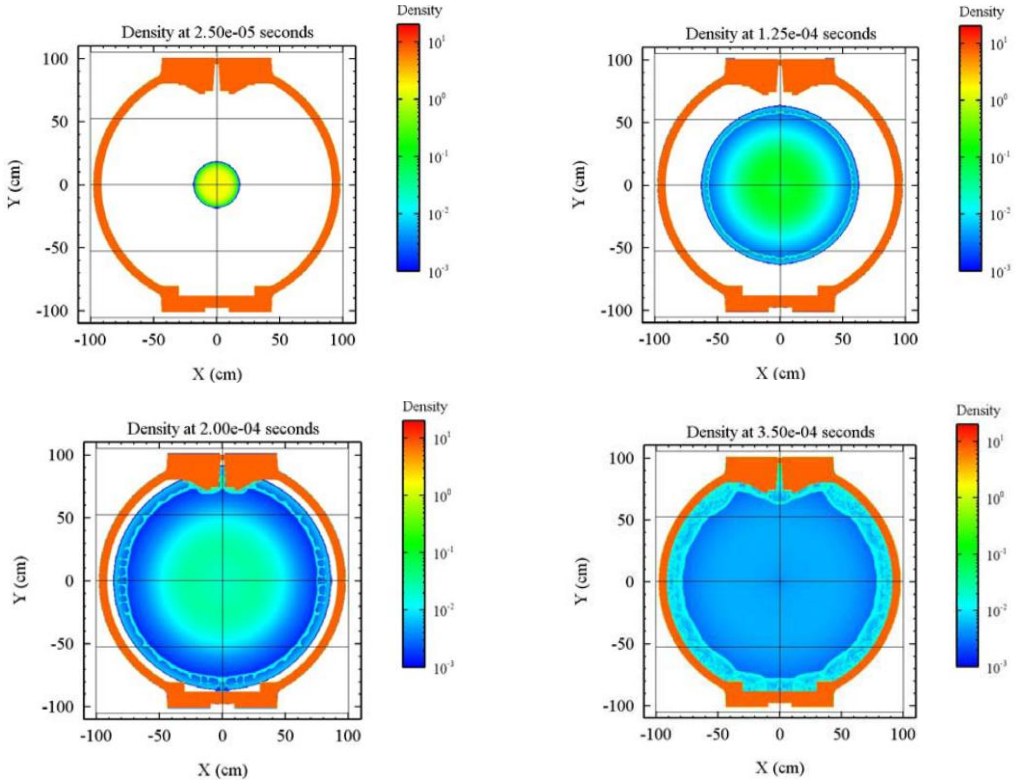

Figure 2-24 Density Contours at 25 µs, 125 µs, 200 µs and 350 µs, respectively [13]

Vagsaether [14] analyzed the blast generated in a generic building and compared experimental data with simulations. 0.5 grams of PETN explosive was detonated at the center of the building which had six distinct small rooms and a hallway (See Figure 2-25) [14]. Two gauges were placed at different rooms of the structure. The simulation study was in 3D domain in which the result of the detonated charge was mapped into the 1mm mesh of axisymmetrical geometry. JWL EOS parameters of PETN were used to model the explosive. The numerical simulations showed that some of the shock peaks were merged in contrast to the experiment result. According to Figure 2-26, the rest of the pressure profile showed good agreement with the experiment result [14].

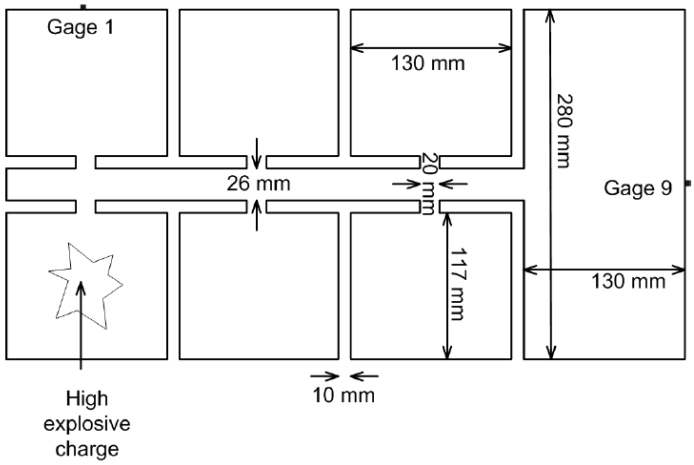

Figure 2-25 Sketch of Experiment Building [14]

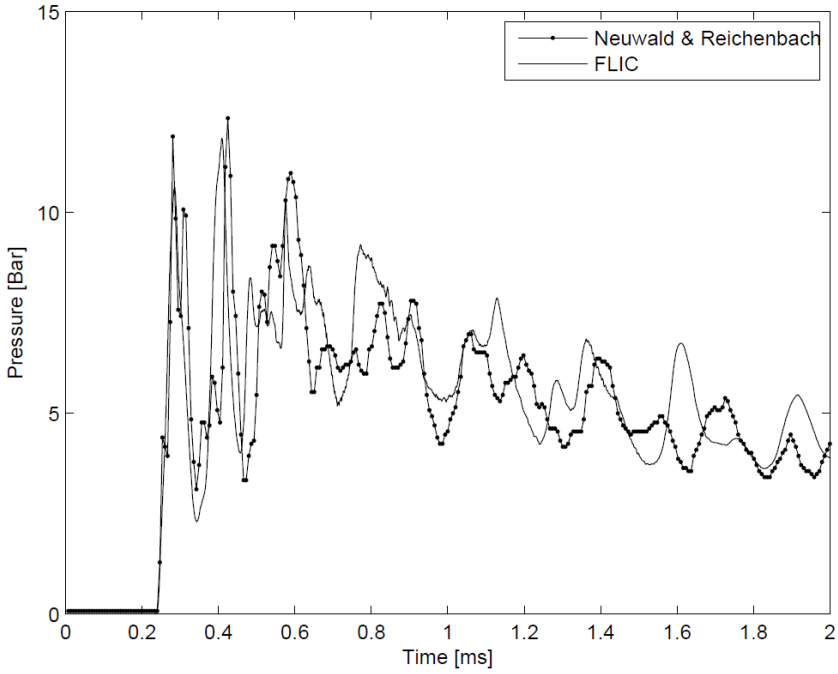

Figure 2-26 Comparison of Numerical and Experimental Results [14]

Ludwig [15] studied the newly developed composition explosives called enhanced blast or thermobaric explosives which have hybrid formulation for small to medium caliber rocket warheads. These hybrid formulations are composed of fuel additives and their combustion energies are tabulated in Table 2-1 [15].

Table 2-1 Some of Fuel Additives and Their Combustion Energies [15]

Fuel Additive	**H_{comb} (cal/g)**
Boron	13970
Aluminum	7560
Titanium	4260
Zirconium	2880
Silicon	7320
Carbon	7840
Magnesium	6020
Hydrocarbons	10000

Ludwig utilized temperature, heat flux and pressure measurement using thermocouples and piezo-resistive pressure transducers. The confined structure was made of reinforced concrete having one door and blocked window which is given in Figure 2-27 [15]. The charge was 1.6 lb mix having 32% aluminum, 40% zirconium, 26.75% isopropyl nitrate and 1.25% gellant in weight. In addition, as a base charge 1 lb C-4 was detonated in the confined structure [15].

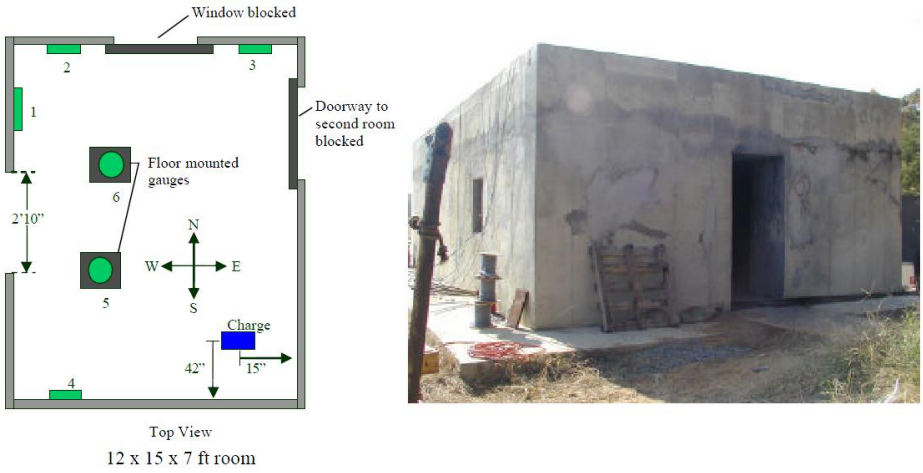

Figure 2-27 Confined Structure [15]

It is stated that thermobaric explosives are designed for personnel and material defeat. The temperature and pressure measurements are given in Figure 2-28 and Figure 2-29 for thermobaric and conventional explosive. It is seen that the total energy in terms of temperature and impulse that thermobaric explosive create is higher than conventional explosives [15].

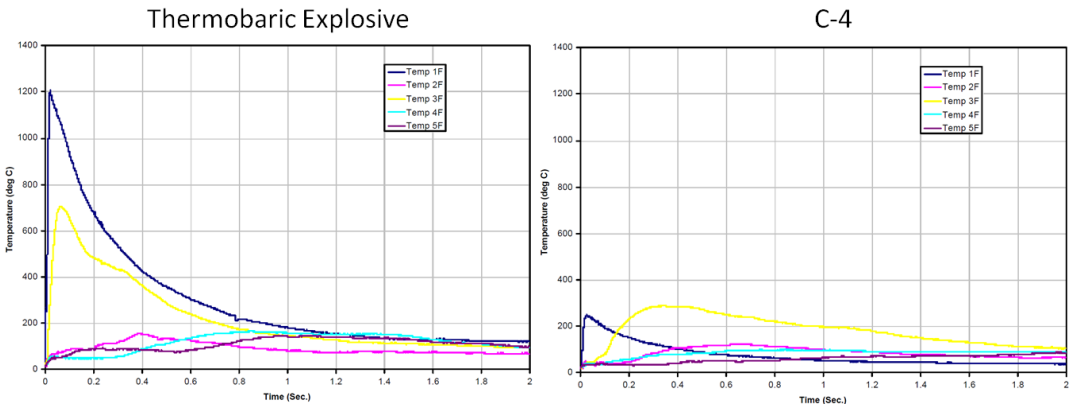

Figure 2-28 Temperature Profiles for Thermobaric Explosive and C-4 [15]

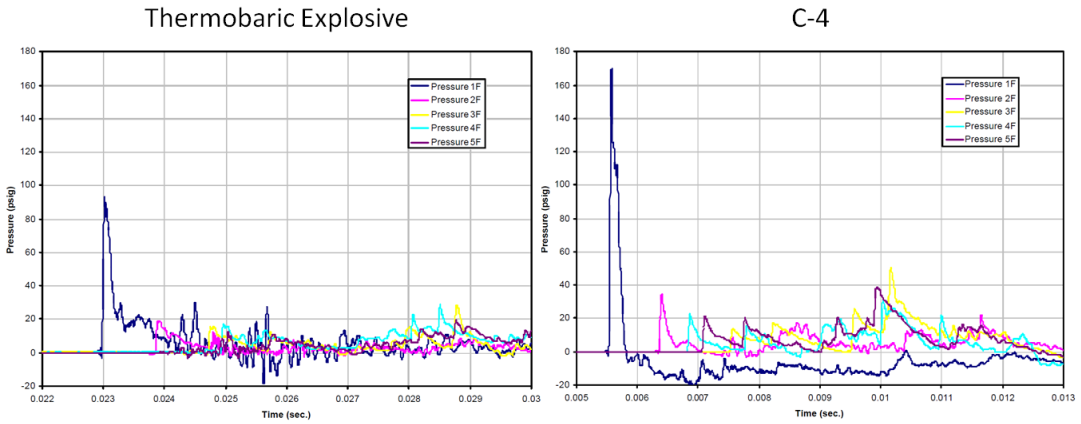

Figure 2-29 Pressure Profiles for Thermobaric Explosive and C-4 [15]

2.2 Open Area Detonation Studies

Simic et al. [16] studied the influence of cast high explosive compositions in open area detonation characteristics. 400 g of thermobaric charges were analyzed in terms of impulse and velocity of air shock. Thermobaric charges which are effective in bunkers, buildings, tunnel and various confined structures have much longer duration of shock wave pressure which corresponds to impulse. It is also stated that enhancement of impulse effect was established by adding metal powder and ammonium perchlorate into explosive composition. The oxidation of metallic elements and ammonium perchlorate will generate an additional energy due to the further combustion. Two different metals, aluminum and magnesium were the additives. The experimental setup which is shown in Figure 2-30 was composed of piezo probes located at different radial stand-off from the center of the charge [16]. In addition, the velocity of detonation of each charge was measured by electrocontact probes. The charges were initiated by booster and detonating caps (See Figure 2-31) [16].

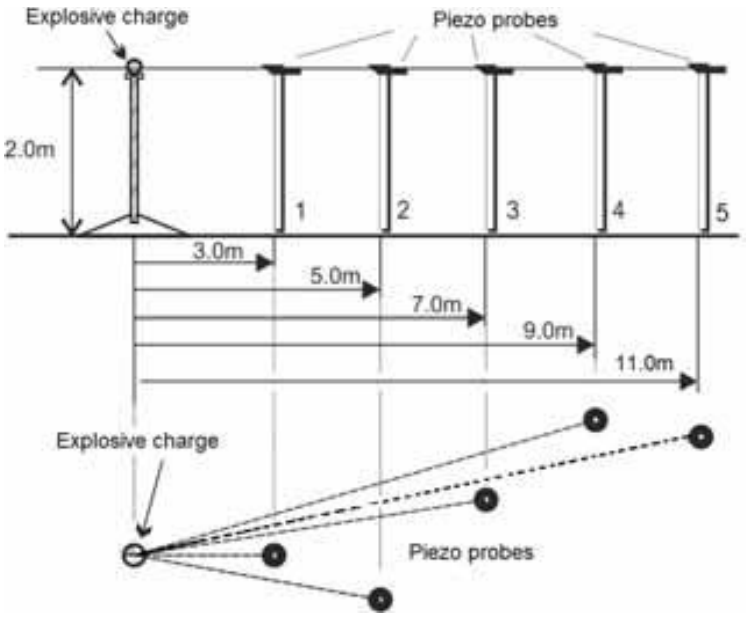

Figure 2-30 Scheme of Experiment Setup [16]

Figure 2-31 Configuration of the Test Item [16]

Similar pressure histories which had a characteristic of combination of discontinuous peak and secondary reflected curve were gathered depending on the stand-off from explosive charge. As the position of the pressure transducer moves upwards from the ground, possibility of eliminating the reflected wave from the ground increases. They stated that at further distances such as 9-11 meters from the center of the charge, the difference between each explosive in terms of maximum peak overpressure gets smaller. They also stated that compositions which had magnesium content give higher values of over pressure and impulse. They selected a specific thermobaric explosive composition based on the ingredients which was a mixture of aluminum, magnesium and ammonium perchlorate [16].

Simoens et al. [17] studied the TNT equivalents of spherical and cylindrical emulsion charges in terms of peak overpressure and impulse. In Figure 2-32, the experimental setup contained circumferential blast sensors from the center of the charge are presented. PCB pencil blast sensors were used to collect data. For each experiment, charges had different aspect ratios. The experiments resulted in that the emulsion charges had a TNT equivalent for overpressure and impulse as 1 and 0.7, respectively [17].

It is also mentioned that in order to calculate the TNT equivalents of various explosive formulations, the geometry of the charges are crucial and it differs with the stand-off distance from the center of the charge [17].

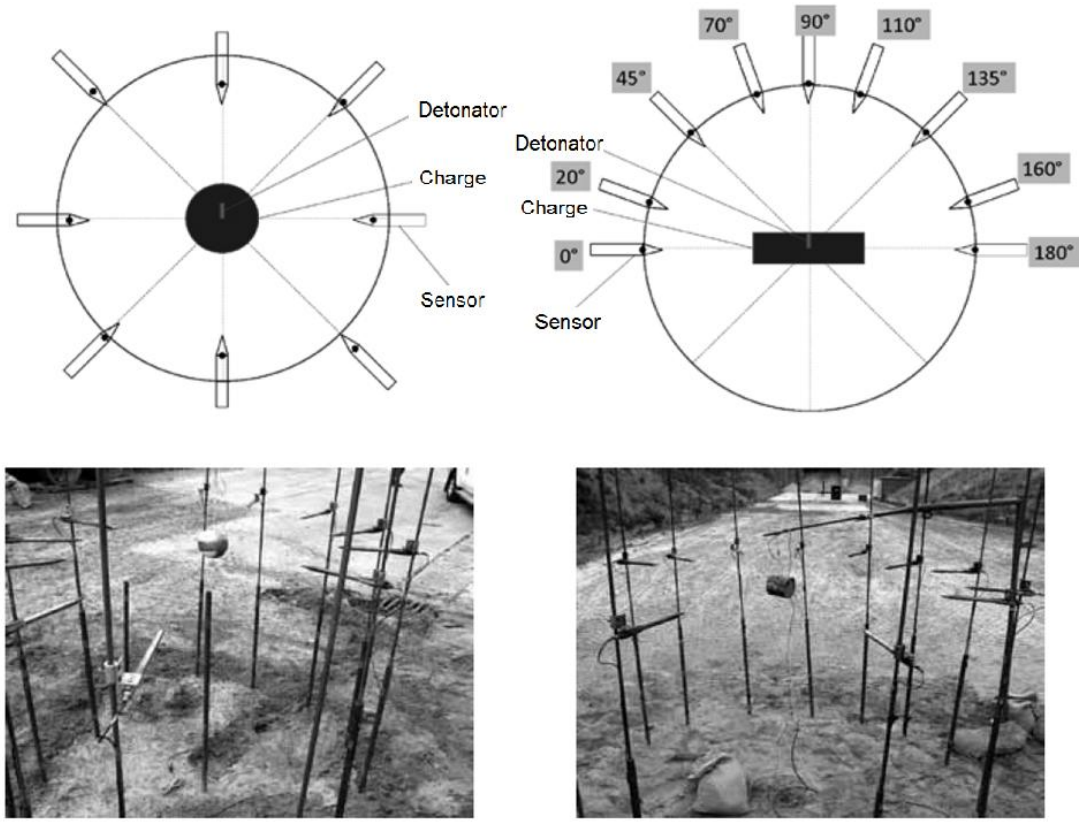

Figure 2-32 Location of Instrumentation to Measure the Pressure [15]

Dilekliоğlu et al. [18] conducted open area blast measurement experiment by detonation of high explosive. The blast measurements were taken at different locations from the center of the charge. Experiment was conducted using cylindrically manufactured explosive. The mass of the main charge was 1 kg. The initiation train was accomplished by a booster charge having mass of 10 grams. In order to collect blast data, PCB pencil blast sensors were used. The experimental test setup which includes explosive charge, pressure sensors and their holders is presented in Figure 2-33 [18]. These sensors were placed circumferentially from the center of the charge.

It is concluded that from the experimental results as the measurement distance from the charge increases, the generated peak over-pressure decreases gradually and the

reflections from the ground surface result in secondary peaks which have amplitudes lower than the first peak [18].

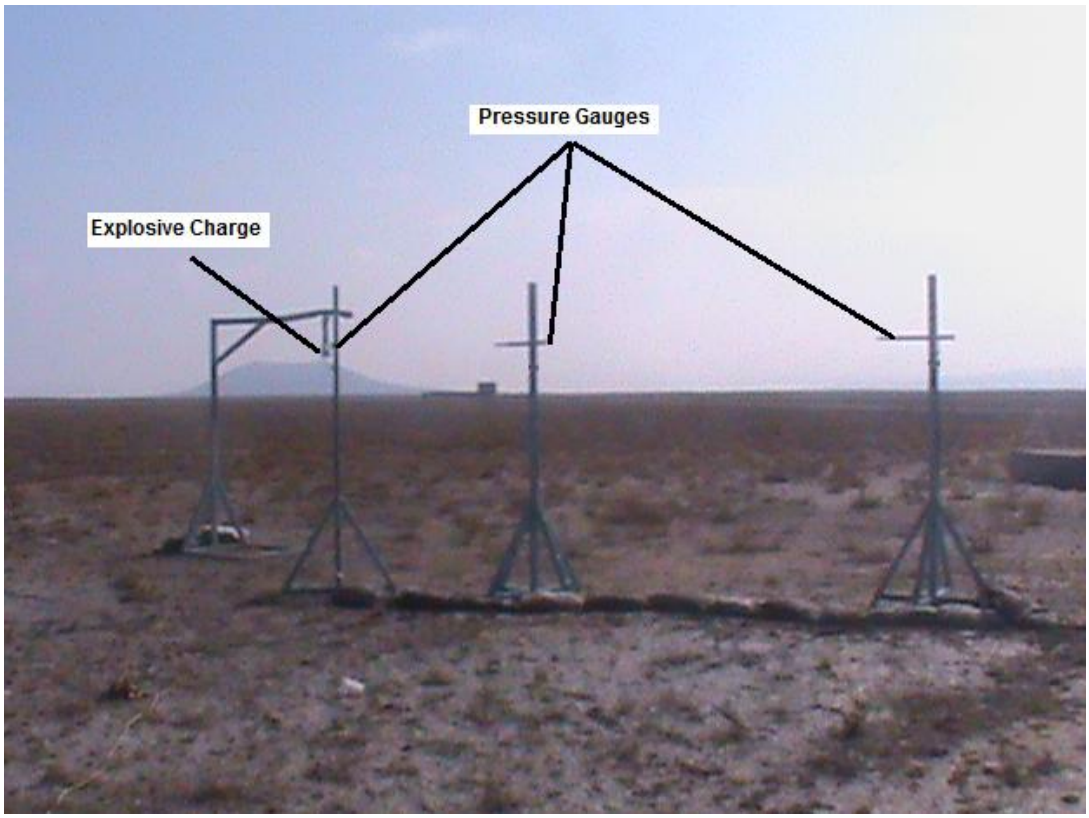

Figure 2-33 Open Area Blast Measurement Test Setup [18]

CHAPTER 3

EXPERIMENTAL METHODOLOGY

A laboratory detonation chamber is used for testing the performance of energetic materials in confined spaces. The detonation chamber body and the technical drawing of the chamber including major dimensions are shown in Figure 3-1 and Figure 3-2, respectively [19]. The dimensions are in [mm]. The chamber has been procured from OZM Research Company and located at ROKETSAN A.Ş. facility.

Figure 3-1 Laboratory Detonation Chamber Body Located at ROKETSAN A.Ş.

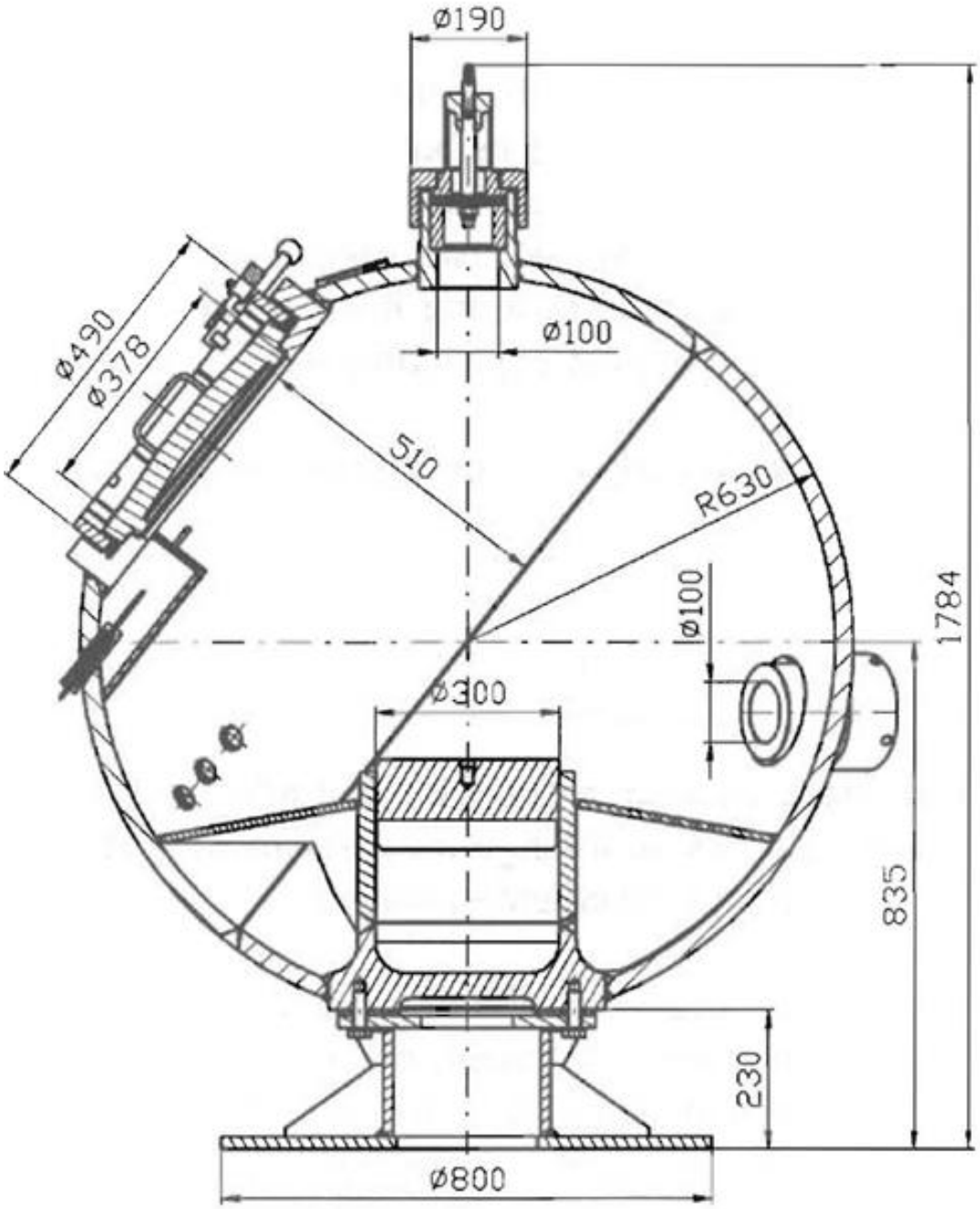

Figure 3-2 Laboratory Detonation Chamber with Major Dimensions [19]

The experimental setup is composed of a detonation chamber body with steel frame supports, the holder of test item, measurement apparatus, data acquisition system and signal converter device. The chamber is formed by two hemispherical bodies with working table which holds the test item and an output valve for further removal of gases. Detonation chamber also consists of two sensor mounting assemblies and electrical measuring inputs for electrical or optical cables with firing input placed at the chamber wall.

This type of laboratory detonation chambers also enable to characterize the mitigation and protective techniques of confined and semi-confined spaces in terms of venting of dust and gaseous products.

The maximum amount of high explosive charges for this specific case study depends on the safety limits of detonation chamber and its equipment. The laboratory detonation chamber is designed such that it can withstand TNT equivalent of up to 250 grams in case of repeated detonation. Therefore, 140 grams of polymer bonded explosive charges including booster pellets are utilized in experiments. Charge assembly includes main charge, booster pellet and aluminum electrial detonator with strength Number 8. The performance characteristic of the main charge in confined spaces is main interest of this work.

All the tests and manufacturing operations of cast explosive and pressed boosters are carried out in ROKETSAN A.Ş. facility. For this case study, three different polymeric bonded explosives labeled as P-2, P-3 and P-4 and one well-known conventional TNT explosive labeled as P-1 are utitlized as shown in Figure 3-3 and Figure 3-4. There are various advantages of conventional TNT since TNT is readily available and has been used for a long time [1]. In addition, TNT has still been used as military explosive due to its low cost [1].

Types of charge assemblies utilized in detonation chamber tests and the main and booster charge diameters and lengths are listed in Table 3-1.

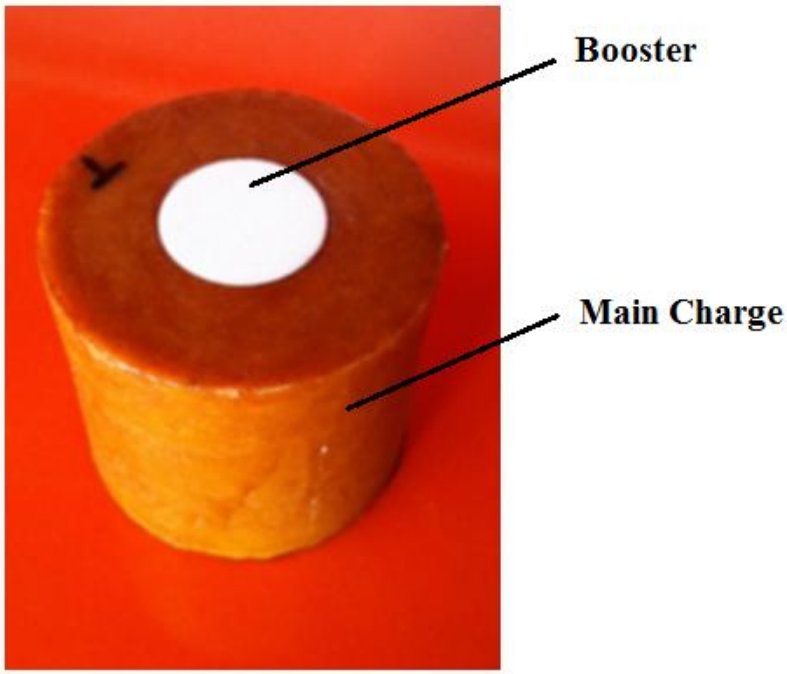

Figure 3-3 Charge Assembly of P-1

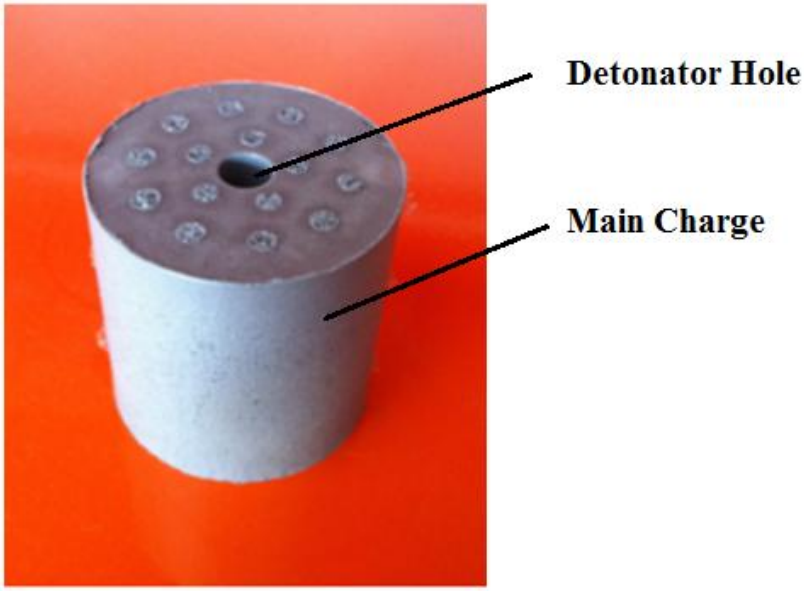

Figure 3-4 Charge Assembly of P-4

Table 3-1 Main and Booster Charge Dimensions

Type of Charge Assembly	Main Charge Diameter (mm)	Main Charge Length (mm)	Main Charge Aspect Ratio (L/D)	Booster Charge Diameter (mm)	Booster Charge Length (mm)
P-1 (TNT)	48	48	1	25.1	10
P-2	48	47.5	0.989	-	-
P-3	48	48.25	1.005	-	-
P-4	48	46.5	0.968	-	-

In order to measure the time of arrival of the shock wave originated from the high explosive charges, signal converter which senses the pulse by fiber-optic cable is used. Fiber-optic cable is taped to detonator to record the detonation instant of detonator. Therefore, velocity of shock front is recorded for each charge with given configuration. Velocity of shock front of explosive depends on the velocity of detonation, total mass and geometry of explosive.

Pressure and impulse performances of each explosive are captured by pressure sensors which are mounted at their housing ports in the detonation chamber body. Two identical pressure sensors are used in every test campaign. The selection of pressure sensors are done such that non-resonant shock wave measurement with instantaneous and reflected energy are main concerns. PCB tourmaline pressure sensor series 134 which has the rise time of 0.2 microseconds with range up to

137900 kPa is utilized. Pressure sensors are connected to a data acqusition system featuring 0.1 microseconds sampling rate which corresponds to 10 MHz. Data acqusition system is triggered by voltage output of fiber-optic cable.

In the tests where shock waves moves at supersonic speed, in addition to the the quality of the pressure sensor and data acqusition system, the quality of sensor mounting apparatus is in a key position since the well-placed sensor eliminates the ringing which results in noise throughout measurements. Therefore, a brand new functional sensor holder apparatus is designed and its solid model and the technical drawing is presented in Figure 3-5 and Figure 3-6, respectively.

Figure 3-5 Solid Model of Sensor Holder Apparatus

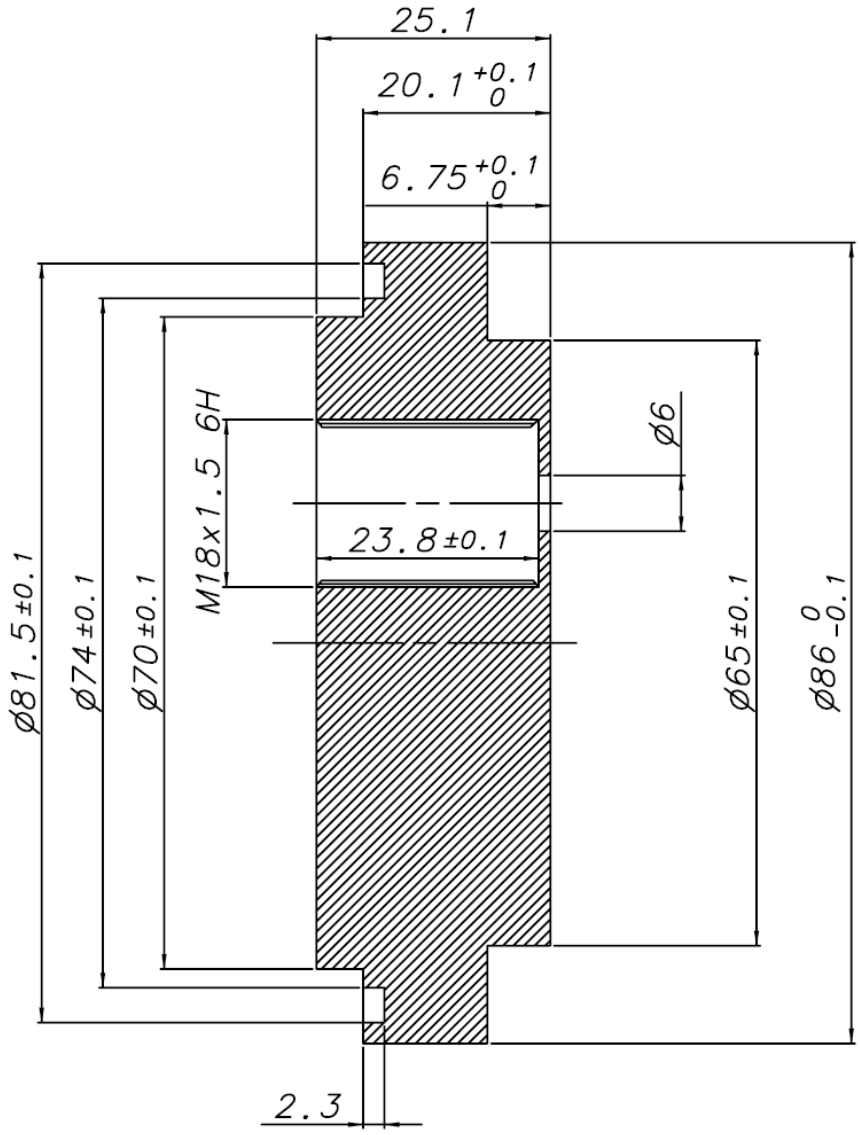

Figure 3-6 Technical Drawing of Sensor Holder Apparatus

The explosive charge assembly is positioned via rubber base plate used for a template in order to guarentee the equal radial distance between the charge assembly and each sensor. The solid model of the base plate is shown in Figure 3-7. The outer diameter of the base plate is equal to the diameter of the holder of the

detonation chamber and the inner diameter is equal to the outer diameter of the charge assembly. The positioned charge assembly is shown in Figure 3-8.

The final test setup assembly is shown in Figure 3-9. Prior to each test, in order to ensure fully confined detonation, exit valve is closed. Therefore, fully-confined structure can be tested in order for evaluating the generated quasi-static pressure inside the chamber. The inner volume of chamber after trials is shown in Figure 3-10.

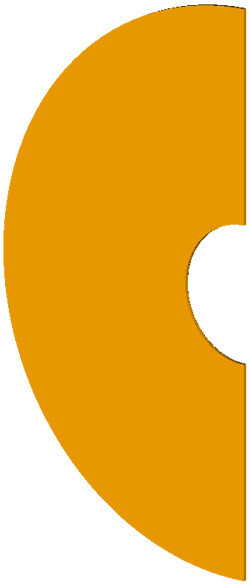

Figure 3-7 Solid Model of Base Plate

Figure 3-8 Positioned Charge Assembly with the Base Plate

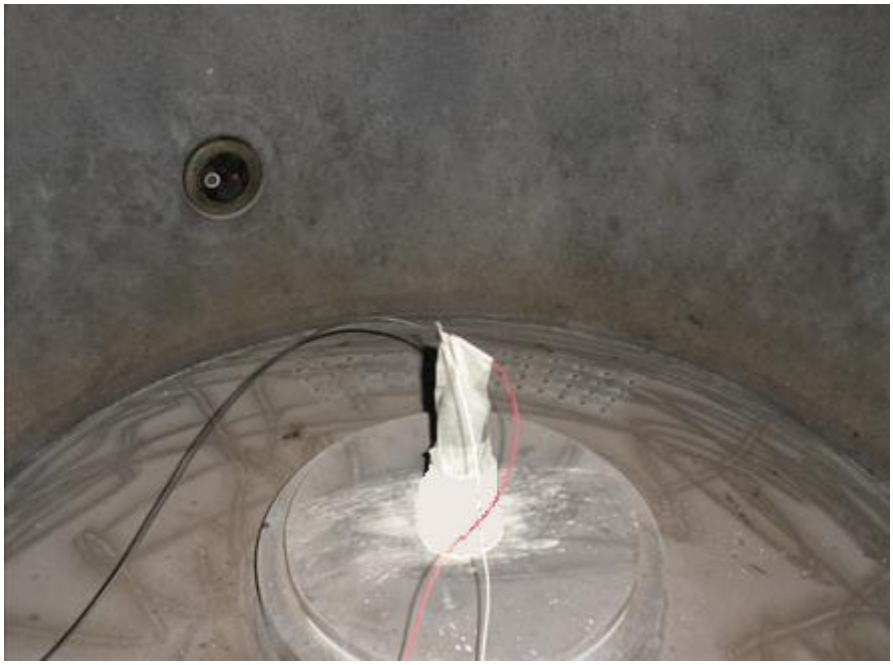

Figure 3-9 Final Test Setup Assembly

Figure 3-10 Inner Volume of Experimental Setup after Each Test

CHAPTER 4

NUMERICAL METHODOLOGY

The behavior of the shock wave created by detonation of explosive is a highly non-linear and time dependent phenomenon and this phenomenon can be modeled using dynamic and transient wave propagation codes, called hydrocodes [20]. Hydrocodes have been in use over 45 years. These complex problems such as blast propagation, perforation and penetration, shock compression and hyper velocity impact have high pressure which means that material strength becomes initially negligible. However, in recent years, material deformation and high explosive initiation become more and more considerable since warhead design tools have been developed rapidly [4]. Nowadays, the most commonly used commercial hydrocodes are Autodyn, Speed, Ls-Dyna and Dytran [1].

Hydrocodes deal with the conservation of momentum, mass and energy equations to solve shock problems where analytical solution is almost impossible unless many assumptions are made. Different techniques are generally used to solve these equations such as Eulerian, Lagrangian and Arbitrary Lagrangian Eulerian (ALE) methods.

Lagrange solvers are interested in the conservation equations in the material frame. The mesh domain deforms with the material as a function of elapsed time. Lagrange mesh is given in Figure 4-1 [21]. In general, these codes solve the conservation equations by using a finite element method. The advantages of these types of codes are that they consume less memory than Eulerian ones and computational requirements for CPU. They have the ability to accurately identify the material surfaces and interfaces. The disadvantages include the difficulty in generating free surfaces for fragmentation and fracture, also the difficulty in developing meshes

especially in three-dimensions, and the difficulty in implementing contact surface interactions [4].

Eulerian solvers deal with the conservation equations in the spatial frame. Therefore, the mesh is fixed in space while the deformation of the material is taken into account as a function of elapsed time. Euler mesh is given Figure 4-2 [21]. A control volume method which utilizes the equations such as conservation of momentum, energy and mass is applied [22]. In general, Eulerian codes solve the conservation equations using a finite difference or finite volume method. The advantages are the computational robustness for large deformation of behavior of material, simple method for generating free surfaces for fragmentation and fracture, easier way to mesh partition and material insertion. The disadvantages include difficulties with material interfaces, computational requirements in CPU and memory, diffusion of shock when poor numerical techniques are employed. Indeed, Eulerian codes solve the conservation equations in Lagrangian form as a part of the solution sequence. The Lagrangian step is followed by an advection step, so called remap step which reverses the physical variables to the original mesh [4].

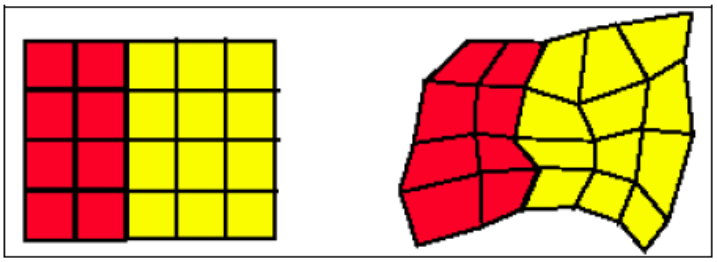

Figure 4-1 Lagrangian Mesh [21]

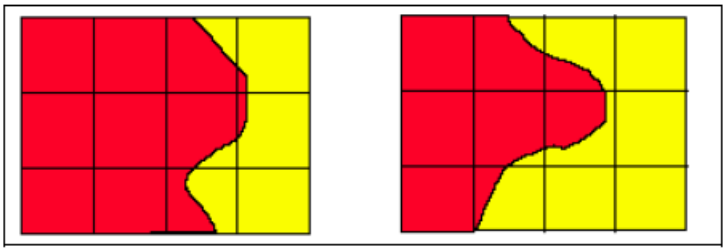

Figure 4-2 Eulerian Mesh [21]

The Arbitrary Lagrangian Eulerian (ALE) [23] solver deals with large shear deformation problems, i.e., metal forming and fluid flow. This method ensures an automatic rezoning which overcomes some of restrictions of Lagrangian and Eulerian solvers [24]. ALE method can be applied for moving boundaries and large volume changes compared to Eulerian methods. This method is composed of a Lagrangian, rezoning and a remapping step. It presents a variation of Lagrangian hydrodynamics that by-passes mesh distortion of Lagrangian in remapping and rezoning steps [23].

Eulerian codes, utilizes a two-step process that includes a Lagrangian step followed by an advection step to solve the conservation equations. The following is a simplified description of the process. In the Lagrangian step, the Lagrangian forms of the governing equations are integrated across a time step. Virtually, the initial mesh distorts to follow the material motions and there is no mass flux across the cell boundaries. The advection step then remaps the distorted cells back to the initial fixed mesh [4].

The whole process begins with cell centered variables. Before the Lagrangian step, face centered variables are calculated using interpolation, which results in a staggered mesh. The hydrocode does not store the face centered variables, but they are temporarily used during the Lagrangian step. In the Lagrangian step, the face centered velocities are updated. Because the time step is known, code virtually calculates the distorted mesh. Then, the advection step remaps the virtually distorted mesh back to the initial fixed mesh, and hence, transports material from

one cell to another. Three advection schemes, 1st order, 2nd order and 3rd order are implemented. After the advection step, the face centered variables are remapped back to cell centered variables, and code stores the new quantities, which include specific internal energy, velocity, total mass, internal energies and volumes of each material contained within a mesh. User defined variables are also stored which may include pressure, the stress tensor and internal state variables [4].

The three advection schemes validate additional flexibility and accuracy. The 1st order advection scheme is the least accurate, but acquires the least computational time. The 2nd order scheme reduces numerical diffusion but requires more computational effort. The 3rd order scheme results in advanced sharpness in shocks by approximately 20% with only a small increase in the computational cost compared to the 2nd order scheme [4].

4.1 Advantages of SPEED Hydrocode

In this thesis, in order to simulate the detonation in closed chamber which is a non-linear transient problem, commercial finite volume Eulerian hydrocode called Speed is used. This code can be described as [25] "a commercial version of Numerics' in-house hydrocode NumHyd. Speed is a multi-material Eulerian hydrocode with explicit solver technique for the computation of highly non-linear problems in 2D and 3D". The hydrocode has been experienced in many engineering problems and research applications. The major advantages of Speed in terms of performance when compared to different commercial hydrocodes such as Autodyn and Ls-Dyna is the superiority of computational effort since no Eulerian-Lagrangian coupling is required for complex interaction problems. This hydrocode also requires low memory with user-friendly competence of post-processing and has sharp shock resolution with robust algorithms for multi-material cells. The most valuable advantage of the code is having extensive material library sets for solids, gaseous

products, explosives, porous solids and soils which enable users to deal with large variety of application fields [25].

The code utilizes multi-material 2D Cartesian and cylindrical; 3D Cartesian and ideal gas solvers with high confidence in the accuracy and material response. As used in this study, geometrical modeling in 2D has many geometric features and includes comprehensive body operations [25].

4.2 Governing Equations

The governing equations that the hydrocode solves can be listed as follows [26]. The velocity can be defined as:

$$\vec{u} = (U, V, W) \tag{4.1}$$

where *U*, *V* and *W* are the x, y and z-components of the velocity vector, respectively. The velocity gradient L_{ij} can be defined in terms of the velocity:

$$L_{ij} = \frac{\partial u_i}{\partial x_j} \tag{4.2}$$

The gradient is split into a symmetric part D_{ij}, the rate of deformation tensor, and a skew part W_{ij}, the rotational spin tensor:

$$D_{ij} = \frac{1}{2}\left(\frac{\partial u_i}{\partial x_j} + \frac{\partial u_j}{\partial x_i}\right) \tag{4.3}$$

$$W_{ij} = \frac{1}{2}(\frac{\partial u_i}{\partial x_j} - \frac{\partial u_j}{\partial x_i}) \quad (4.4)$$

In Eulerian approach, partial differential equations of conservation of mass, energy and momentum should be involved as the main equations. In differential form the law of mass conservation or equation of continuity can be expressed in the following form:

$$\frac{d\rho}{dt} = \frac{\partial \rho}{\partial t} + u_i \frac{\partial \rho}{\partial x_i} \quad (4.5)$$

Here, ρ is the density of the fluid. Conservation of linear momentum is expressed by the following:

$$\rho \frac{d\vec{u}}{dt} = \rho\vec{b} + div\bar{\sigma} \quad (4.6)$$

In addition, conservation of energy can be written as:

$$\rho \frac{d(e+k)}{dt} = div(\bar{\sigma}\vec{u}) + \rho\vec{b}.\vec{u} \quad (4.7)$$

where *e* is the specific internal energy and k is the specific kinetic energy. In addition to the balance laws or equations of motion, the behavior of materials should be identified. Usually the stress tensor is split into a stress deviator S_{ij} and the hydrostatic pressure *p*:

$$\sigma_{ij} = S_{ij} - \delta_{ij}p \quad (4.8)$$

$$p = -\frac{1}{3}\sigma_{ii} \quad (4.9)$$

The pressure is assumed to be known through an equation of state as a function of specific internal energy, density and a set of state variables λ_k:

$$p = p(e, \rho, \lambda_k) \tag{4.10}$$

The equation of state for air and the explosives are implemented by constitutive models which are ideal gas and JWL equation of states, respectively. To begin with, the pressure of an ideal gas is a function of density and temperature:

$$p = \rho R_s T \tag{4.11}$$

where p is the pressure, ρ is density of the gas, R_s is specific gas constant and T is the temperature. This relation implies that the specific internal energy must be a function of the temperature alone. It is assumed a polynomial dependence:

$$e(T) = (c_0 T + \frac{c_1}{2} T^2) R_s \tag{4.12}$$

It follows for the heat capacity:

$$c_v = \frac{d}{dT} e(T) \tag{4.13}$$

which is equal to;

$$c_v = (c_0 + c_1 T) R_s \tag{4.14}$$

where e is the specific internal energy and c_v is the specific heat capacity at constant volume. The specific gas constant is calculated from the molecular weight:

$$R_s = \frac{R_u}{M} \tag{4.15}$$

where R_u is the universal gas constant which is equal to 8.314 J/mol.K and M is molecular weight of the gas. In order to obtain the sound speed, the following equations are applied:

$$C = \sqrt{\gamma R_s T} \tag{4.16}$$

The numerical simulation setup includes main charge assembly, detonation chamber body and gauge points located at the exact location with experiments. The walls of the detonation chamber are modeled as rigid in analyses since Speed cannot handle solid material deformation properly in high strain rate problems such as detonation. As an initial condition, detonation of the explosive at t=0 is applied. The problem definition with the initial and boundary conditions of the control volume of the study is presented in Figure 4-3.

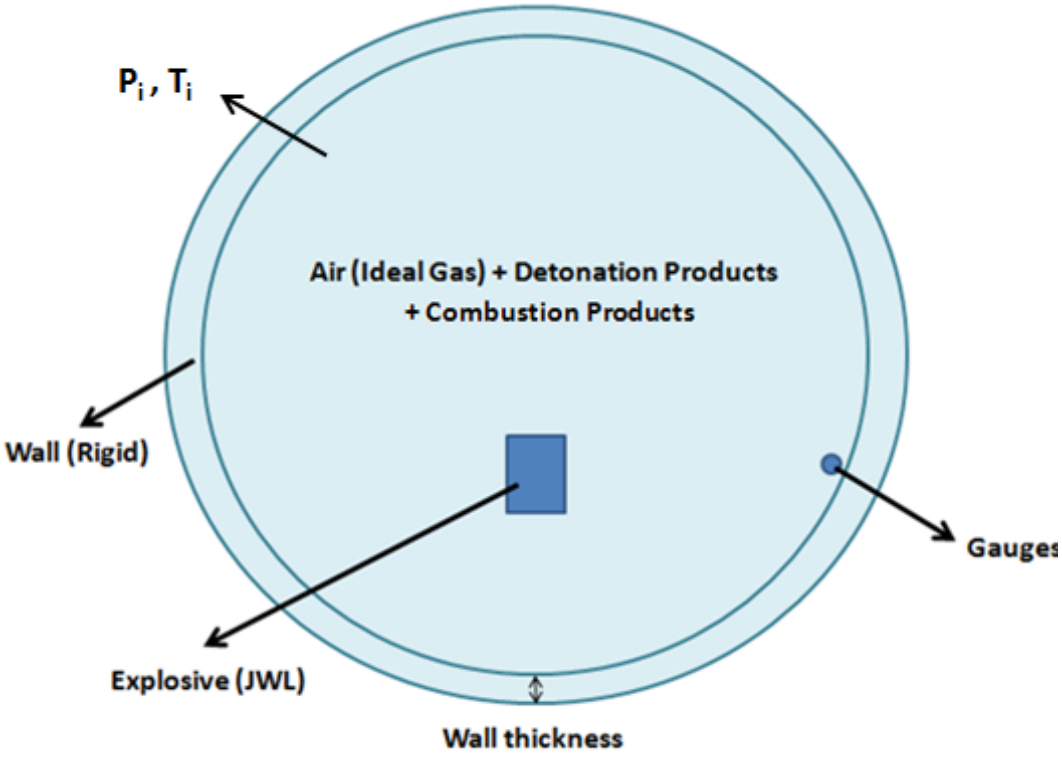

Figure 4-3 Control Volume of the Study

For the modeling of explosives, almost all commercial softwares require equation of state parameters of high explosives where detonation pressure is the main concern. In order to model this phenomenon, the hydrodynamic detonation theory is used. This theory utilizes some assumptions such that the reaction time is zero and the velocity of the detonation wave propagation throughout the explosive is constant. This propagation of detonation wave is given in Figure 4-4 [27]. With the detonation of explosive, gaseous products compress the medium and extend rapidly. In the generated sharp boundary, called shock front, the pressure rises in a discontinuous manner. These peak pressure and impulse are the two main damage mechanism of blast effect. Peak pressure can be defined as the highest pressure at the shock front of the shock wave. Impulse is the measure of force multiplied by the duration of blast phase. Hence, positive impulse corresponds to the integral of the

pressure-time curve over the positive phase duration [2]. A typical air blast curve is given in Figure 4-5 [28]. Here, t_a is the time of arrival of the shock wave that creates a positive phase over atmospheric pressure, P_o. In other words, time of arrival is the time from the onset of the detonation till the arrival of the shock wave to the measurement location.

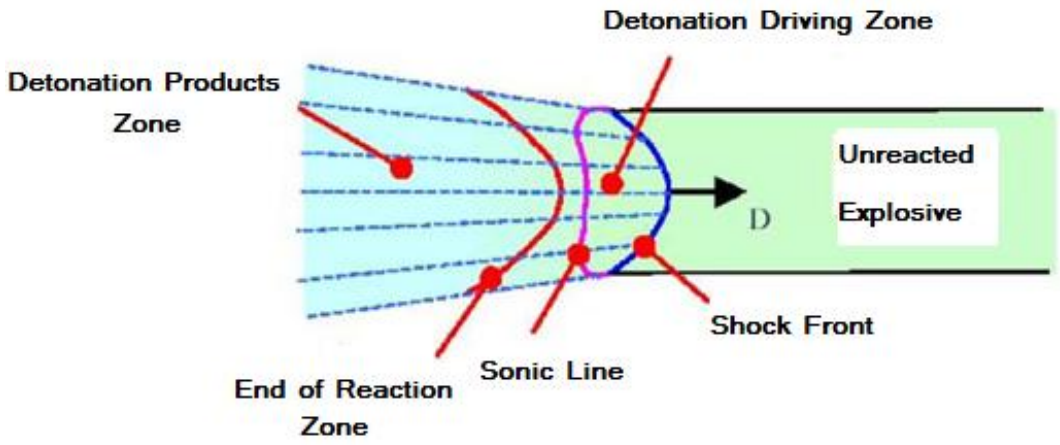

Figure 4-4 Representation of the Hydrodynamic Theory [27]

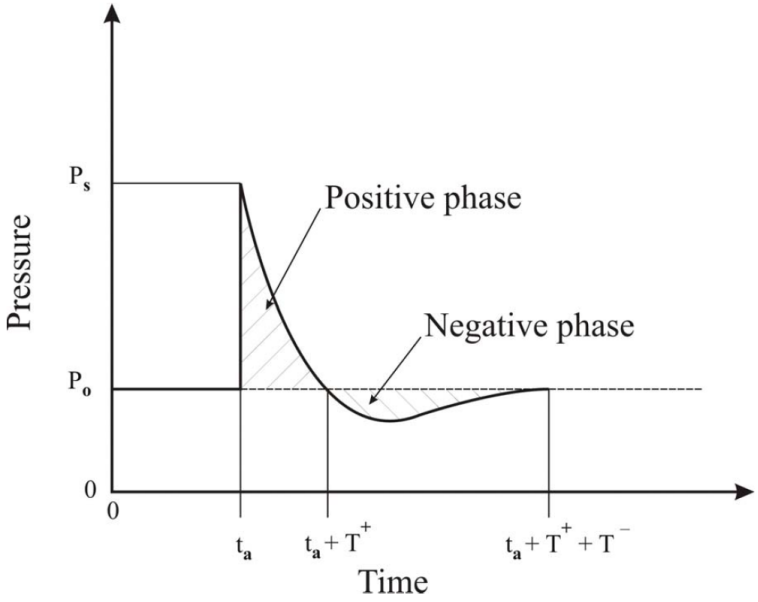

Figure 4-5 Typical Air Blast Curve [28]

A modern approach that hydrocodes apply for the determination of the relation between specific volume of the reaction products and the pressure generated is obtained from thermo-mechanical analysis of measured values and their fit of related equation of state [29], [30] .

The widely used non-linear Jones-Wilkins-Lee (JWL) equation of state is employed in various numerical codes. The JWL equation of state that represents the detonation characteristics of energetic materials is given in Equation (1.1). In Equation (1.1), the parameters A, B, C, R_1, R_2 and ω are the constants that are obtained from cylinder expansion test.

The JWL parameters that are used in this study are obtained from [31] for P-1, P-2, P-3 and P-4. These parameters that are derived from the cylinder expansion tests for the explosives are listed in Table 4-1[31].

Table 4-1 JWL Equation of Parameters for P-1, P-2, P-3 and P-4 [31]

Parameter / Property	**Unit**	**P-1**	**P-2**	**P-3**	**P-4**
V_d	m/s	6632	7059	7237	7273
ρ	g/cm^3	1.59	1.66	1.62	1.70
E_o	kJ/m^3	5.675×10^6	4.892×10^6	5.431×10^6	4.977×10^6
P_{cj}	kPa	2.033×10^7	1.892×10^7	2.009×10^7	1.967×10^7
A	kPa	4.531×10^8	1.813×10^8	1.362×10^9	2.143×10^9
B	kPa	1.560×10^7	2.217×10^7	2.384×10^7	2.152×10^7
C	kPa	5.765×10^5	6.247×10^5	8.464×10^5	1.213×10^6
R_1	-	5.15	6.623	6.250	6.64
R_2	-	1.00	1.367	1.350	1.37
ω	-	0.344	0.137	0.170	0.134

Since the JWL EOS parameters of the booster charge which is made of PBXN-5 type explosive are not determined, the widely used, most relevant to PBXN-5 and validated explosive, LX-10-1 is modeled in Speed. The JWL EOS parameters of LX-10-1 are listed in Table 4-2 [32].

Table 4-2 JWL Equation of Parameters for LX-10-1 [32]

Parameter / Property	**Unit**	**LX-10-1**
V_d	m/s	8819.78
ρ	g/cm^3	1.865
E_o	kJ/m^3	1.040×10^7
P_{cj}	kPa	3.749×10^7
A	kPa	8.807×10^8
B	kPa	1.835×10^7
C	kPa	1.296×10^6
R_1	-	4.62
R_2	-	1.32
ω	-	0.38

4.3 Validation of Speed Code

The validation of Speed hydrocode is split into different application areas such as cylinder expansion test, open area blast measurement experiment by detonation of high explosive and explosive dent test. The main idea of these validation studies is to compare the experimental results available in literature with the numerical results obtained from Eulerian Speed software code. These experimental studies are modeled in Speed code and corresponding results are discussed.

4.3.1 Cylinder Expansion Test

The cylinder expansion test which is used to characterize the explosive parameters was modeled using Speed software. Topkaraoğlu [31] conducted cylinder expansion test in order to obtain the JWL parameters of explosive, P-1. As presented in Figure 4-6, the setup consists of copper cylinder filled with the main explosive for which the JWL parameters are desired and contact ionization pins that measure the consecutive radial expansion of the copper tube with the detonation of main explosive. The main explosive is detonated by booster charge assembly composed of two booster pellets. In the numerical model, pins were modeled as fixed gauges and placed at the exact radial positions utilized in the experiment. Copper cylinder with inner diameter of 60 mm, outer diameter of 72 mm and length of 800 mm was filled with P-1 explosive. In order to model copper material Cu (OFHC) material, Johnson-Cook material strength model was used, which was already presented in Speed material library. These parameters are presented in Appendix B. To model the booster charge, JWL equation of state parameters for LX-10-1 was applied [32]. Solver type was selected to be axisymmetrical 2D. In order to save computational time, mesh sensitivity studies were conducted. Five different sets of runs were performed and the corresponding total number of elements for each model is given in Table 4-3.

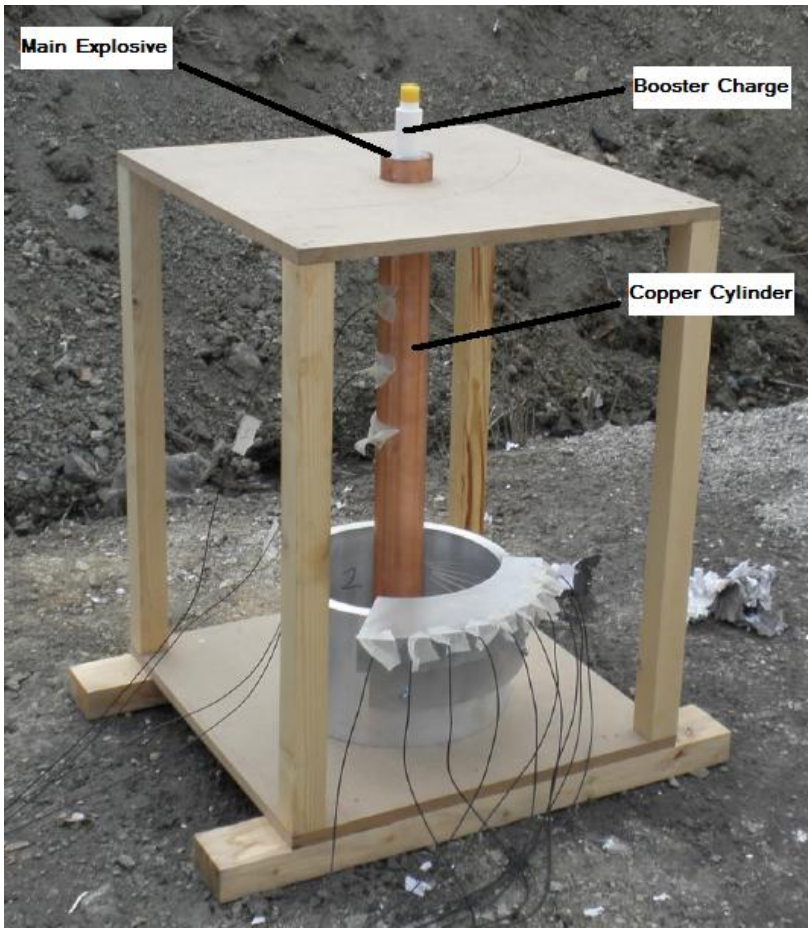

Figure 4-6 Cylinder Expansion Test Setup [31]

Table 4-3 Total Number of Elements in Cylinder Expansion Test Model

Model	The Total Number of Elements
1	300000
2	450000
3	675000
4	1012500
5	1518750

In Table 4-4, calculated and measured pin signal times with the relative difference of the test results with respect to model 5 are presented for the 9 pins which were positioned radially.

Table 4-4 Comparison of Experimental and Numerical Contact Time

Pin Radial Distance (mm)	**Experimental Contact Time (μs)**	**Numerical Contact Time Model 5 (μs)**	**Relative Difference of the Test Results with respect to Model 5**
0.10	0.0	0.0	0.0%
8.10	9.3	9.55	2.15%
16.10	16.3	17.65	2.76%
24.10	23.1	24.9	3.90%
32.10	29.7	30.25	6.90%
40.10	35.2	33.2	-6.53%
48.10	41.5	39.8	-9.04%
56.10	47.5	47.2	-3.68%
64.10	53.4	51.15	-5.62%

The numerical contact time results of the pin which was located at 40.1 mm away from the copper tube are shown in Figure 4-7 for different number of elements. After certain mesh density, as the number of elements increases in the numerical model, a certain convergence is observed.

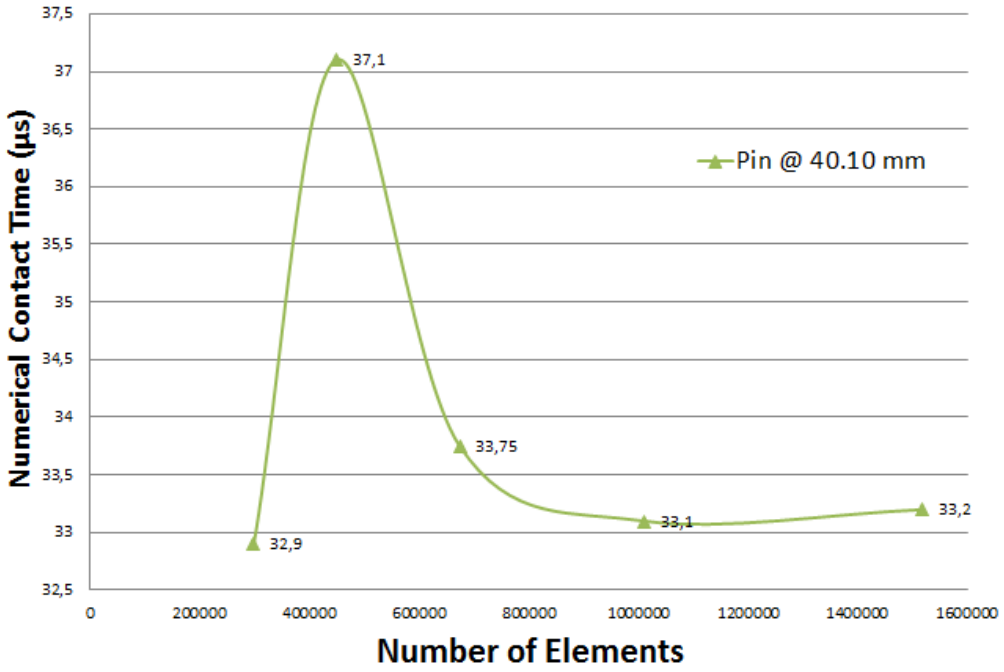

Figure 4-7 Mesh Independency Results - Contact Time

In Figure 4-8, representation of the pressure wave at different times are given. The magnitude of pressure of the shock wave is also given.

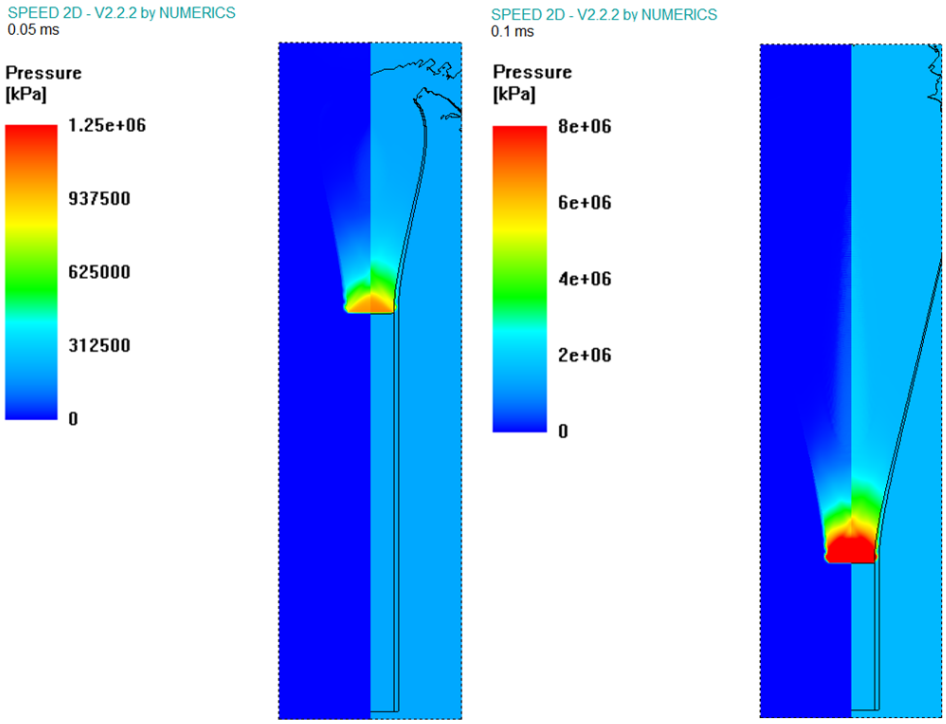

Figure 4-8 Representation of the Pressure Wave at Different Times

According to the numerical and experimental pin contact times presented in Table 4-4, it can be concluded that there is a certain consistency of the numerical results with respect to experimentally measured values. It implies that the deformation response of solid materials can be simulated properly with Eulerian methodology.

4.3.2 Open Area Blast Measurement Experiment by Detonation of High Explosive

The aim of this application is to investigate the accuracy of the shock wave and its magnitude in open area generated from high explosive, P-1. The related explosive blast performance characteristics were tested and the results are presented in [18]. In the numerical model, the explosive P-1 was used with the previously gathered JWL parameters. To model the booster charge, JWL equation of parameters for LX-10-1 was applied [32]. Solver type was selected as axisymmetrical 2D in order to save computational time. The gauges were placed at the exact radial positions which were 2 m, 3 m and 4 m radially from the center of charge as utilized in the experiment. Geometrical constrains that applied in experiment were utilized in the simulation. That is, the height of the explosive from the ground was 2.1 m. Also, the mass of the charge assembly was 1 kg including the booster charge. The outer boundaries were selected as transmissive in order for the shock wave to flow out except the lower boundary which implies the ground. As an initial condition, detonation of booster charge was used in the simulation setup.

In order to select an optimum mesh size, mesh sensitivity studies were conducted. Five different sets of runs were performed and the corresponding total number of elements for each model is given in Table 4-5.

Table 4-5 Total Number of Elements in Blast Measurement Test Model

Model	The Total Number of Elements
1	300000
2	450000
3	675000
4	1012500
5	1518750

Pressure-time histories were recorded by using gauges for each model. The peak over-pressure results with the relative difference of the test results with respect to model 5 are presented in Table 4-6.

Table 4-6 Comparison of Experimental and Numerical Results

Model	**Measurement Distance (m)**	**Calculated Peak Over-Pressure (kPa)**	**Experimental Peak Over-Pressure (kPa)**	**Relative Difference of the Test Results with respect to Model 5**
5	2	179.30	183.12	-2.08%
	3	78.26	83.43	-6.19%
	4	42.24	43.70	-3.34%

The calculated peak over-pressure values taken from 2 m are also shown in Figure 4-9 for different number of elements. After certain mesh density, as the number of elements in the numerical model increase, a certain convergence is observed.

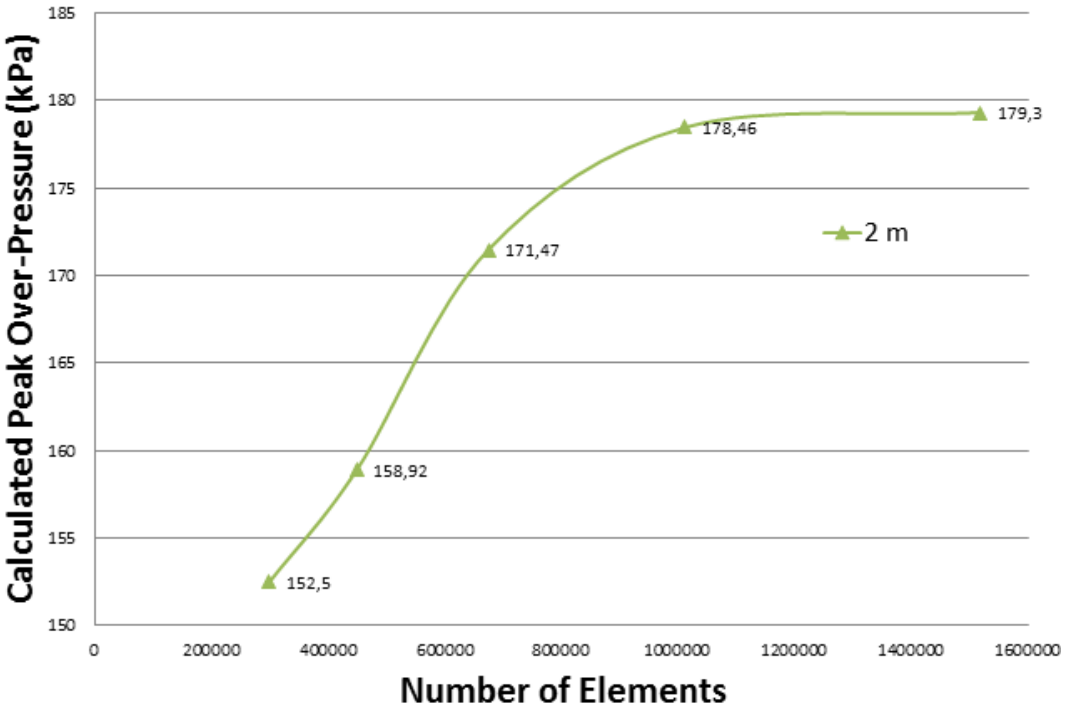

Figure 4-9 Mesh Independency Results – Peak Over-Pressure

Shock waves at different times obtained from simulation are presented in Figure 4-10. The magnitude of pressure of the shock wave is also given.

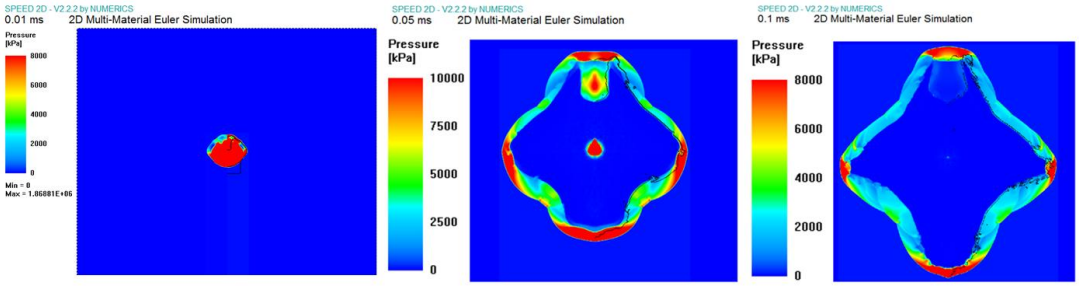

Figure 4-10 Shock Wave at Different Times

According to the Table 4-6, it can clearly be identified that, the calculated peak over-pressure results obtained from model 5 is in good agreement with the experimental measurements at 2 m, 3 m, and 4 m.

4.3.3 Explosive Dent Test

Dent test of high explosive is performed to analyze whether the detonation occurs for the explosive with the designed initiation train. The methodology of this test can be expressed by using a thick witness steel plate which is deformed by the detonation of explosive placed directly on it. Then, the dent characteristic of the explosive is investigated by measuring the plate dent depth. The aim of this study is to observe the capability of Speed code in terms of material response against high explosive detonation. The explosive dent experiment was conducted and the results are presented in [33]. The experimental test setup is given in Figure 4-11. One hundred and forty five grams of PBXN-5 explosive with steel casing was detonated on the witness plate and dent depth was recorded. The material type of the witness plate and the casing was Steel 4340. In the numerical simulation, in order to measure the depth of the dent, a moving gauge was placed on the upper side of the plate. The plate thickness and width were 25 and 75 mm, respectively. The numerical model consists of HE, its casing and witness plate. Solver type was selected to be axisymmetrical 2D. To model the witness plate and the outer casing of the explosive, Johnson-Cook material strength model of Steel 4340 was used, which is obtained from the material library. These material parameters are presented in Appendix B. The outer boundaries of the setup were transmissive in order for the shock wave to flow out. As an initial condition, detonation of the explosive charge was used.

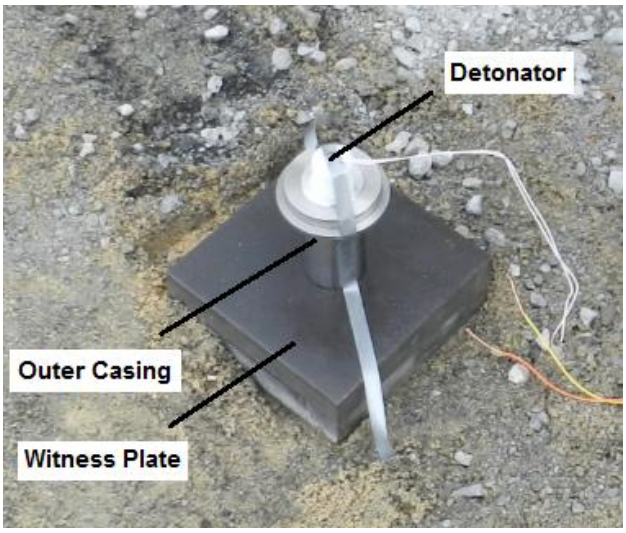

Figure 4-11 Explosive Dent Test Setup [33]

In the numerical study, to define an optimum mesh edge length, mesh sensitivity studies were conducted. Since the dimensions of the experiment and simulation setup are comparably small with respect to previous studies, the maximum number of elements of the finest model is 506250. Five different sets of runs were performed and the corresponding total number of elements for each model is given in Table 4-7.

Table 4-7 Total Number of Elements in Dent Test Model

Model	**The Total Number of Elements**
1	100000
2	150000
3	225000
4	337500
5	506250

Dent depth histories were recorded for each model. Results of the model 5 are presented in Table 4-8 with experimental results.

Table 4-8 Comparison of the Experimental and Numerical Dent Depths

Model	**Calculated Dent Depth (mm)**	**Experimentally Measured Dent Depth (mm)**	**Relative Difference of the Test Results with respect to Model 5**
5	12.74	13.20	-3.48%

The calculated dent depth values are also shown in Figure 4-12 for different number of elements. After certain mesh density, as the number of elements in the numerical model increase, a certain convergence is obtained.

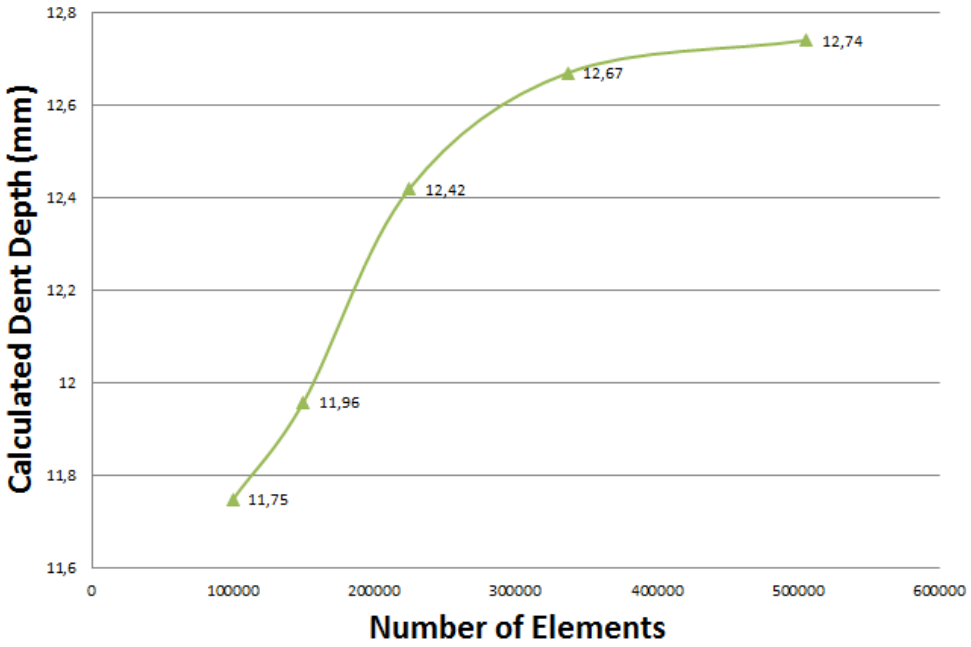

Figure 4-12 Mesh Independency Results – Dent Depth

The corresponding calculated dent depth history for model 5 and final capture of the simulation is also presented in Figure 4-13 and Figure 4-14, respectively.

Figure 4-13 Simulation Model of Dent Test

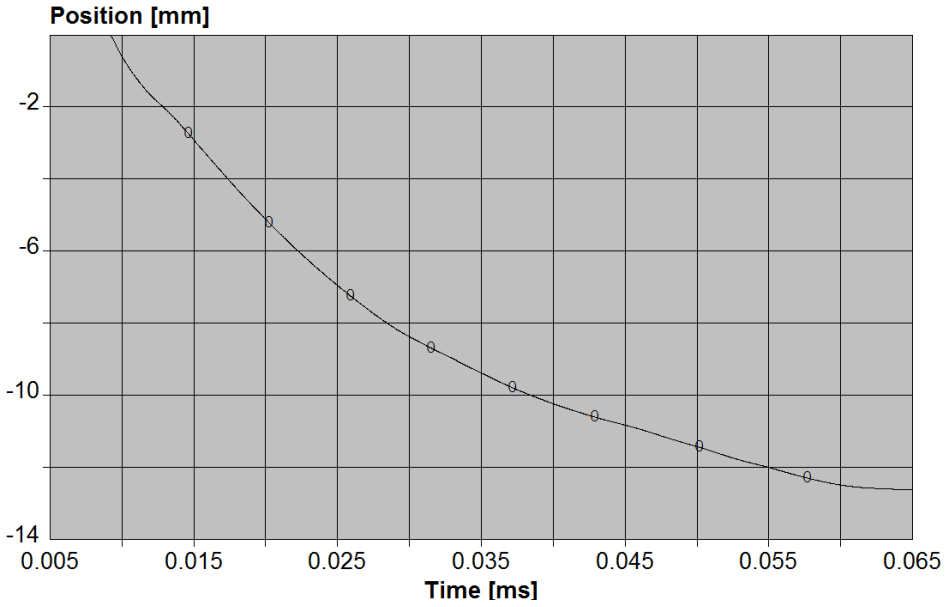

Figure 4-14 Calculated Dent Depth History – Model 5

The numerical data indicates that as the number of elements in the numerical model increase, the calculated dent depth converges to the experimental results and remains constant after certain mesh density. According to the numerical and experimental measured depth distances, it can be concluded that there is a certain consistency of the numerical results with respect to experimental ones.

CHAPTER 5

NUMERICAL AND EXPERIMENTAL RESULTS

In this chapter, results of numerical simulation studies and experimental results obtained from the detonation chamber are presented. Experimental results include the pressure measurements during the detonation of explosives having different compositions in the detonation chamber. Numerical results include the sensitivity analysis according to mass and distance, effects of uncertainties on the utilized JWL equation of state parameters for each explosive and mesh independency studies. Additionally, over-pressure and impulse data obtained from both experiment and numerical study are presented. The pressure contour outputs of numerical hydrocode are given. Also, filtering of experimental data is utilized in this chapter.

5.1 Numerical Studies

As stated in Chapter 4, numerical studies are conducted using multi-material Eulerian Speed hydrocode software.

5.1.1 Mesh Independency Studies

Subsequent to the modeling the test setups in Eulerian grid, in order to investigate the effect of mesh independency, several runs are accomplished for the same model by altering the cell sizes of whole Eulerian domain. This study is applied only for the explosive P-4. The comprehensive results shall be gathered for the explosive which has higher velocity of detonation since the time step calculations are based on the maximum velocity in whole Eulerian domain. Six different sets of runs are

done and the corresponding numbers of elements with the minimum size for each model are given in Table 5-1. A general method is applied for incrementation of total mesh size of models. Each consecutive model is 1.5 times finer than the previous one. In the same manner, mesh rezoning adopted near the gauge points is kept similar for each model. The six different mesh grids around the gauge points are also presented in Figure 5-1. Here, the finest model which is the model 6 has number of elements of 3000000 that is approximately 2 times finer than model 5. The difference between model 5 and 6 is to be analyzed in terms of effect of high quality mesh size on peak-over pressure.

Table 5-1 Total Number of Elements and Minimum Edge Length in Mesh Independency Studies

Model	**The Total Number of Elements in Eulerian Domain**	**The Minimum Size of the Element (mm)**
1	300000	1.3
2	450000	1
3	675000	0.75
4	1012500	0.5
5	1518750	0.3
6	3000000	0.15

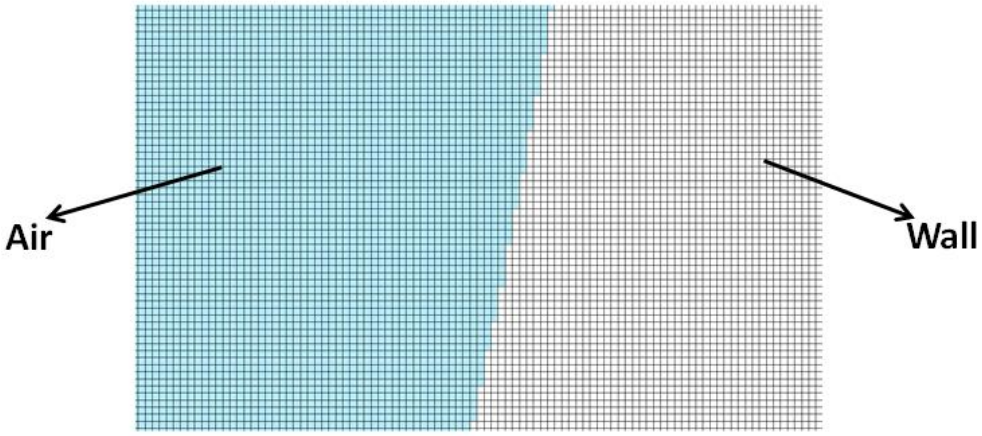

(a)

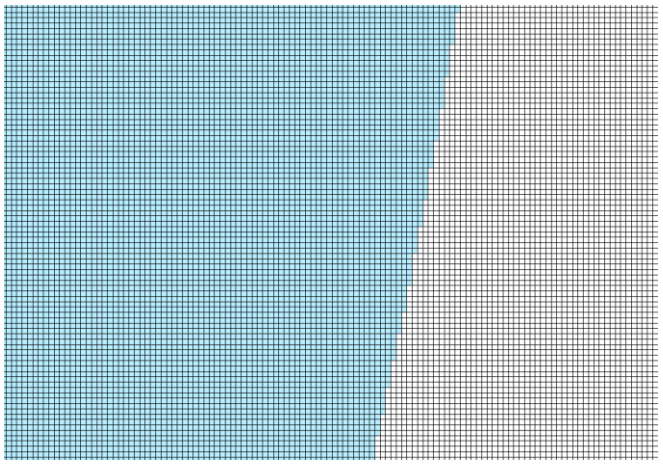

(b)

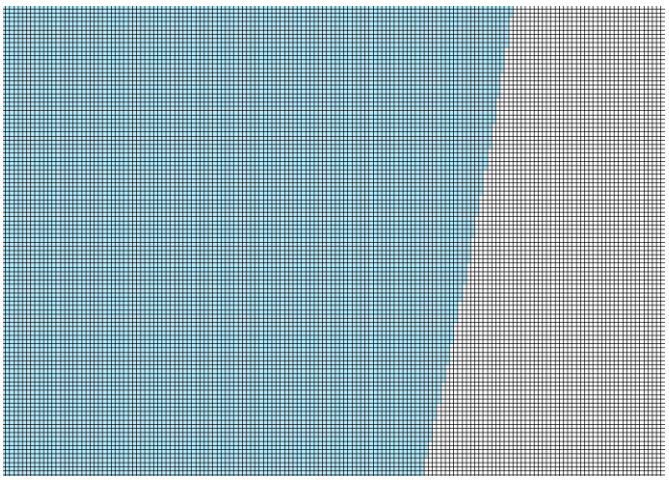

(c)

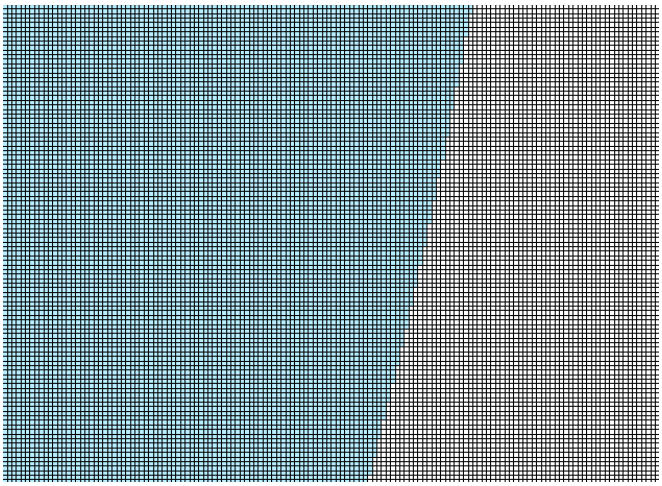

(d)

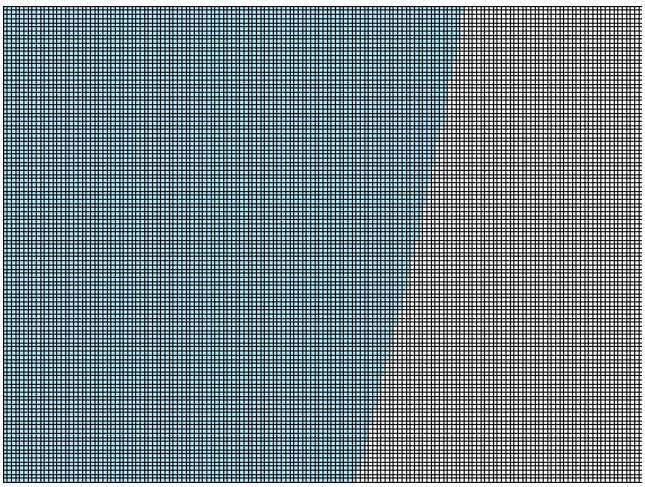

(e)

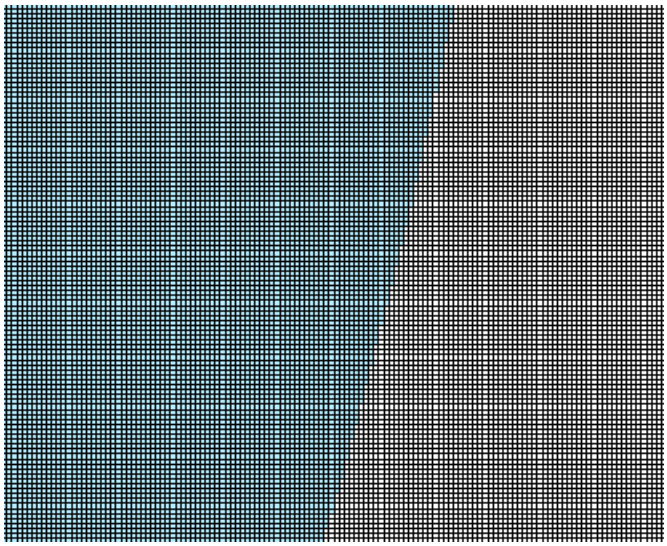

(f)

Figure 5-1 Representations of Cell Arrangement

(a) Model 1 (b) Model 2 (c) Model 3 (d) Model 4 (e) Model 5 (f) Model 6

For the all models, the mesh distribution around the locations of both explosive and gauge points have mesh rezoning. That is, the minimum size of elements around explosive and gauge locations is lower than the rest of the areas throughout the mesh grid.

In explicit analyses, time step calculated from the minimum cell size and the maximum velocity highly affects the run-time of simulations. The minimum cell size determines the stable time step which affects the run time and stability of the simulation and it is calculated by Equation (5.1) and (5.2) [26];

$$\Delta t_{ijk} = \min \{ \frac{\Delta x_i}{U_{ijk} + C_{ijk}}, \frac{\Delta y_j}{V_{ijk} + C_{ijk}}, \frac{\Delta z_k}{W_{ijk} + C_{ijk}} \} \tag{5.1}$$

The actual time step is

$$\Delta t = f_{safety} \min(\Delta t_{ijk}) \tag{5.2}$$

where f_{safety} is the safety factor which scales down the time step and the adiabatic sound speed C is expressed by Equation (4.16).

In order to save time for a bunch of analyses, the optimum number of total Eulerian elements is selected and the comparison of mesh independency study is based on the peak over-pressure results. The peak over-pressure results of explosive P-4 are shown in Figure 5-2 for different number of elements. It is deducted that the asymptotic line is achieved while moving from Model 4 to 5. Since the finest model which is model 6 has nearly the same peak-over pressure with model 5, the rest of the analyses including all type of explosives are conducted by the same domain of mesh count of 1518750 in order to save computational time for the bunch of the analyses**.**

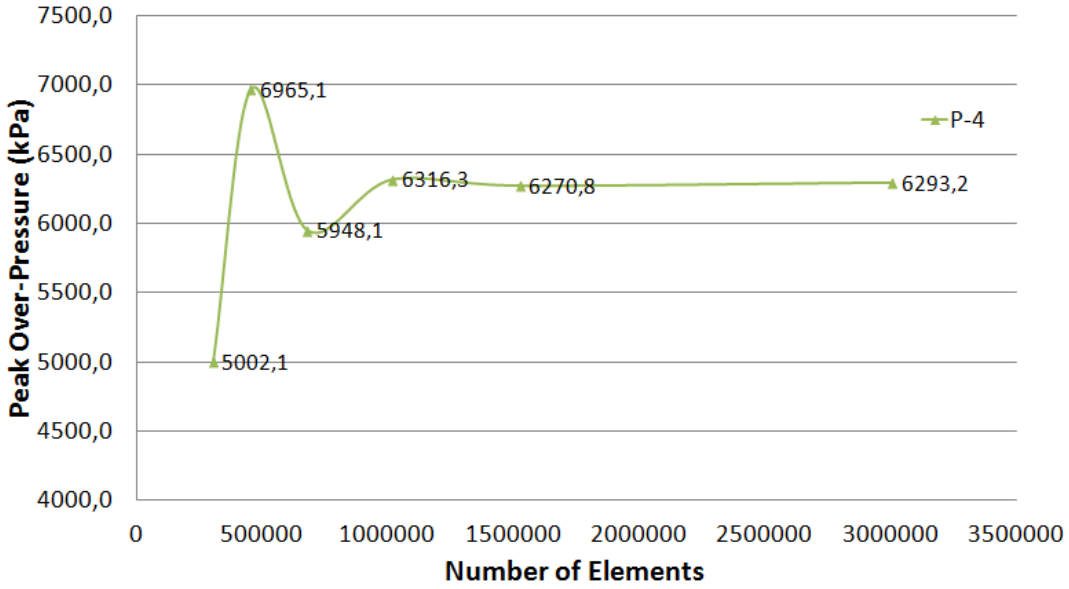

Figure 5-2 Mesh Independency Runs According to Explosive P-4

5.1.2 Sensitivity Analysis of Numerical Studies

In the numerical studies examining the blast performance of explosives, there are two different key parameters that affect the peak over-pressure calculations which are the explosive mass and the distance from the detonation point of explosive to the gauge location. To account for the sensitivity effects, these parameters are investigated in detail.

5.1.2.1 Sensitivity Analysis on the Distance between the Detonation Point of the Explosive and the Pressure Sensor

The position of the pressure sensor is measured before the tests and in numerical simulation; a set of gauges are placed at the experimentally measured location of pressure sensor. The variations of the position of the pressure sensor measured in experiments are in the range of 3 mm. That is to say, since pressure sensors are located on the wall of the chamber, the deviation is negative with respect to measured distance. Therefore, to investigate the effect of uncertainties in the measurement of the distance between the detonation point of the explosive and the pressure sensor, a total of 11 differently oriented gauge points (See Figure 5-3) are located having maximum distance of 3.37 mm from the measured value. The distances of the gauges from the measured distance are tabulated in Table 5-2.

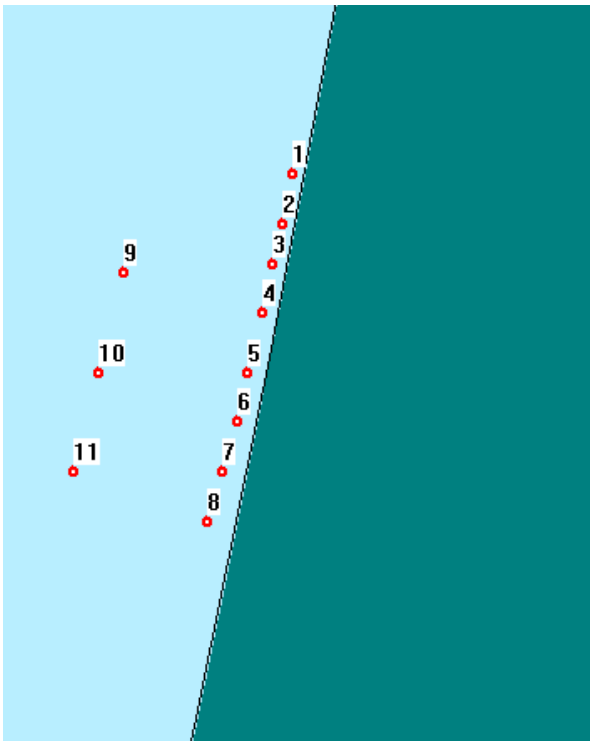

Figure 5-3 Orientation of Gauge Points

Table 5-2 Gauge Positions Relative to Measured Gauge

Gauge Number	Distance From Measured Gauge (mm)
1	0.68
2	0.53
3	0.38
4	0.23
5	0.00
6	-0.14
7	-0.38
8	-0.62
9	-2.61
10	-2.99
11	-3.37

The simulation runs are conducted using explosive P-4 and the peak over-pressure results are presented in Figure 5-4 and tabulated in Table 5-3 for each gauge points.

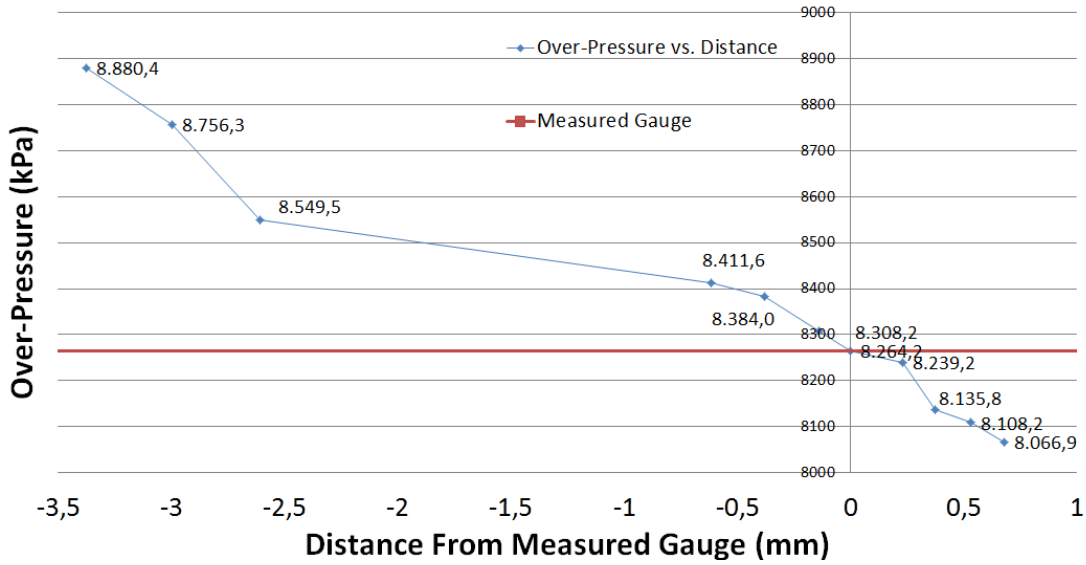

Figure 5-4 Over-Pressure Calculations from Each Gauge Points for P-4

Table 5-3 Comparison of Peak Over-Pressure Results

Gauge Number	Calculated Peak Over-Pressure (kPa)	Relative Difference – Peak Over-Pressure (kPa)
1	8066.9	-2.39%
2	8108.2	-1.88%
3	8135.8	-1.53%
4	8239.2	-0.30%
5	8264.2	0.00%
6	8308.2	0.50%
7	8384.0	1.35%
8	8411.6	1.78%
9	8549.5	3.45%
10	8756.3	5.95%
11	8880.4	7.46%

According to the results presented in Figure 5-4 and Table 5-3, the over-pressure calculated from closest gauges to the detonation point are higher than the ones that are located near the wall of the chamber. It can be deducted that the maximum deviation from the measured distance is 7.5% in terms of peak over-pressure when 0.6% alteration occurs in the distance.

5.1.2.2 Sensitivity Analysis on the Mass of the Explosive

In order to conduct sensitivity analysis according to the mass of explosive, the variation of masses of explosives are measured and related sensitivity analysis is conducted only for P-4 as in the previous studies. The mass variation of P-4 is given in Table 5-4.

Table 5-4 Variation of Mass

Explosive Type	Variation of Mass (g)
P-4	138
	140
	143

The deviation of the mass is in maximum 2% according to the mass measurements. Corresponding over-pressures obtained from altering the explosive mass in the simulation from 138 grams to 143 grams is shown in Figure 5-5.

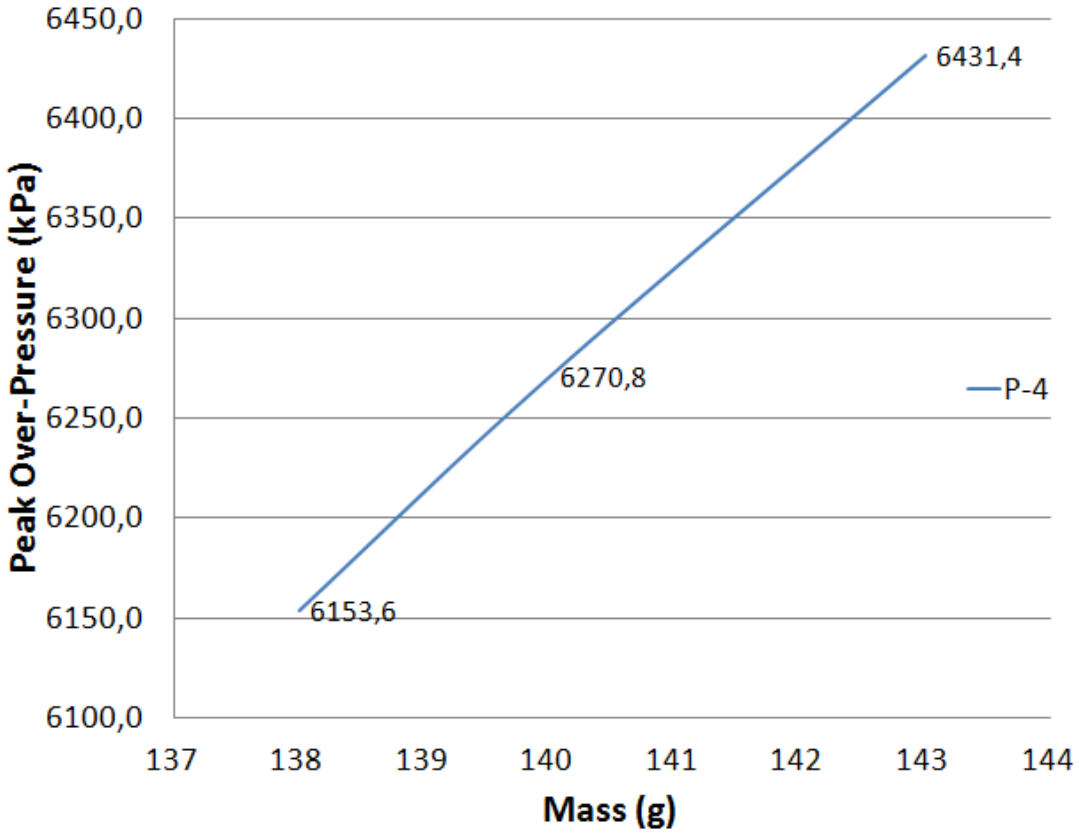

Figure 5-5 Peak Over-Pressure Calculations According to Explosive Mass

According to the results presented in Figure 5-5, 2% alteration in mass of explosive results in relatively minor variation which is 2.5% difference in peak over-pressure calculations.

5.1.3 Effects of Uncertainties on the Calculated JWL Parameters

As stated in Chapter 4, Jones-Wilkins-Lee equation of state can be adopted for modeling traditional and newly synthesized explosives in numerical hydrocodes. Therefore, the JWL parameters that are listed in Table 4-1 are used in Speed for each explosive. There are many uncertainties while gathering these parameters from

cylinder expansion test. These deviations are due to the manufacturing and mounting tolerances of cylinder expansion tests. Topkaraoğlu [31] studied the effects of uncertainties of cylinder expansion test for the well-known explosive TNT, namely P-1. In addition, TNT that Topkaraoğlu used in his research was manufactured in ROKETSAN A.Ş. facilities and his explosive and the one that is used in this case study were from the same production batch. He calculated the broad limits of JWL parameters by determining the quantity sets which gave lowest and highest limits of pressure-specific volume curves of explosives [31]. He concluded that the nominal values of JWL parameters of P-1 explosive were within the ±2% interval with the upper and lower boundary limits. The result is presented in Figure 5-6 [31].

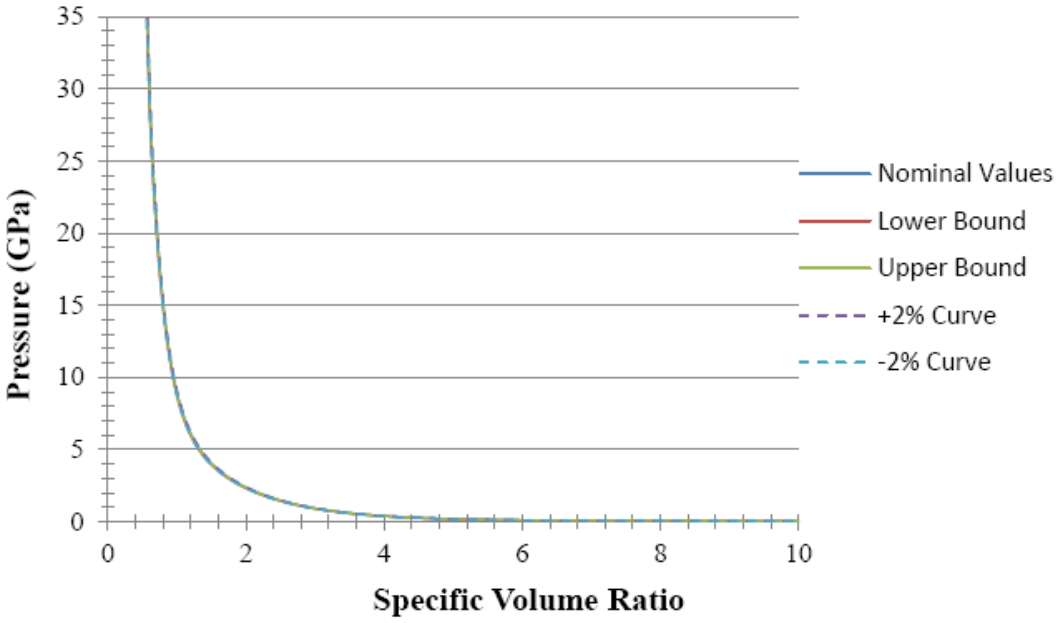

Figure 5-6 Upper and Lower Limits of P-ν Curves for Explosive P-1 [31]

According to the lower and upper bounds of new sets of JWL parameters which are given in Table 5-5 [31], two additional runs are conducted in Speed by keeping all other inputs as constant and the related nominal, lowest and highest peak over-pressure results of explosive P-1 are listed in Table 5-6. The results indicate that variations in JWL parameters which correspond to lowest and highest pressure-specific volume curve result in maximum of ±1.5% deviation in peak over-pressure.

Table 5-5 Boundary Limits of JWL Parameters of Explosive P-1 [31]

Parameter	**Unit**	**Nominal**	**Value Resulting Lowest Values of Pressure**	**Value Resulting Highest Values of Pressure**
V_d	m/s	6632	6629	6656
ρ	g/cm^3	1.59	1.57	1.60
E_o	kJ/m^3	5.675×10^6	5.672×10^6	5.678×10^6
P_{cj}	kPa	2.033×10^7	2.031×10^7	2.038×10^7
A	kPa	4.531×10^8	4.372×10^8	4.607×10^8
B	kPa	1.560×10^7	1.591×10^7	1.540×10^7
C	kPa	5.765×10^5	5.692×10^5	5.833×10^5
R_1	-	5.15	5.15	5.15
R_2	-	1.00	1.00	1.00
ω	-	0.334	0.336	0.334

Table 5-6 Analyses Results with Nominal, Lowest and Highest Values of JWL Parameters

Explosive Type	**Nominal Over-Pressure Obtained Using the Nominal Values of JWL Parameters (kPa)**	**Over-Pressure Obtained Using the Lowest Values of JWL Parameters (kPa)**	**Over-Pressure Obtained Using the Highest Values of JWL Parameters (kPa)**
P-1	10377.9	10244.9	10491.0

5.1.4 Numerical Results

Pressure contours inside the detonation chamber at different times obtained from numerical simulations are presented in Figure 5-7 for explosive P-1. The related figures for the rest of the explosives, P-2, P-3 and P-4 are provided in Appendix A.

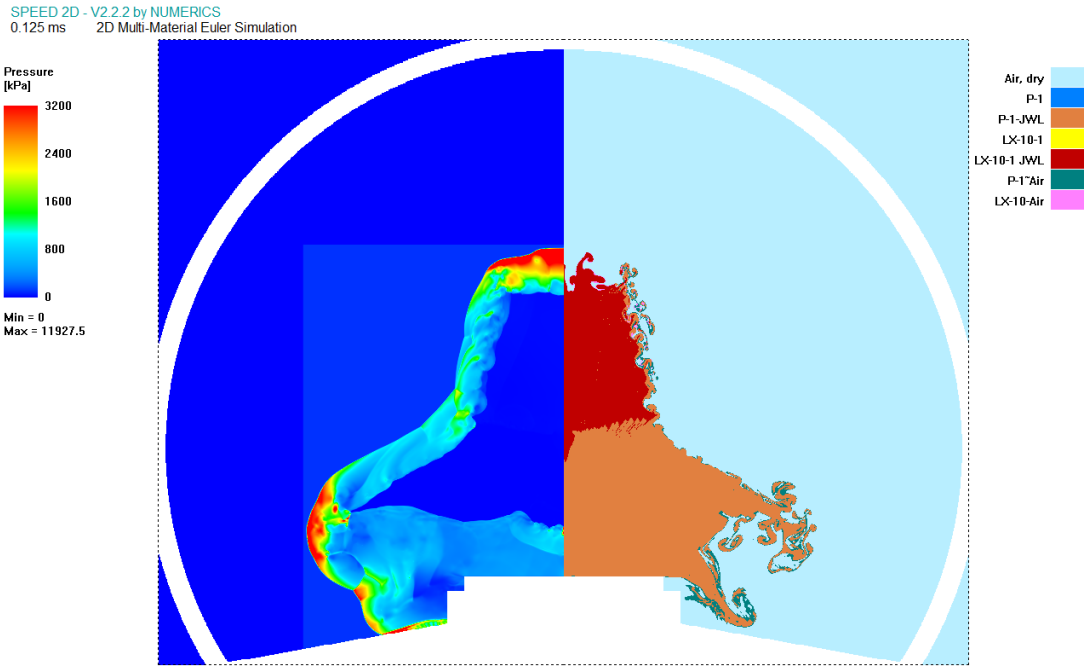
SPEED 2D - V2.2.2 by NUMERICS
0.125 ms 2D Multi-Material Euler Simulation
Pressure
[kPa]
3200
2400
1600
800
0
Min = 0
Max = 11927.5
Air, dry
P-1
P-1-JWL
LX-10-1
LX-10-1 JWL
P-1~Air
LX-10-Air

(a)

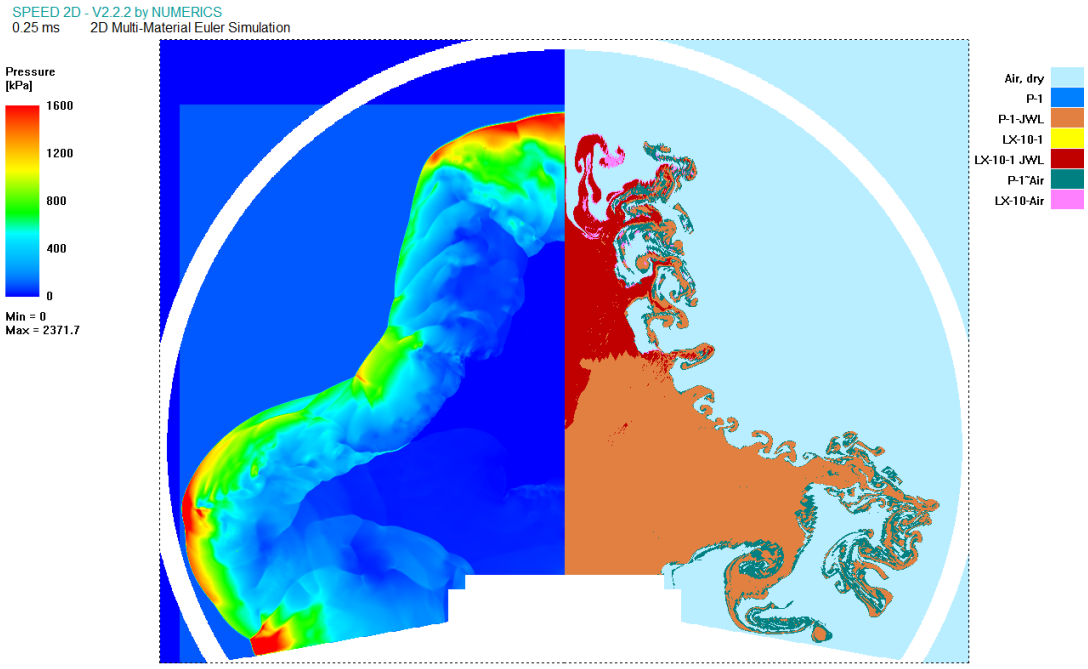
SPEED 2D - V2.2.2 by NUMERICS
0.25 ms 2D Multi-Material Euler Simulation
Pressure
[kPa]
1600
1200
800
400
0
Min = 0
Max = 2371.7
Air, dry
P-1
P-1-JWL
LX-10-1
LX-10-1 JWL
P-1~Air
LX-10-Air

(b)

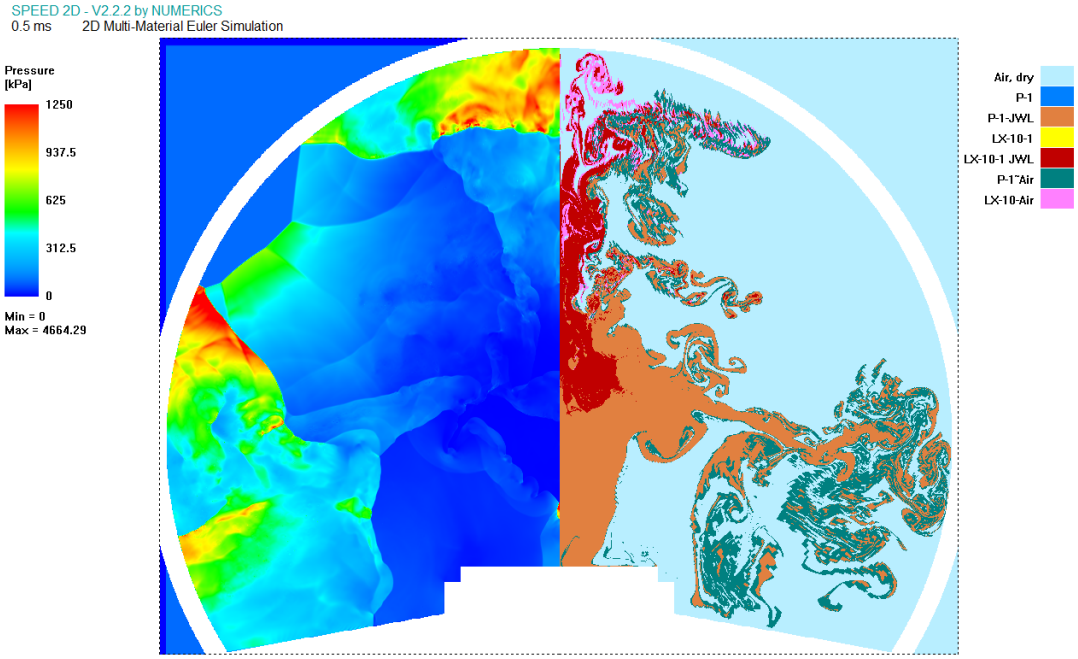
SPEED 2D - V2.2.2 by NUMERICS
0.5 ms 2D Multi-Material Euler Simulation
Pressure
[kPa]
1250
937.5
625
312.5
0
Min = 0
Max = 4664.29
Air, dry
P-1
P-1-JWL
LX-10-1
LX-10-1 JWL
P-1~Air
LX-10-Air

(c)

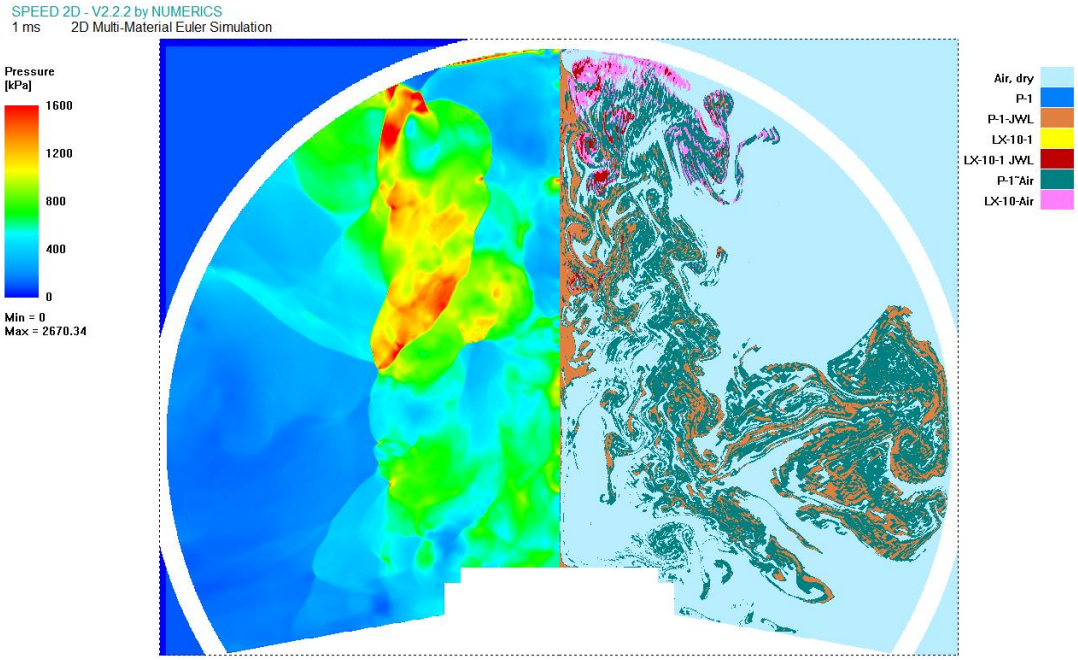
SPEED 2D - V2.2.2 by NUMERICS
1 ms 2D Multi-Material Euler Simulation
Pressure
[kPa]
1600
1200
800
400
0
Min = 0
Max = 2670.34
Air, dry
P-1
P-1-JWL
LX-10-1
LX-10-1 JWL
P-1~Air
LX-10-Air

(d)

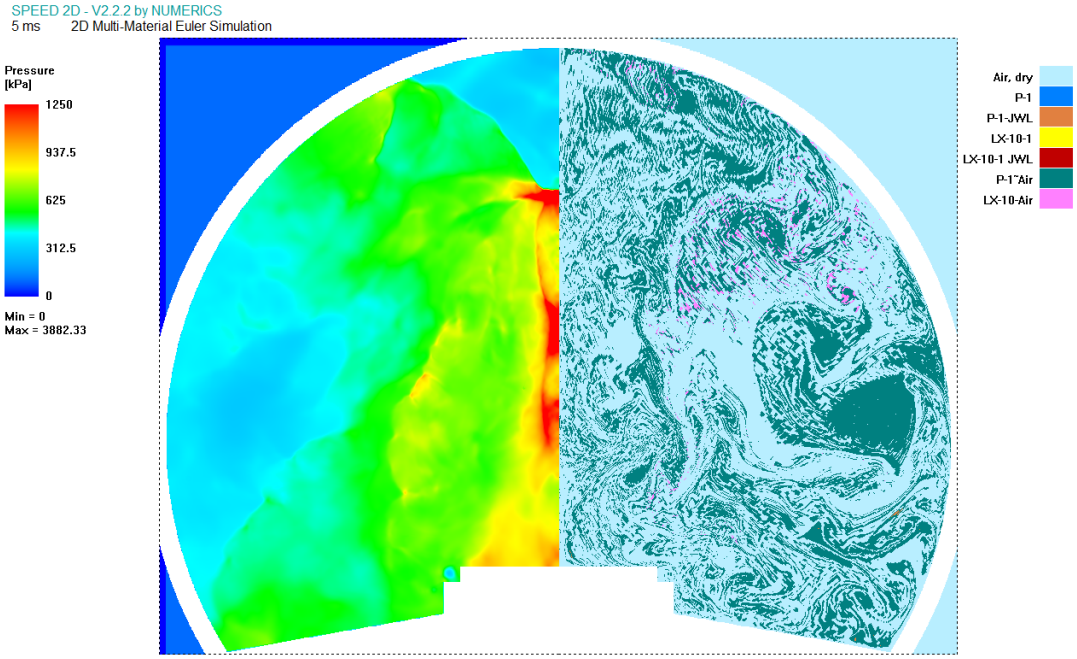
SPEED 2D - V2.2.2 by NUMERICS
5 ms 2D Multi-Material Euler Simulation
Pressure
[kPa]
1250
937.5
625
312.5
0
Min = 0
Max = 3882.33
Air, dry
P-1
P-1-JWL
LX-10-1
LX-10-1 JWL
P-1^Air
LX-10-Air

(e)

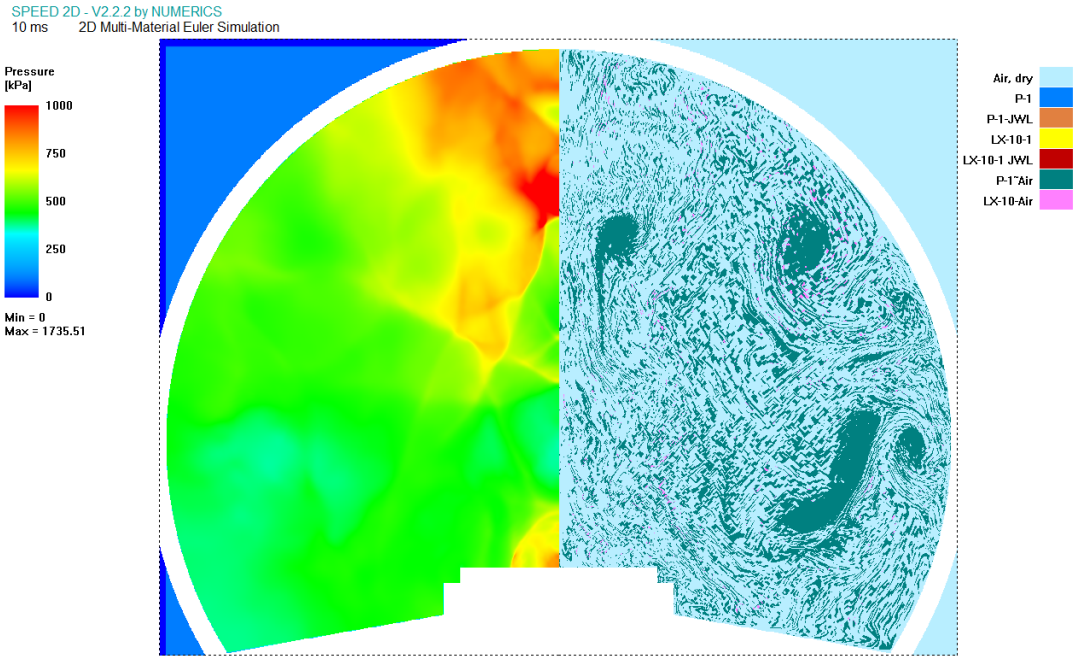
SPEED 2D - V2.2.2 by NUMERICS
10 ms 2D Multi-Material Euler Simulation
Pressure
[kPa]
1000
750
500
250
0
Min = 0
Max = 1735.51
Air, dry
P-1
P-1-JWL
LX-10-1
LX-10-1 JWL
P-1^Air
LX-10-Air

(f)

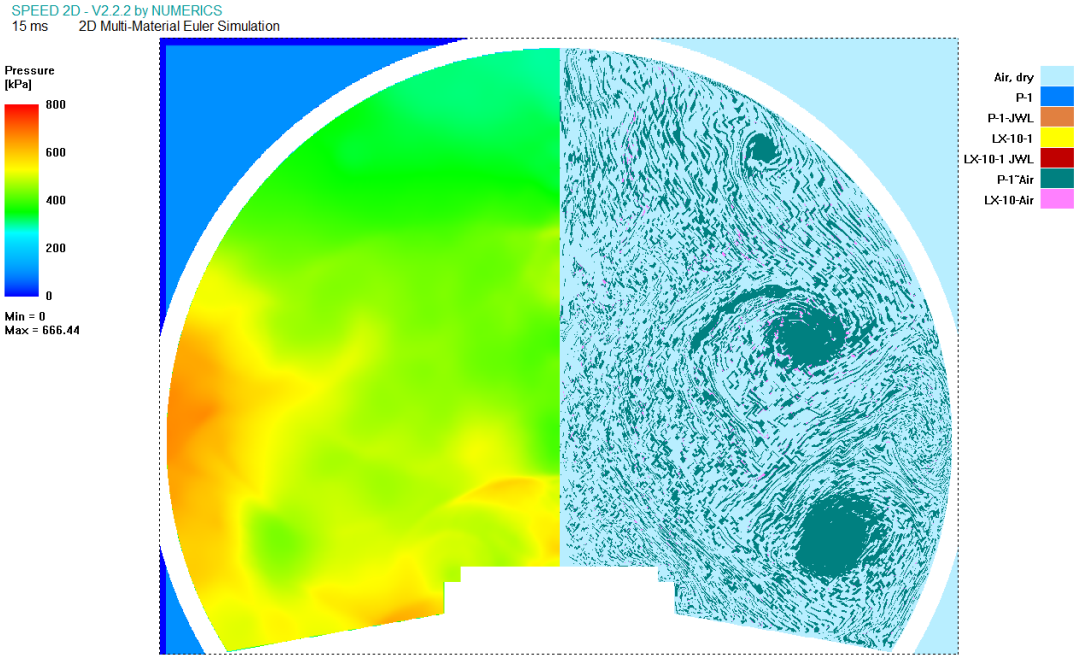
SPEED 2D - V2.2.2 by NUMERICS
15 ms 2D Multi-Material Euler Simulation
Pressure
[kPa]
800
600
400
200
0
Min = 0
Max = 666.44
Air, dry
P-1
P-1-JWL
LX-10-1
LX-10-1 JWL
P-1^Air
LX-10-Air

(g)

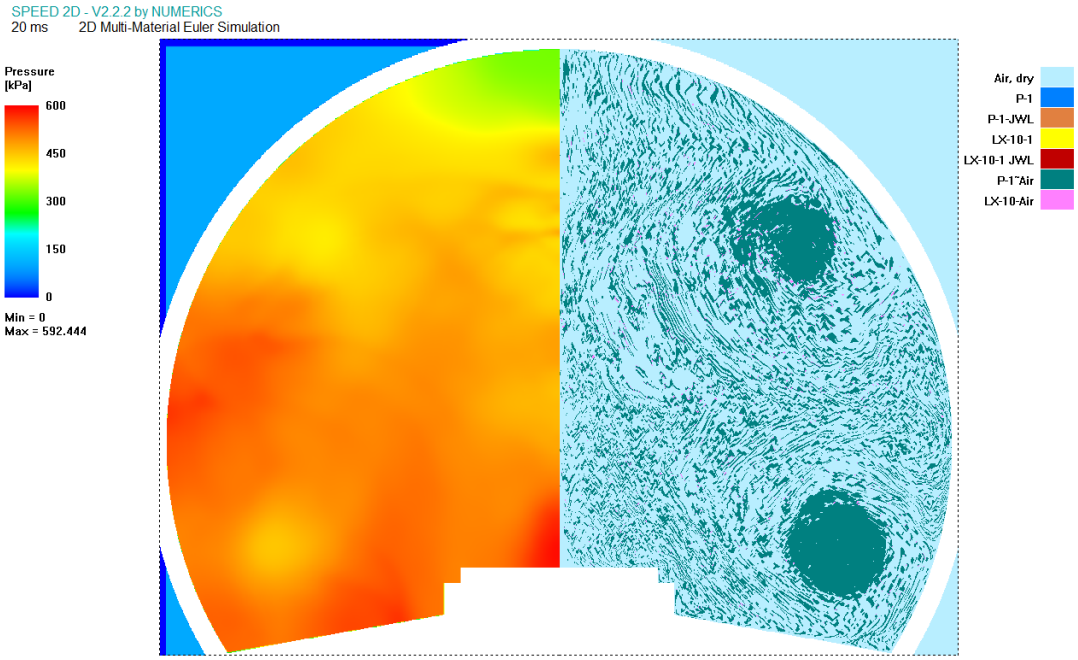
SPEED 2D - V2.2.2 by NUMERICS
20 ms 2D Multi-Material Euler Simulation
Pressure
[kPa]
600
450
300
150
0
Min = 0
Max = 592.444
Air, dry
P-1
P-1-JWL
LX-10-1
LX-10-1 JWL
P-1^Air
LX-10-Air

(h)

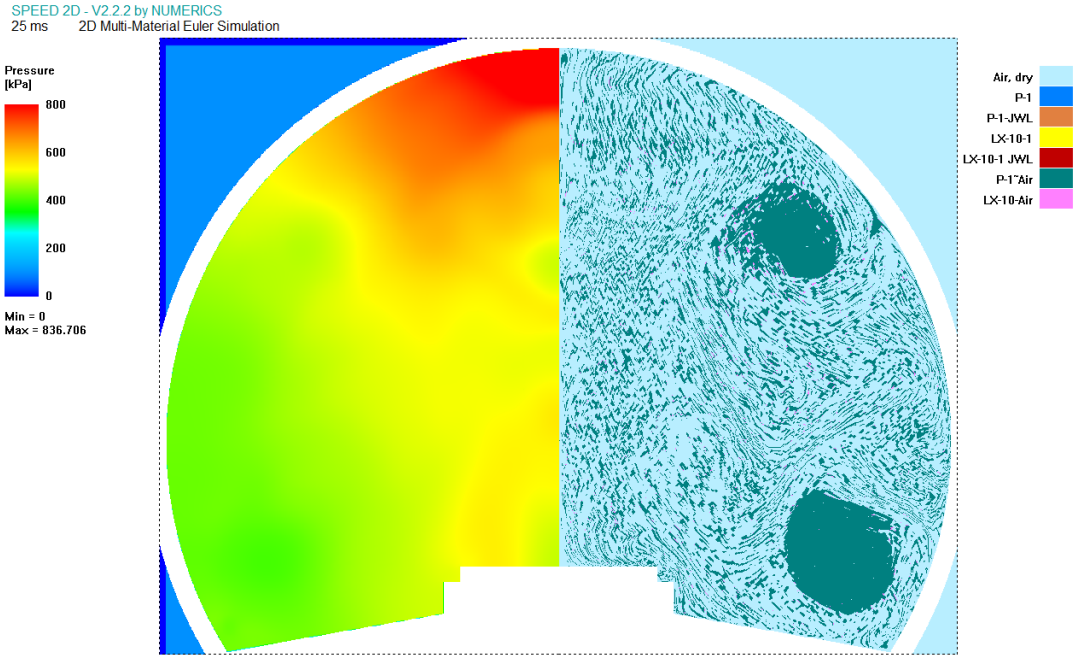
SPEED 2D - V2.2.2 by NUMERICS
25 ms 2D Multi-Material Euler Simulation
Pressure
[kPa]
800
600
400
200
0
Min = 0
Max = 836.706
Air, dry
P-1
P-1-JWL
LX-10-1
LX-10-1 JWL
P-1-Air
LX-10-Air

(i)

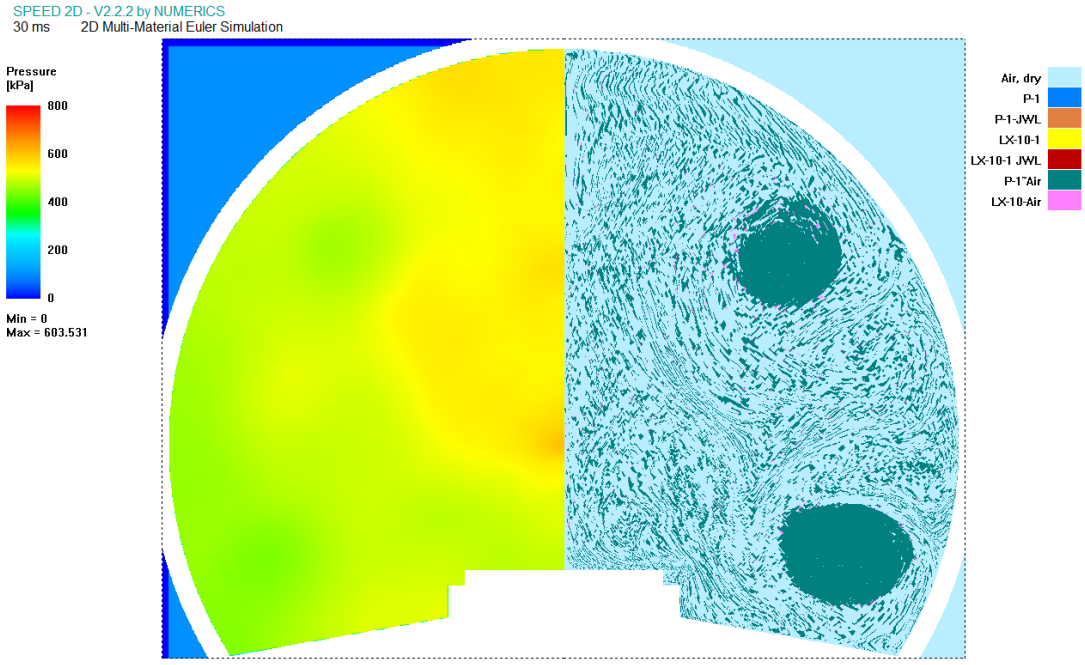

(j)

Figure 5-7 Pressure and Material Distribution after Detonation of Explosive P-1 at Different Times:

(a) 0.125 ms (b) 0.25 ms (c) 0.5 ms (d) 1 ms (e) 5 ms (f) 10 ms (g) 15 ms (h) 20 ms (i) 25 ms (j) 30 ms

In these figures, the left portion indicates the pressure variation, whereas the right one designates the material distribution inside the rigid chamber. The material legend lines up the materials that are used in simulations. P-1 and LX-10-1 indicates the main and the booster charge, respectively. Also, JWL detonation products and combustion products are involved both for the main and booster charge. Here, P1-JWL and LX-10-1-JWL indicate the detonation products, whereas P-1-AIR and LX-10-AIR represent the combustion products. These gaseous reaction products could be CO_2, H_2O, N_2, CO, H_2, C and CH_4. Speed considers these gaseous reaction products as a single reaction material.

In Figure 5-7 (a), pressure distribution after 0.125 ms from the detonation instance is presented. Here, the detonation products of the main and the booster charge

expand and they are in contact with the base of the chamber. In Figure 5-7 (b), pressure distribution after 0.25 ms from the detonation instance is given. This is the time that the pressure wave nearly interacts with gauge points which are located on the wall. The secondary shock wave created from the reflection from the base also expands through the side of the wall. As the shock wave re-reflects from the inner surfaces, the detonation products of the main and the booster charge are combusted and the combustion products starts to generate the quasi-static pressure inside the chamber. This phenomenon takes places approximately after 1 ms (d) when prior reflections are accomplished from all over the chamber. Thus, 100% percent combustion of detonation products occurs at 30 ms as presented in Figure 5-7 (j).

Speed hydrocode deals with the combustion model distinct from JWL equation of state. An additional term is applied and added to specific internal energy. It is an optional property that materials which are modeled by JWL EOS have. When combustion model is activated, the following equation is applied and directly added as a term to specific internal energy [26].

$$\frac{d\lambda}{dt} = a(1-\lambda)^m(\frac{p}{p_u})^n \tag{5.3}$$

In Equation (5.3), λ represents the burn fraction of the products, p is pressure and p_u reference pressure. Also, a, m and n are the energy release constant, exponent and pressure exponent, respectively [26]. These constants are JWL detonation products parameters that are calculated by the code.

All the simulations presented here are conducted using the finest mesh having 1518750 numbers of total elements. The time of arrivals which is the time from the onset of the detonation till the arrival of the shock wave to the gauge location differ for each explosive due to the difference between velocity of detonation values and geometrical design. The time of arrival values are tabulated in Table 5-7 for each explosive.

Table 5-7 Time of Arrivals Obtained from Numerical Simulations

Explosive Type	**Time of Arrivals (ms)**
P-1	0.259
P-2	0.292
P-3	0.267
P-4	0.288

Similarly, the peak over-pressure and positive impulse values obtained from each explosive are shown in Table 5-8 and the pressure with the corresponding positive impulse curves are given in Figure 5-8 and Figure 5-9 for 0-32 ms and for 0-4 ms time periods, respectively.

Table 5-8 Peak Over-Pressure and Positive Impulse Values Obtained from Numerical Simulations

Explosive Type	**Peak Over-Pressure (kPa)**	**Positive Impulse (kPa.ms)**
P-1	10377.9	15303.6
P-2	5086.9	20984.1
P-3	8124.7	19620.4
P-4	6270.7	21693.6

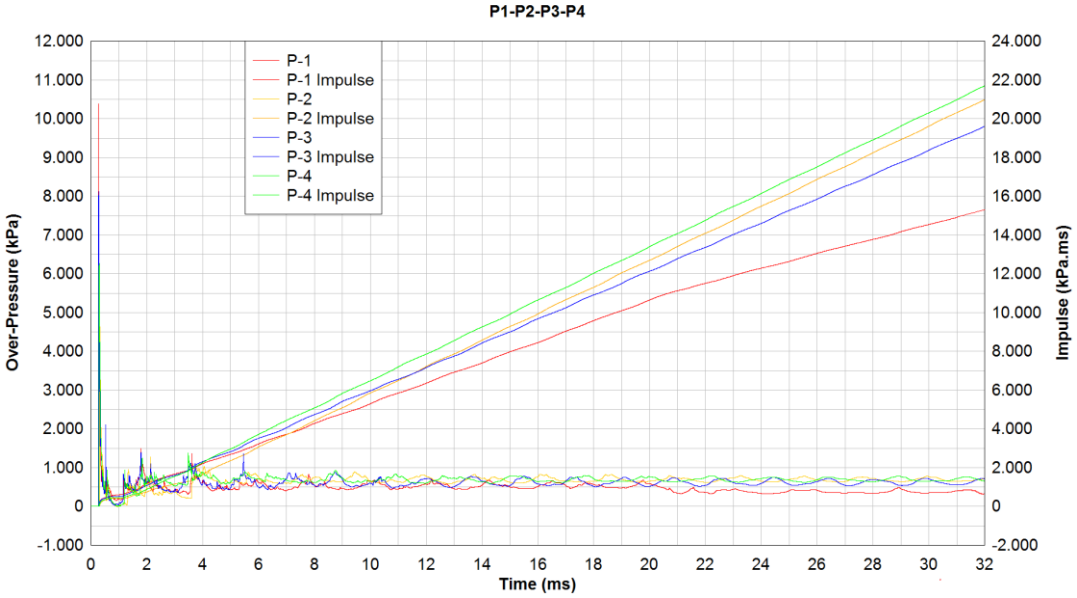

Figure 5-8 Pressure and Impulse Curves Obtained from Numerical Simulations (0-32 ms)

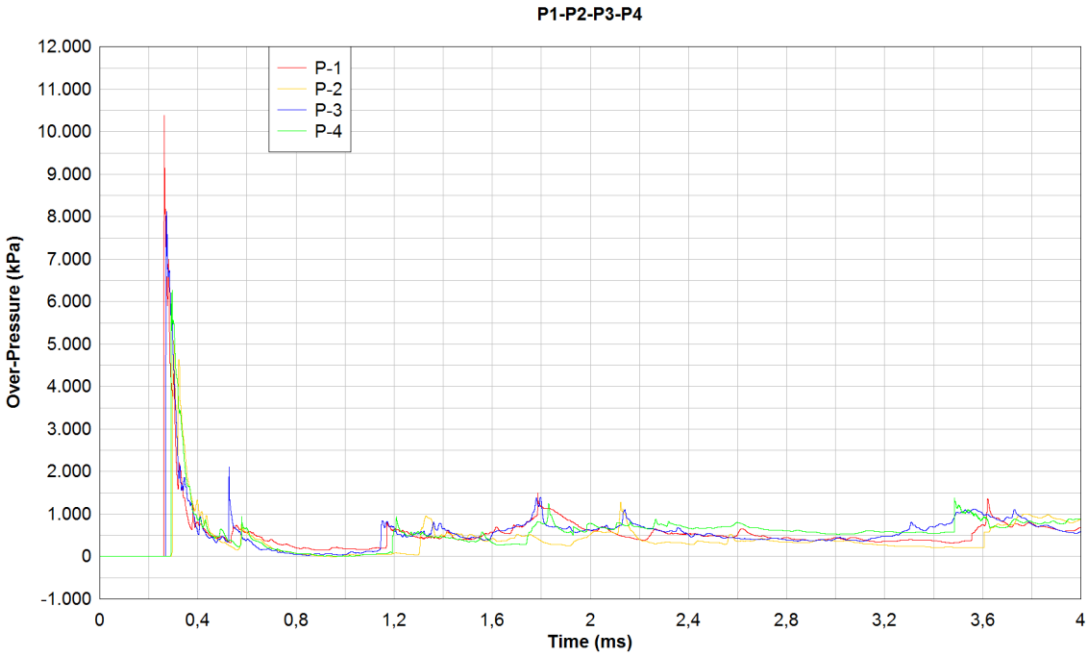

Figure 5-9 Pressure Curves Obtained from Numerical Simulations (0-4 ms)

According to Figure 5-8, the positive impulses do not converge to a specific value in numerical simulations since walls are modeled as rigid in Speed. Rigid modeling of the wall of the detonation chamber will not affect the peak over-pressure values since only the base interacts with the shock wave which is expanding throughout the detonation point. However, rigid modeling method makes a difference in calculation of impulse with respect to the experimental study. That is to say, wall of chamber absorbs certain amount of the energy of the shock wave during the reflections from the chamber wall in experiments. Therefore, the positive impulse phase will never converge to specific value in numerical simulations when walls are modeled as rigid. So, in numerical simulations the impulse calculations are made until 32 milliseconds, which is the time when all pressure curves converge to gauge pressure in experiments.

5.2 Experimental Results

As stated in Chapter 3, experimental case studies are conducted in a laboratory detonation chamber using four different types of explosives. For each explosive, two tests with two sensors are conducted. In these eight tests, pressure-time data are gathered successfully. The mass of explosives utilized in each test is presented in Table 5-9. In Table 5-10, calculated impulse from experimental and Speed simulation results are presented. In order to capture the time of arrivals of shock front, fiber-optic cable is used to sense the time of detonation of the detonator. Each face-on sensors are located approximately 590 mm from the detonation point. The time of arrivals of each explosive is tabulated in Table 5-11. Each data pair is gathered from single shot test. The pressure and corresponding positive impulse curves obtained from experiments and numerical simulations are given for each explosive in Figure 5-10, Figure 5-11 and Figure 5-12.

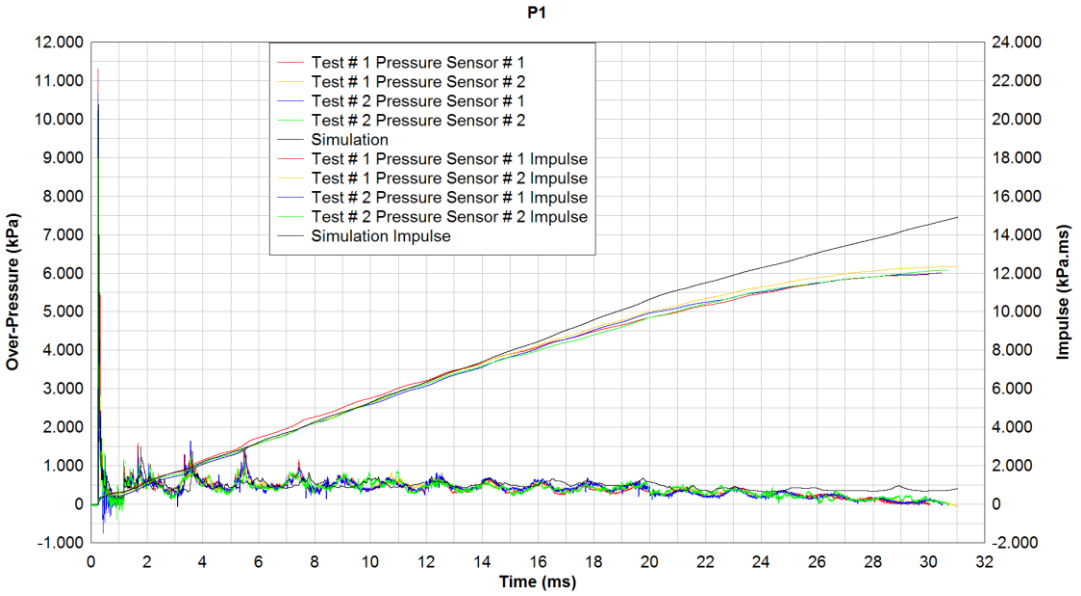
P1
Test # 1 Pressure Sensor # 1
Test # 1 Pressure Sensor # 2
Test # 2 Pressure Sensor # 1
Test # 2 Pressure Sensor # 2
Simulation
Test # 1 Pressure Sensor # 1 Impulse
Test # 1 Pressure Sensor # 2 Impulse
Test # 2 Pressure Sensor # 1 Impulse
Test # 2 Pressure Sensor # 2 Impulse
Simulation Impulse
Over-Pressure (kPa)
Impulse (kPa.ms)
Time (ms)

(a)

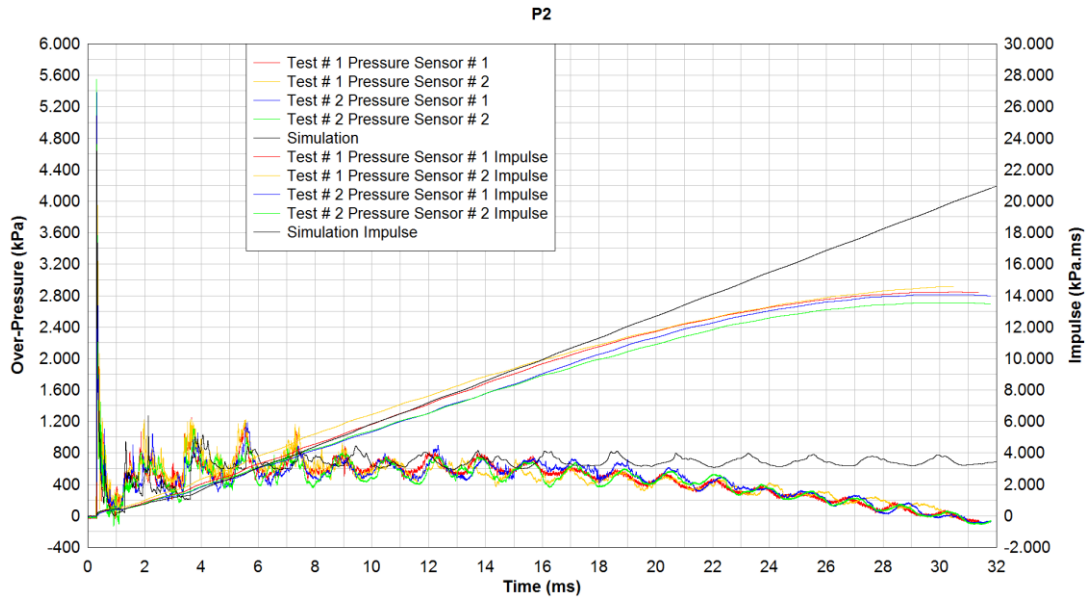
P2
Test # 1 Pressure Sensor # 1
Test # 1 Pressure Sensor # 2
Test # 2 Pressure Sensor # 1
Test # 2 Pressure Sensor # 2
Simulation
Test # 1 Pressure Sensor # 1 Impulse
Test # 1 Pressure Sensor # 2 Impulse
Test # 2 Pressure Sensor # 1 Impulse
Test # 2 Pressure Sensor # 2 Impulse
Simulation Impulse
Over-Pressure (kPa)
Impulse (kPa.ms)
Time (ms)

(b)

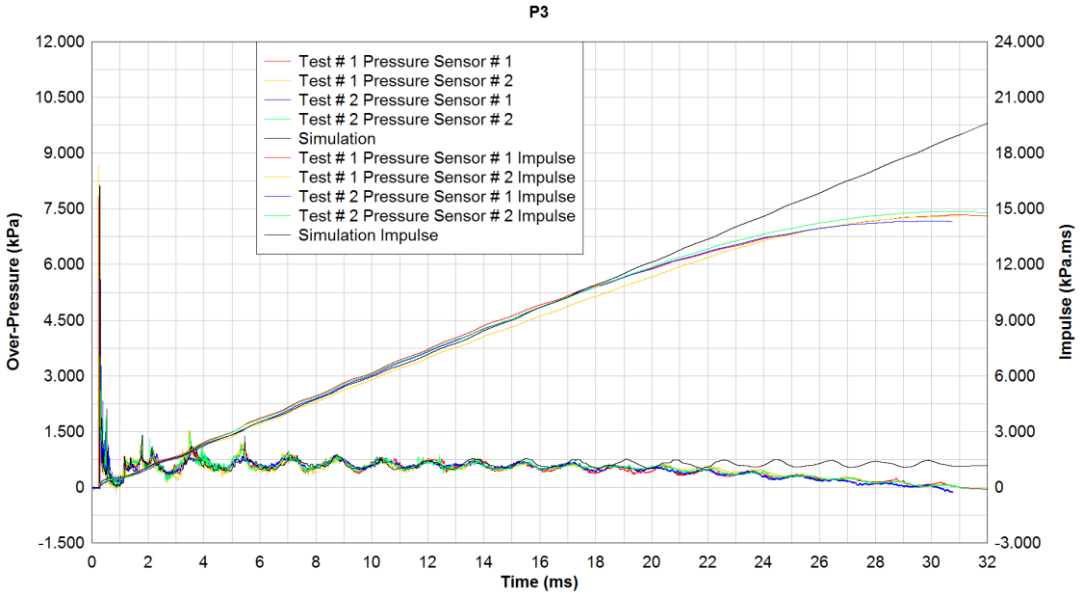

(c)

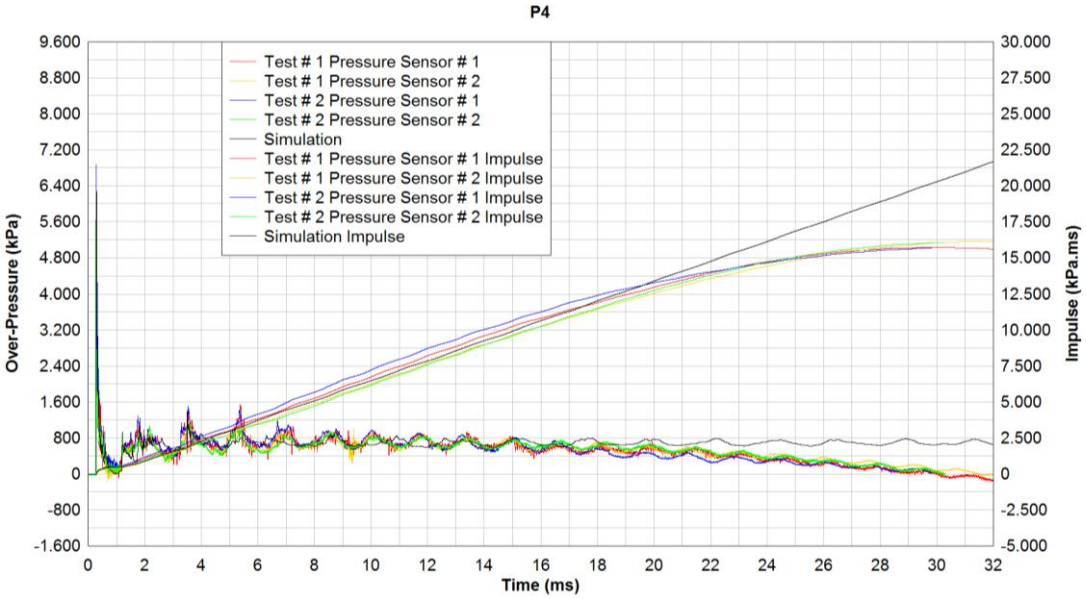

(d)

Figure 5-10 Pressure and Impulse Curves for 0-32 ms

(a) P-1 (b) P-2 (c) P-3 (d) P-4

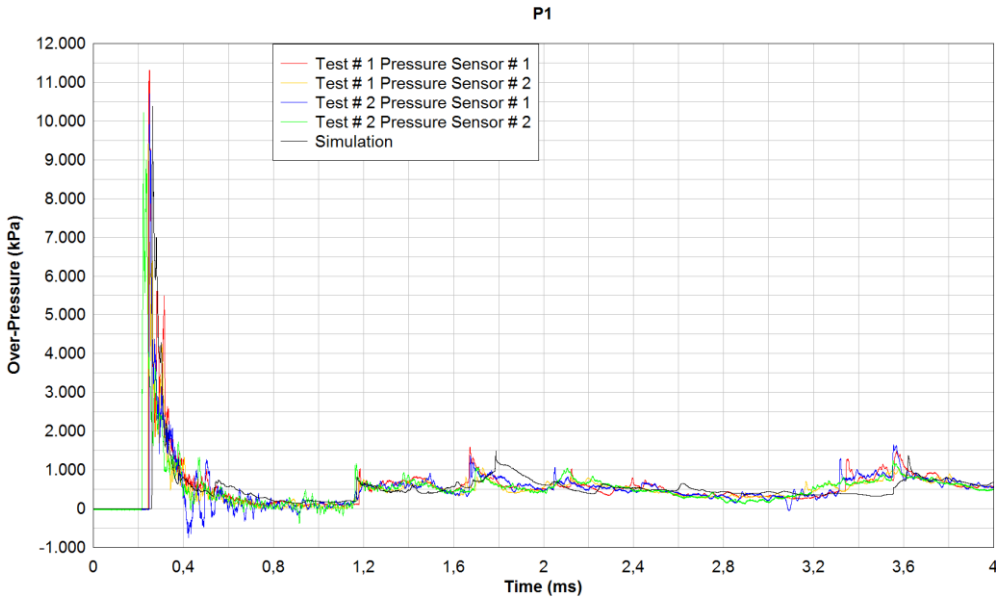
P1
Test # 1 Pressure Sensor # 1
Test # 1 Pressure Sensor # 2
Test # 2 Pressure Sensor # 1
Test # 2 Pressure Sensor # 2
Simulation
Over-Pressure (kPa)
12.000
11.000
10.000
9.000
8.000
7.000
6.000
5.000
4.000
3.000
2.000
1.000
0
-1.000
0
0,4
0,8
1,2
1,6
2
2,4
2,8
3,2
3,6
4
Time (ms)

(a)

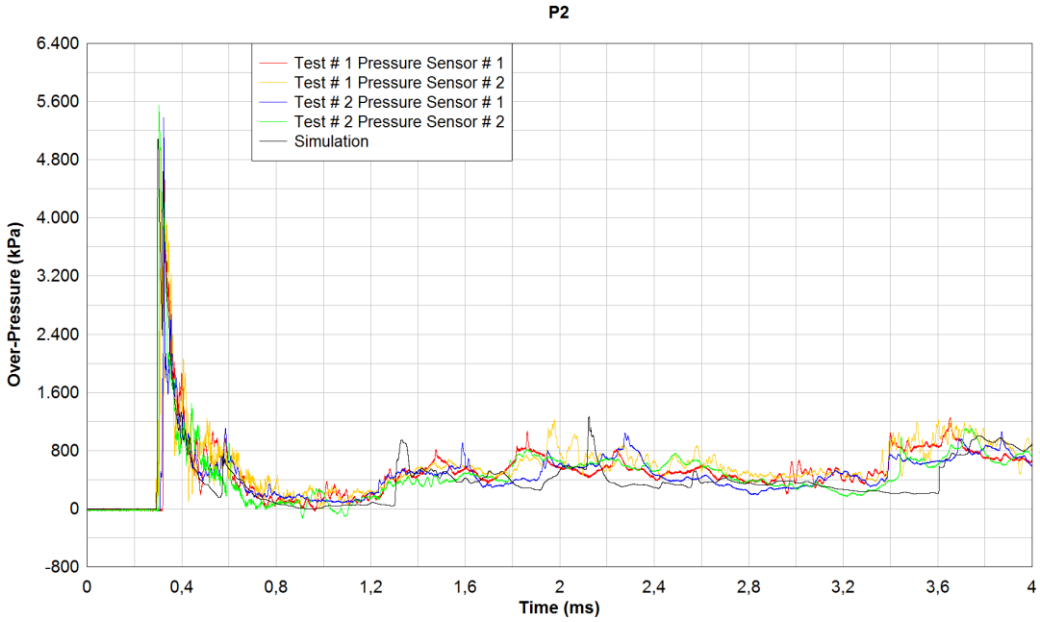
P2
Test # 1 Pressure Sensor # 1
Test # 1 Pressure Sensor # 2
Test # 2 Pressure Sensor # 1
Test # 2 Pressure Sensor # 2
Simulation
Over-Pressure (kPa)
6.400
5.600
4.800
4.000
3.200
2.400
1.600
800
0
-800
0
0,4
0,8
1,2
1,6
2
2,4
2,8
3,2
3,6
4
Time (ms)

(b)

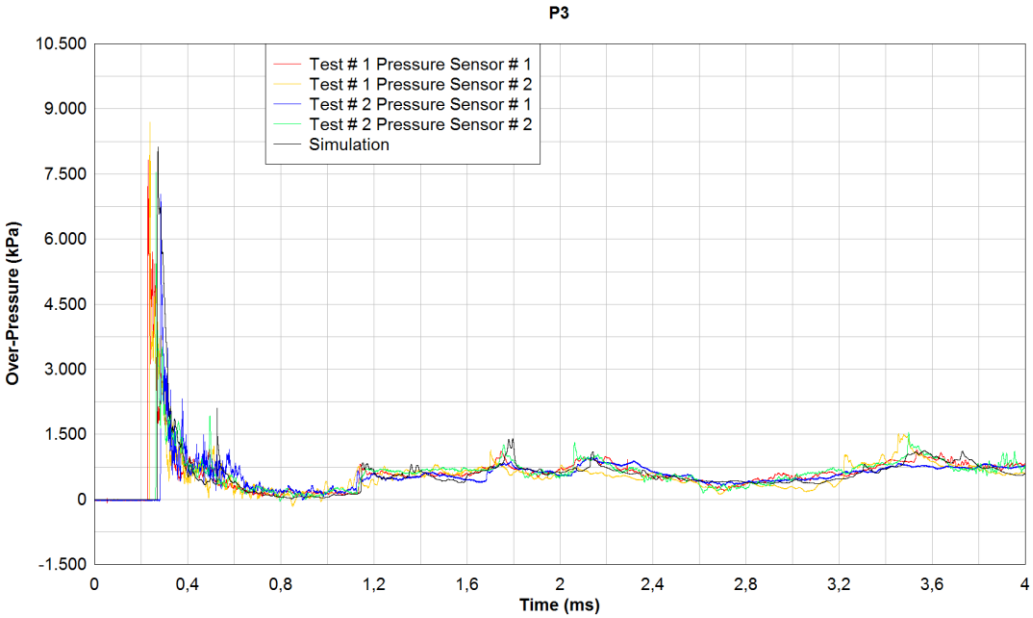

(c)

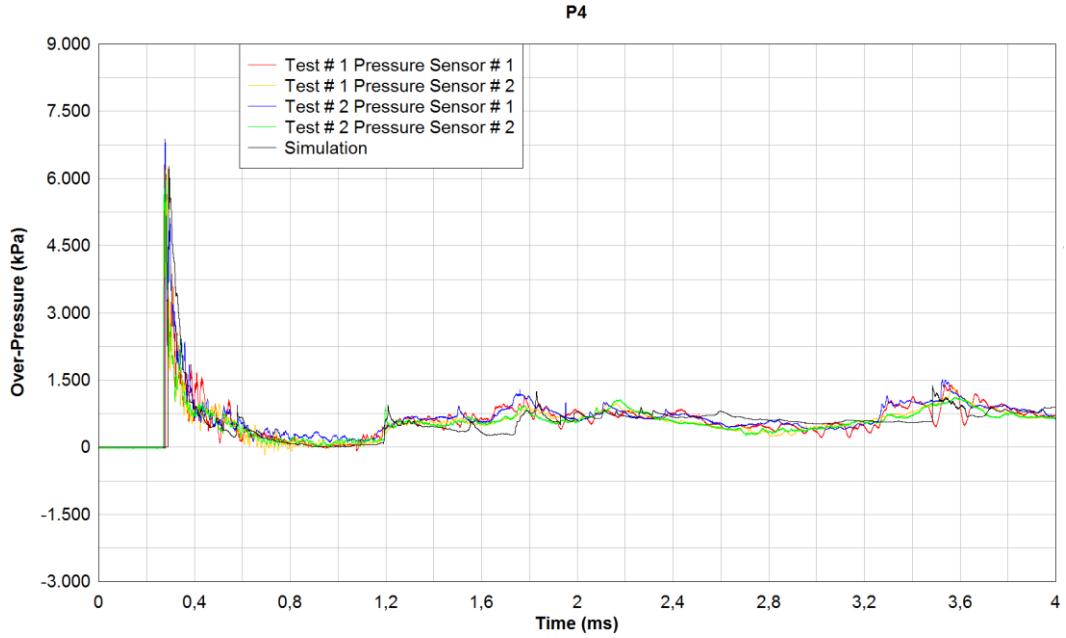

(d)

Figure 5-11 Pressure Curves for 0-4 ms

(a) P-1 (b) P-2 (c) P-3 (d) P-4

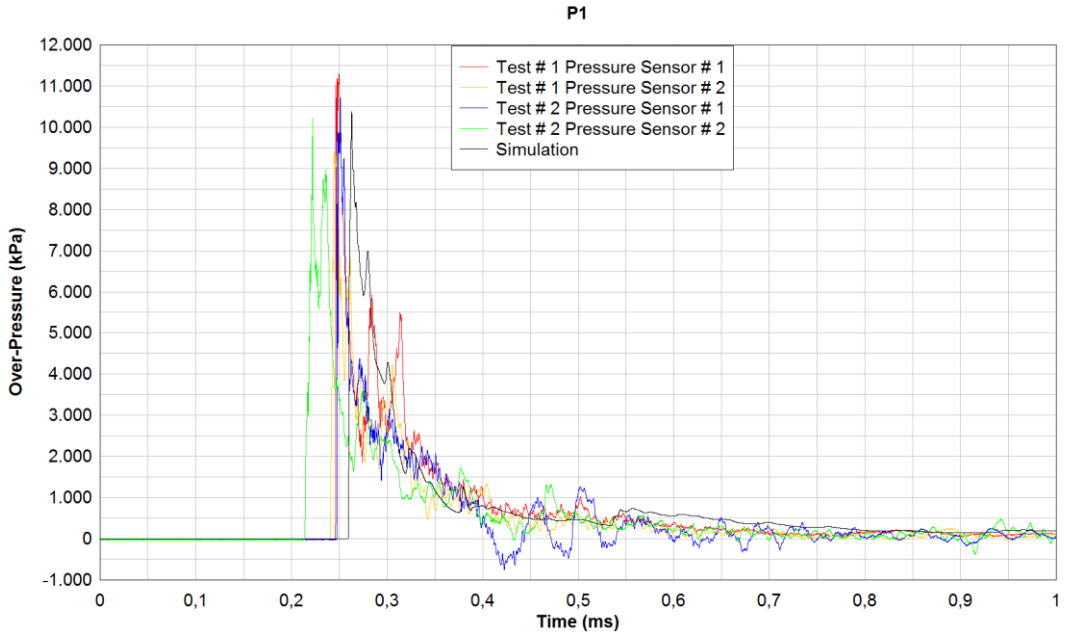
P1
Test # 1 Pressure Sensor # 1
Test # 1 Pressure Sensor # 2
Test # 2 Pressure Sensor # 1
Test # 2 Pressure Sensor # 2
Simulation
Over-Pressure (kPa)
12.000
11.000
10.000
9.000
8.000
7.000
6.000
5.000
4.000
3.000
2.000
1.000
0
-1.000
0
0,1
0,2
0,3
0,4
0,5
0,6
0,7
0,8
0,9
1
Time (ms)

(a)

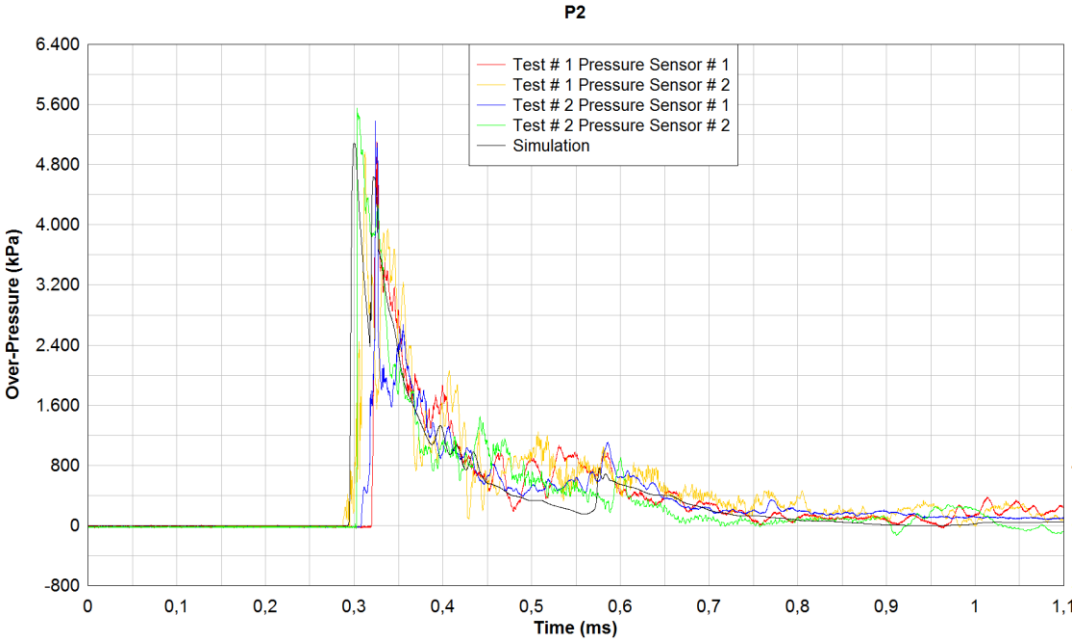
P2
Test # 1 Pressure Sensor # 1
Test # 1 Pressure Sensor # 2
Test # 2 Pressure Sensor # 1
Test # 2 Pressure Sensor # 2
Simulation
Over-Pressure (kPa)
6.400
5.600
4.800
4.000
3.200
2.400
1.600
800
0
-800
0
0,1
0,2
0,3
0,4
0,5
0,6
0,7
0,8
0,9
1
1,1
Time (ms)

(b)

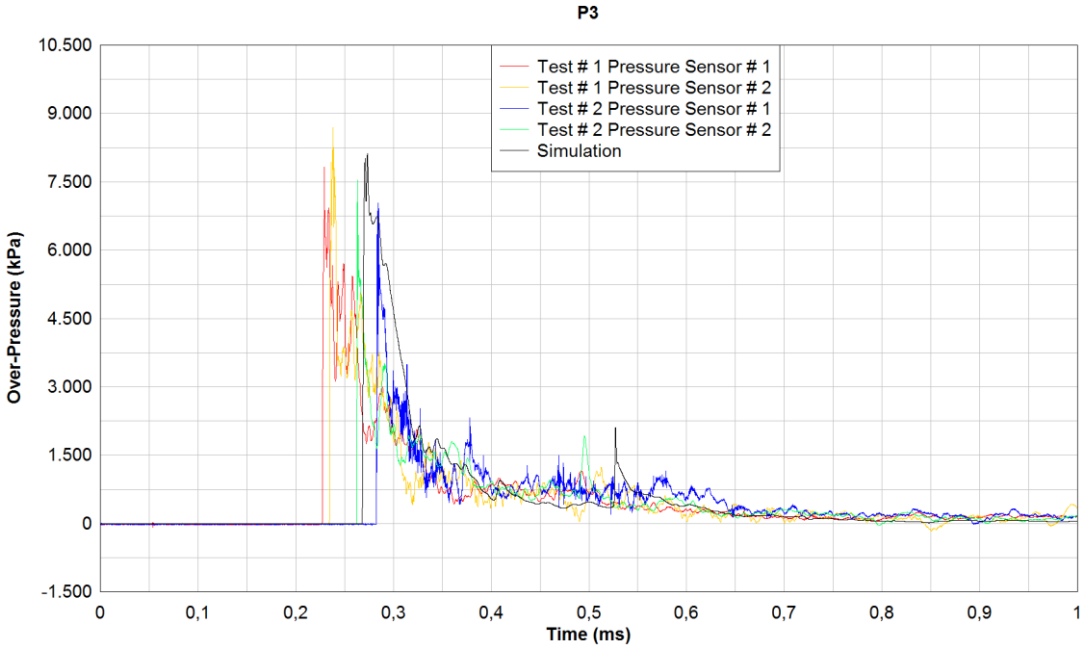

(c)

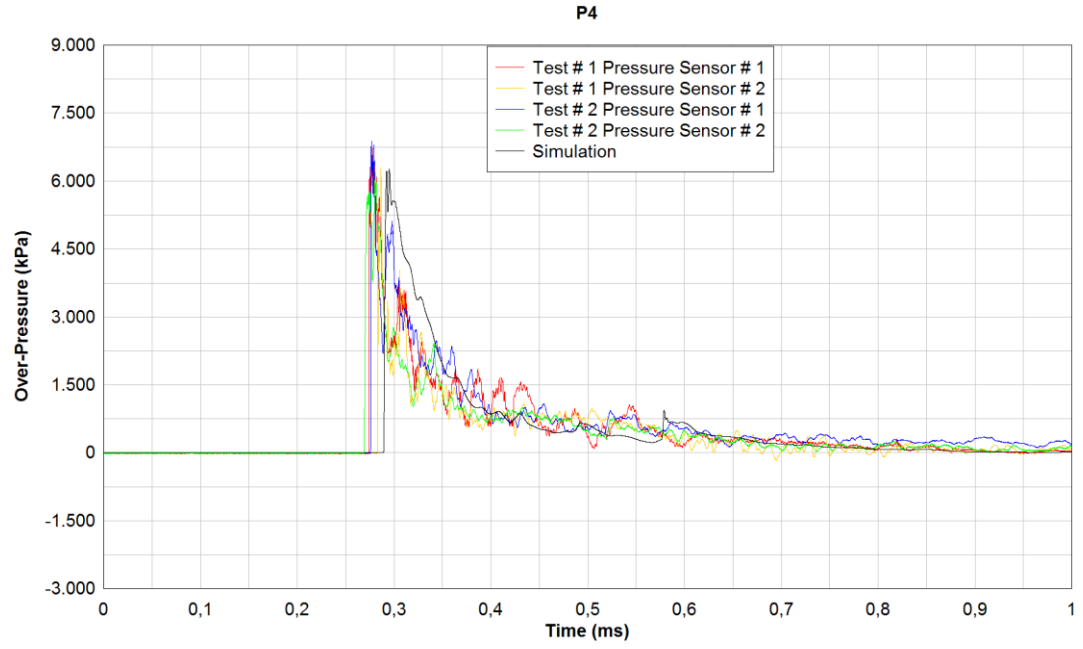

(d)

Figure 5-12 Pressure Curves for 0-1 ms

(a) P-1 (b) P-2 (c) P-3 (d) P-4

Table 5-9 Mass of Explosive Utilized in Each Test

Explosive Type	**Mass of Explosive (g)**	
	Test # 1	**Test # 2**
P-1	140.6	139.7
P-2	138.3	140.4
P-3	141.4	139.6
P-4	138.1	142.8

Table 5-10 Peak Over-Pressure and Positive Impulse Values Obtained from Experiments and Simulations

Explosive Type	**Peak Over-Pressure (kPa)**				
	Test # 1 Pressure Sensor # 1	**Test # 1 Pressure Sensor # 2**	**Test # 2 Pressure Sensor # 1**	**Test # 2 Pressure Sensor # 2**	**Simulation**
P-1	11335.6	9427.8	10700.6	10223.5	10377.9
P-2	5105.5	4964.9	5382.0	5546.8	5086.9
P-3	8690.1	7826.2	7542.8	7040.9	8124.7
P-4	6726.5	6276.9	6878.8	6191.4	6270.7
Explosive Type	**Impulse (kPa.ms)**				
	Test # 1 Pressure Sensor # 1	**Test # 1 Pressure Sensor # 2**	**Test # 2 Pressure Sensor # 1**	**Test # 2 Pressure Sensor # 2**	**Simulation**
P-1	11932.7	12351.2	12014.1	12163.7	15303.6
P-2	14225.2	14567.2	14065.9	13564.0	20984.1
P-3	14614.8	14667.9	14868.5	14341.7	19620.4
P-4	15742.8	16146.1	15690.4	16066.1	21693.6

Table 5-11 Time of Arrivals Obtained from Experiments and Simulations

Data No	Explosive Type / Time of Arrival (ms)							
	P-1		P-2		P-3		P-4	
	Exp.	Sim.	Exp.	Sim.	Exp.	Sim.	Exp.	Sim.
1	0.213	0.259	0.286	0.292	0.227	0.267	0.269	0.288
2	0.241		0.301		0.233		0.274	
3	0.245		0.307		0.261		0.276	
4	0.247		0.319		0.282		0.282	

Peak over-pressure values obtained from each test campaign show that there is a margin between the lowest and the highest values. The most important factor that alters the collected over-pressure of explosive charges is the manufacturing techniques. The non-uniform casting of charges results in variations in density which directly affects the detonation pressure and velocity of detonation. Also, sensitivity differences mentioned in previous sections according to mass and distance are the secondary effects that contribute to the peak over-pressure measurements. Due to the nature of internal fully-confined detonation, the generated pressure becomes complex since as the shock wave reflects from the wall of the chamber, it strengthens and re-reflects from the inside of the wall of the body continuously. Many subsequent reflections occur throughout 32 ms interval since the air blast is bounded by fully-confined structure. Pressure histograms of the detonation in detonation chamber show that many superposed reflections of the shock wave occur at least 15 times for 32 ms interval. After 32 ms, pressure dissipates and shock phase converges to gauge pressure. In case of vented structures, relief of the internal pressure increases gradually compared to unvented structures.

For the all simulations, numerical results normalize experimental values for each explosive charge. That is to say, numerical peak-over pressure values are in the limits of maximum and minimum of the test data. Additionally, since bare charges which are not confined within any warhead casing are analyzed, absorption of energy due to any casing material shall not occur. Outer casing that covers the explosive charge circumferentially would affect the shock propagation velocity and hence, there would be an increase in the time of arrivals of the shock wave since confinement slows down the rate of expansion of the decomposition products. The time of arrivals gathered from fiber-optical cables depends on the detonation pressure, velocity of detonation and the geometrical constraints of the explosives. P-3 and P-4 give relatively close results since their velocity of detonation values are nearly the same. The average time of arrivals obtained from experimental results for each explosive is tabulated in Table 5-12 with relative difference with respect to numerical results. The maximum difference between experimental and numerical simulation results is within 10%.

Table 5-12 Comparison of the Performances of Explosives P-2, P-3, and P-4 with respect to P-1 – Time of Arrival

Explosive Type	**Time of Arrivals (ms)**		**Relative Difference with Numerical Results**
	Experimental Average	**Numerical Results**	
P-1	0.23650	0.259	9.51%
P-2	0.30325	0.292	3.70%
P-3	0.25075	0.267	6.48%
P-4	0.27525	0.288	4.63%

The average peak over-pressures obtained from experimental results for each explosive are tabulated in Table 5-13 with relative difference with respect to numerical results. Numerical studies result in maximum of 4.3% relative error when compared to experimental average. This indicates that an excellent agreement with respect to experimental average can be observed with the assumptions stated and the numerical method applied.

Table 5-13 Comparison between Experimental and Numerical Results – Peak Over-Pressure

Explosive Type	**Peak Over-Pressure (kPa)**		**Relative Difference with Numerical Results**
	Experimental Average	**Numerical Results**	
P-1	10421.8	10377.9	0.42%
P-2	5249.8	5086.9	3.20%
P-3	7775.0	8124.7	4.30%
P-4	6518.4	6270.7	3.95%

Explosive P-1, namely TNT, has higher peak over-pressure than the others according to both simulation and experiment results. However, the impulse is relatively lower compared to the rest of the explosives, as expected. The impulse values of P-2, P-3 and P-4 make big differences with respect to P-1 since the compositions are designed and optimized in order to have massive impulsive damage in closed spaces. The relative difference of average positive impulse and average peak over-pressure obtained from experiments between P-2, P-3 and P-4 with respect to P-1 is tabulated in Table 5-14. P-4 has relatively high impulse compared to P-2 and P-3; in addition, P-4 is superior in terms of peak over-pressure

with respect to P-2. The relative difference between the P-4 and P-1 in average positive impulse is 31% according to experimental results. Impulsive loading can be enhanced applying metallic fuel additive into explosive formulation. Also, ingredients and their manufacturing techniques result in alterations in pressure, velocity of detonation and energy. It can be deducted from the peak over-pressure results that as the mass percentage of the metallic fuel additive increases in the composition, generated peak over-pressure decreases proportionally. The relative difference between the P-1 and P-4 in experimental average peak over-pressure is 37%. Such comparison should be evaluated when hard target defeat is main concern for warhead applications.

Table 5-14 Comparison of the Performances of Explosives P-2, P-3, and P-4 with respect to P-1 – Peak Over-Pressure and Positive Impulse

Explosive Type	**Peak Over-Pressure (kPa)**	**Positive Impulse (kPa.ms)**	**% Difference of Peak Over-Pressure Relative to P-1**	**% Difference of Positive Impulse Relative to P-1**
P-1	10421.8	12115.4	-	-
P-2	5249.8	14105.5	-49%	16%
P-3	7775.0	14623.2	-25%	20%
P-4	6518.4	15911.3	-37%	31%

5.3 Filtering of Raw Experimental Data

As stated in Chapter 3, in explicit applications where warhead systems are utilized, high frequency is needed to capture the pressure of the shock waves that move at high velocities. Additionally, the experimental equipments such as data acquisition systems, cables and sensors can result in noise in the history of data due to the disturbances. For the applications that include noise, low pass filtering method is applied to smooth the collected raw data. One of the methods of low-pass filtering that is widely used in explicit scenarios such as detonation is Butterworth filtering [34]. [35], [36] have studied the Butterworth filtering in their detonation problems. It is a signal processing type which is developed for flat frequency response in pass band. Butterworth filtering is also called maximally flat magnitude filter [34]. The amplification of a Butterworth low-pass of the order n is [4]:

$$|A|^2 = \frac{1}{1 + \Omega^{2n}} \tag{5.4}$$

The denominator polynoms for Butterworth low passes up to 6^{th} order is listed in Table 5-15. As the order increases, the amplitude and duration of the ringing of the filtered data increases. Therefore, by increasing the filter order, elimination of noise frequency is even more possible [4].

Table 5-15 Denominator Polynoms of Butterwort Filtering [26]

n	
1	$1 + P$
2	$1 + 2^{1/2}P + P^2$
3	$(1 + P)(1 + P + P^2)$
4	$(1 + 1.848P + P^2)(1 + 0.765P + P^2)$
5	$(1 + P)(1 + 1.618P + P^2)(1 + 0.618P + P^2)$
6	$(1 + 1.932P + P^2)(1 + 1.414P + P^2)(1 + 0.517P + P^2)$

The corresponding transfer function of a 6th order Butterworth low-pass is [37]:

$$H(s) = \frac{1}{(1 + 1.932s + s^2)\,(1 + 1.414s + s^2)(1 + 0.517s + s^2)} \tag{5.5}$$

The main idea of low-pass filtering is described as "The nature of the original signal (the result as a function of time) limits the range of meaningful cut frequencies to use for filtering. If the cut frequency is too low, all signal features will be lost and a constant value may remain. On the other hand, if the cut frequency is too high, the signal may remain unaltered" [24]. The determination of cut frequency depends on the frequency rate. The sampling frequency limits the cut frequency which is the input of low-pass filtering. That is, the cut frequency should not be higher than quarter of sampling frequency to eliminate such noise [24]. Therefore, the ideal cut frequency should be derived from the sampling rate of the data acquisition system.
Throughout all experiments, the sampling rate of the data acquisition system is set to be 10 MHz. Hence, the maximum of resultant cut frequency can be calculated as 2.5 MHz. Since the raw pressure data consists of high amplitude of nearly discontinues peak over-pressure values, the experimental data are low-pass filtered by Butterworth digital filtering with filtering frequency of 180 Hz which is recommended in most researches for explicit applications [35]. Filtering process of raw experimental data is conducted for the explosive P-4 which has the highest velocity of detonation. This technique is utilized by 6th order Butterworth low-pass filtering. The filtered data for four different experimental sets with the raw data are given in Figure 5-13, Figure 5-14 and Figure 5-15 0-32 ms, 0-4 ms and 0-1 ms time periods, respectively. The peak over-pressure and positive impulse results of raw and filtered data are tabulated in Table 5-16 with relative differences.

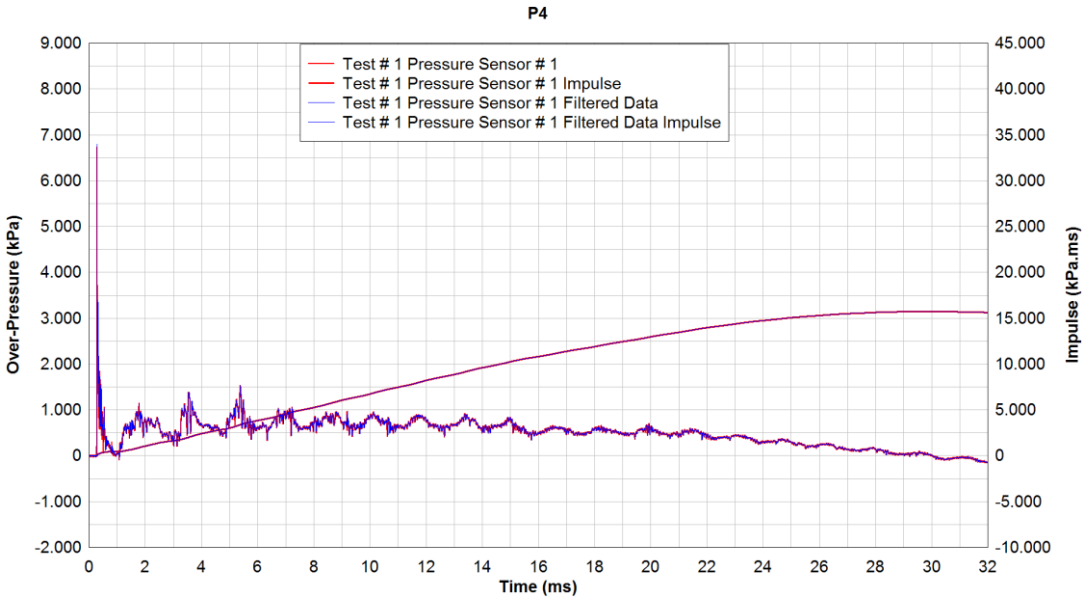
P4
Test # 1 Pressure Sensor # 1
Test # 1 Pressure Sensor # 1 Impulse
Test # 1 Pressure Sensor # 1 Filtered Data
Test # 1 Pressure Sensor # 1 Filtered Data Impulse
Over-Pressure (kPa)
Impulse (kPa.ms)
Time (ms)

(a)

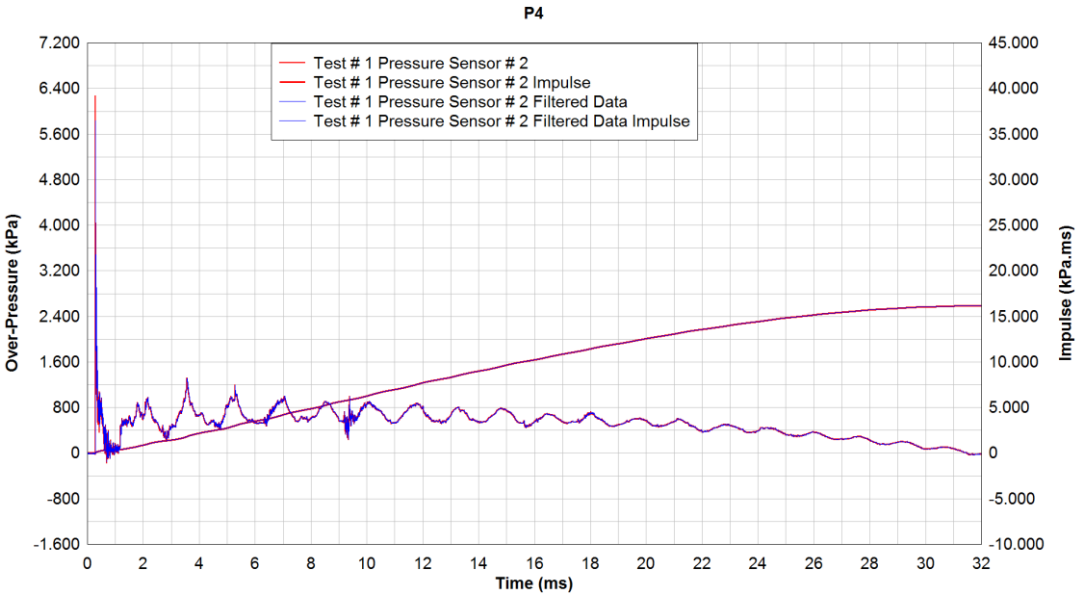
P4
Test # 1 Pressure Sensor # 2
Test # 1 Pressure Sensor # 2 Impulse
Test # 1 Pressure Sensor # 2 Filtered Data
Test # 1 Pressure Sensor # 2 Filtered Data Impulse
Over-Pressure (kPa)
Impulse (kPa.ms)
Time (ms)

(b)

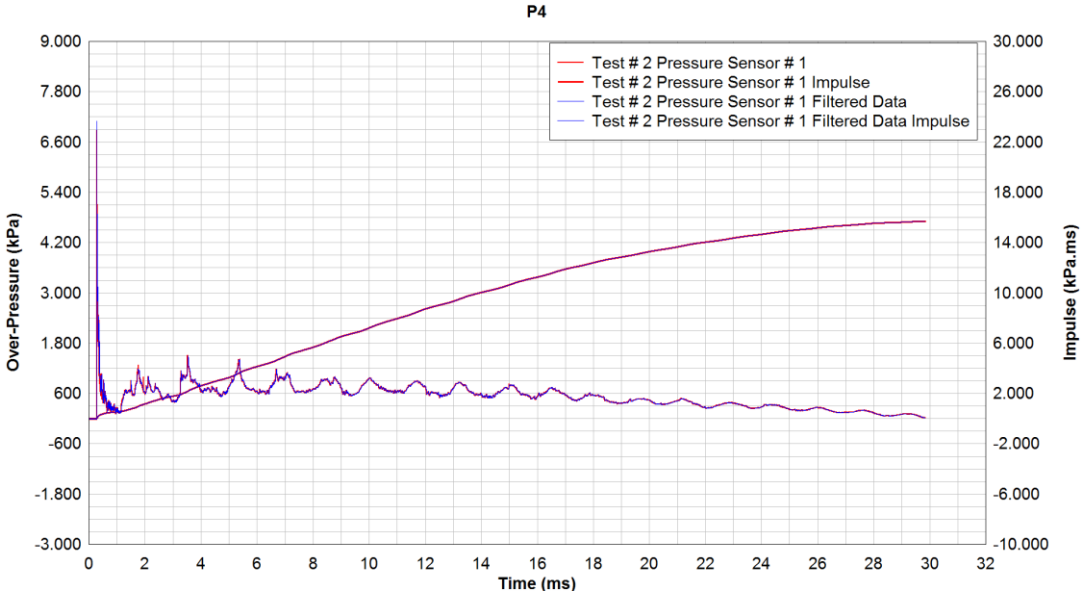

(c)

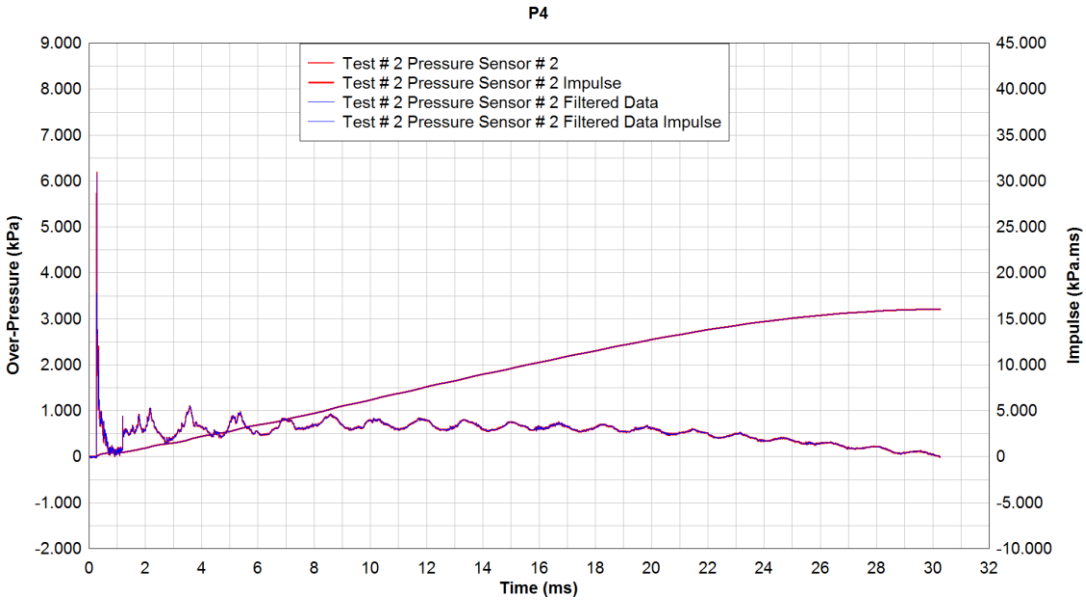

(d)

Figure 5-13 Raw and Filtered Data for P-4 (0-32 ms)

(a) Data #1 (b) Data #2 (c) Data #3 (d) Data #4

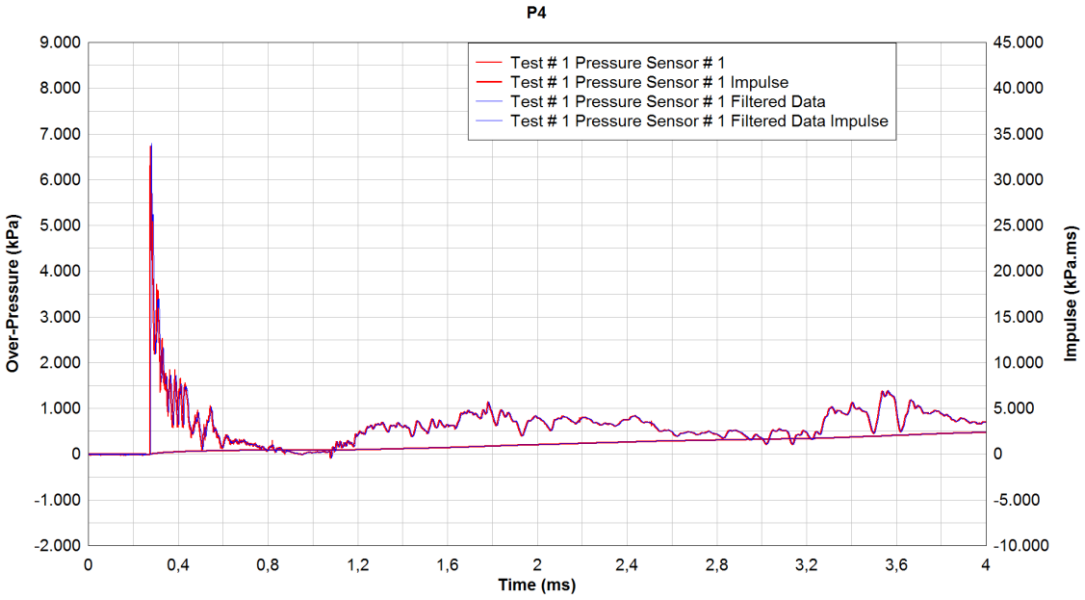
P4
Test # 1 Pressure Sensor # 1
Test # 1 Pressure Sensor # 1 Impulse
Test # 1 Pressure Sensor # 1 Filtered Data
Test # 1 Pressure Sensor # 1 Filtered Data Impulse
Over-Pressure (kPa)
Impulse (kPa.ms)
Time (ms)
9.000
8.000
7.000
6.000
5.000
4.000
3.000
2.000
1.000
0
-1.000
-2.000
45.000
40.000
35.000
30.000
25.000
20.000
15.000
10.000
5.000
0
-5.000
-10.000
0
0,4
0,8
1,2
1,6
2
2,4
2,8
3,2
3,6
4

(a)

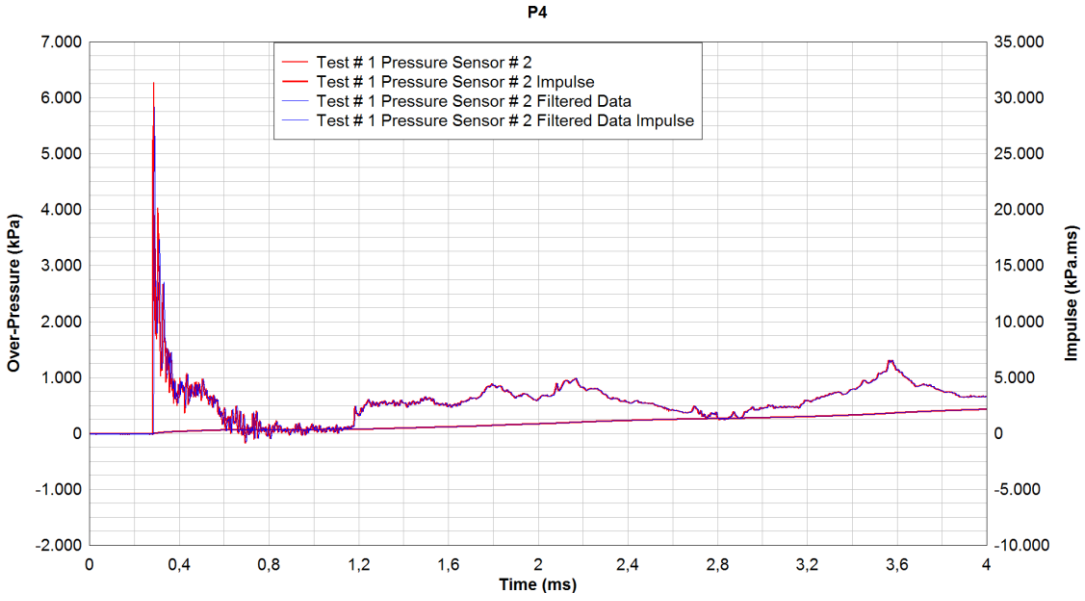
P4
Test # 1 Pressure Sensor # 2
Test # 1 Pressure Sensor # 2 Impulse
Test # 1 Pressure Sensor # 2 Filtered Data
Test # 1 Pressure Sensor # 2 Filtered Data Impulse
Over-Pressure (kPa)
Impulse (kPa.ms)
Time (ms)
7.000
6.000
5.000
4.000
3.000
2.000
1.000
0
-1.000
-2.000
35.000
30.000
25.000
20.000
15.000
10.000
5.000
0
-5.000
-10.000
0
0,4
0,8
1,2
1,6
2
2,4
2,8
3,2
3,6
4

(b)

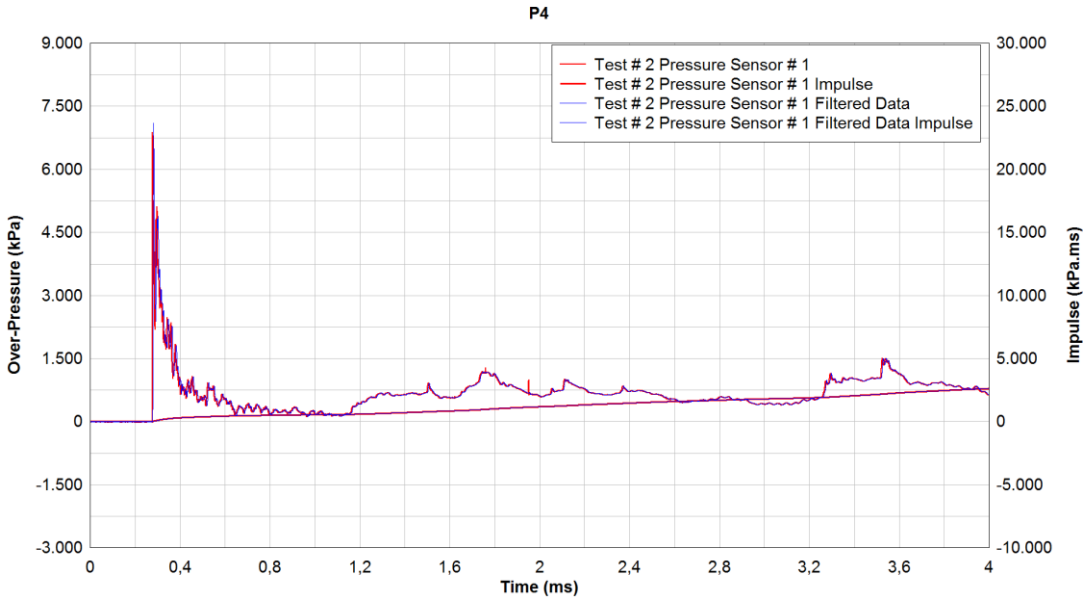

(c)

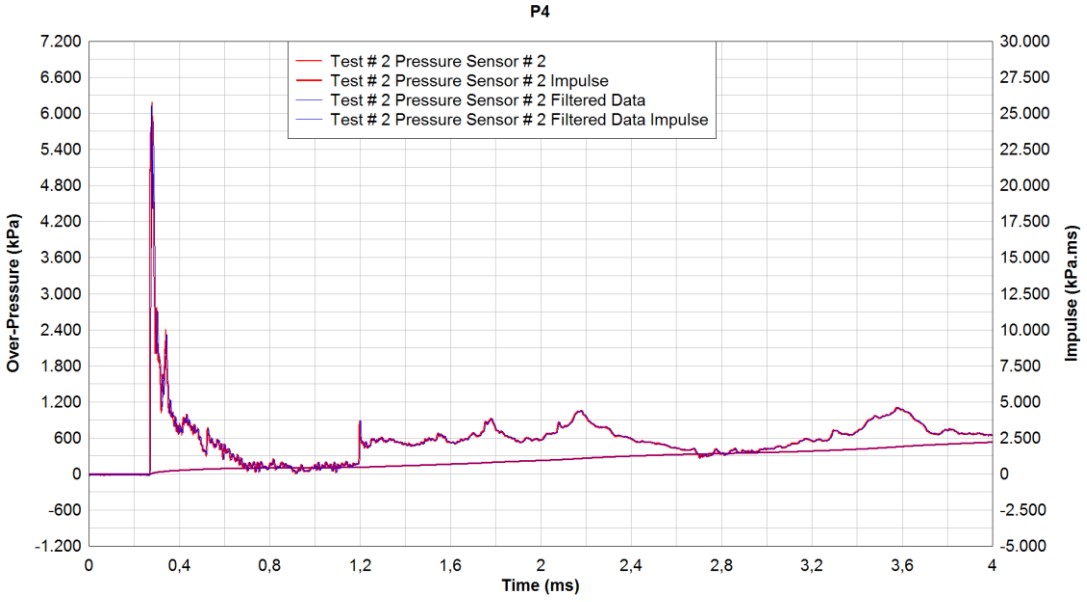

(d)

Figure 5-14 Raw and Filtered Data for P-4 (0-4 ms)

(a) Data #1 (b) Data #2 (c) Data #3 (d) Data #4

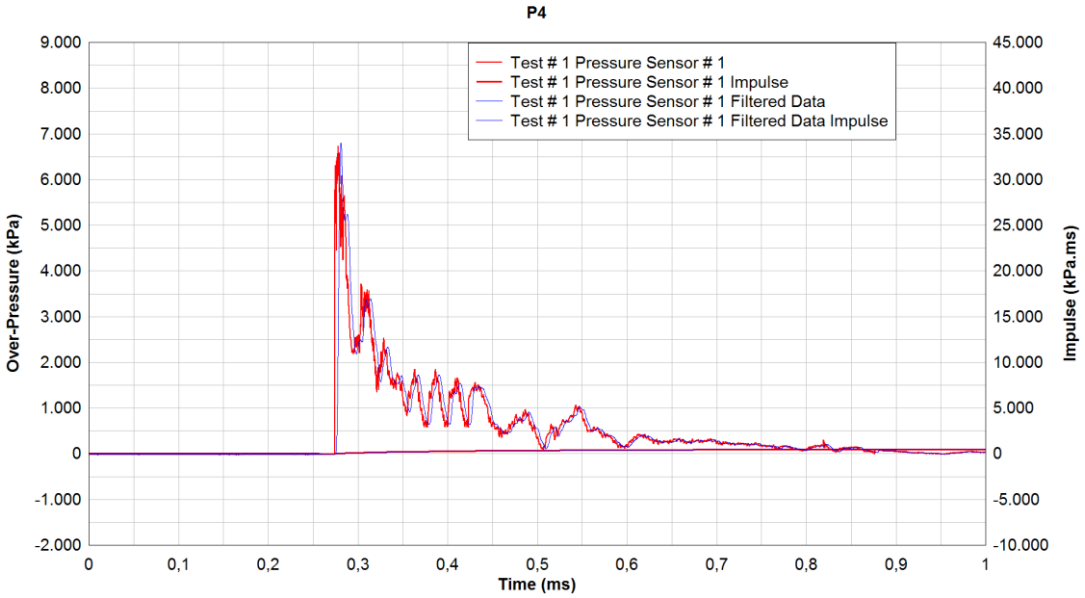
P4
Test # 1 Pressure Sensor # 1
Test # 1 Pressure Sensor # 1 Impulse
Test # 1 Pressure Sensor # 1 Filtered Data
Test # 1 Pressure Sensor # 1 Filtered Data Impulse
Over-Pressure (kPa)
Impulse (kPa.ms)
Time (ms)
9.000
8.000
7.000
6.000
5.000
4.000
3.000
2.000
1.000
0
-1.000
-2.000
45.000
40.000
35.000
30.000
25.000
20.000
15.000
10.000
5.000
0
-5.000
-10.000
0
0,1
0,2
0,3
0,4
0,5
0,6
0,7
0,8
0,9
1

(a)

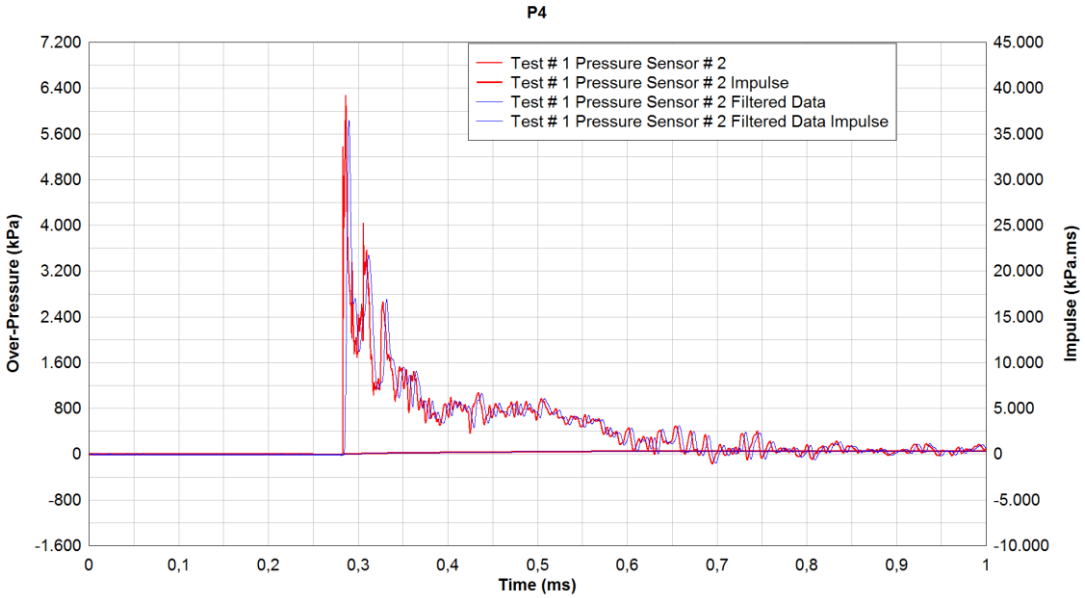
P4
Test # 1 Pressure Sensor # 2
Test # 1 Pressure Sensor # 2 Impulse
Test # 1 Pressure Sensor # 2 Filtered Data
Test # 1 Pressure Sensor # 2 Filtered Data Impulse
Over-Pressure (kPa)
Impulse (kPa.ms)
Time (ms)
7.200
6.400
5.600
4.800
4.000
3.200
2.400
1.600
800
0
-800
-1.600
45.000
40.000
35.000
30.000
25.000
20.000
15.000
10.000
5.000
0
-5.000
-10.000
0
0,1
0,2
0,3
0,4
0,5
0,6
0,7
0,8
0,9
1

(b)

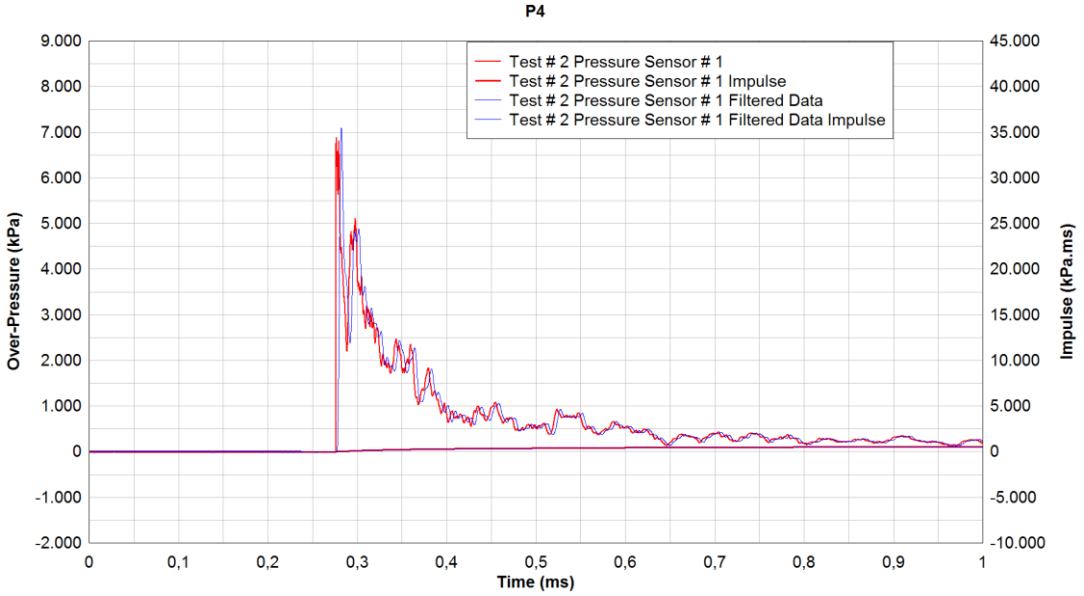

(c)

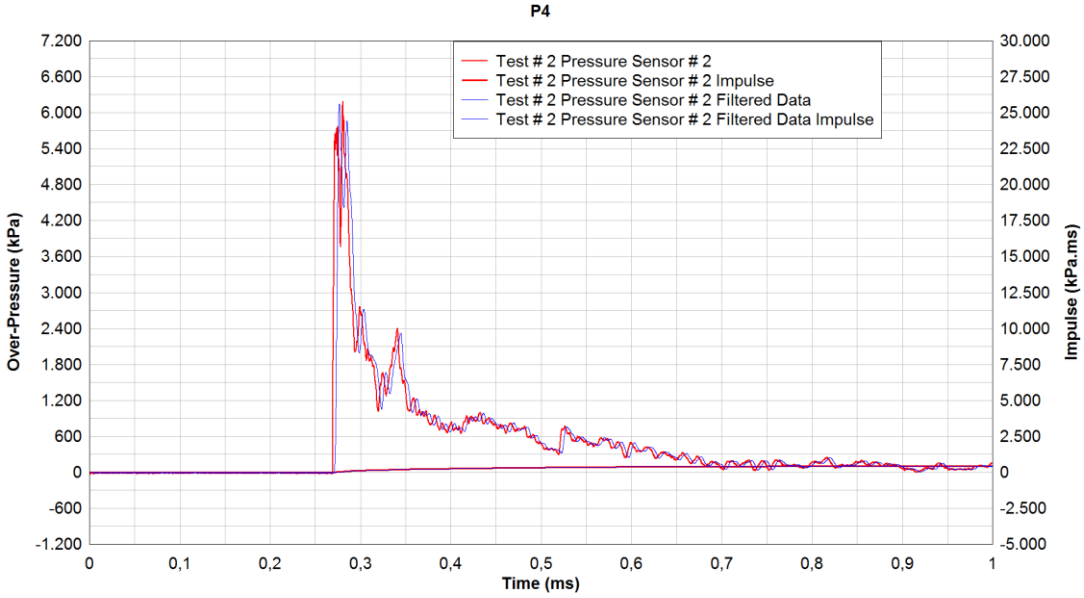

(d)

Figure 5-15 Raw and Filtered Data for P-4 (0-1 ms)

(a) Data #1 (b) Data #2 (c) Data #3 (d) Data #4

Table 5-16 Raw and Filtered Test Results of P-4

Data	Peak Over-Pressure (kPa)	Positive Impulse (kPa.ms)	Relative Difference - Peak Over-Pressure	Relative Difference –Positive Impulse
Data # 1	6726.5	15742.8	1.02%	0.0019%
Data # 1 Filtered	6796.1	15743.1		
Data # 2	6276.9	16146.1	7.49%	0.0049%
Data # 2 Filtered	5839.1	16146.9		
Data # 3	6878.8	15690.4	3.07%	0.0006%
Data # 3 Filtered	7097.2	15690.5		
Data # 4	6191.4	16066.1	0.74%	0.0024%
Data # 4 Filtered	6145.6	16066.5		

According to the results that are derived from the collected raw and filtered results of explosive P-4, low-pass filtering of data which have high frequency sampling rate reduces undesired noisy peaks. There are many things that can generate noise in the system such as cables, mounting details, design details of electronic and mechanical equipment. At several points including the peak over-pressure of raw data low-pass filtering smoothes the peak values. Table 5-16 indicates that low-pass filtering makes minor differences between raw and filtered data. The maximum difference observed is 7.5% in peak over-pressure for data # 3. In terms of positive impulse, since generated impulse is calculated for 32 ms interval the magnitude of the dramatically increased peak values do not contribute much in impulse calculation. The maximum difference observed is 0.0049% in positive impulse for data # 3 as in peak over-pressure results.

CHAPTER 6

CONCLUSION

6.1 Summary and Discussions

In this thesis, experimental and numerical studies have been carried out in detailed manner to investigate the blast performance of bare high explosive charges in closed detonation chamber. This study consisted of comparison of four different high explosives which have different compositions.

For the experimental study, explosive charges were manufactured and initiation train was assembled to have reliable detonation of charge assemblies. Mechanical components of the detonation chamber which are sensor holder apparatus and base plate were also manufactured.

Blast performance characteristic based on peak over-pressure and positive impulse have been analyzed with the time of arrivals that was measured by fiber-optic cables. Pressure and impulse measurements were taken by face-on pressure sensors having high data sampling rate which enables to capture peak pressure of shock wave moving at high velocity.

Numerical studies were conducted using 2D multi-material Eulerian hydrocode called Speed commercial software. The detonation chamber test setup was modeled in software and gauge points were located at the exact positions of the pressure sensors in experiments. The JWL EOS parameters which determine the pressure–specific volume curves of the explosives were adapted from cylinder expansion test results obtained in a companion work for the same batch of the explosives, P-1, P-2, P-3 and P-4. The numerical method consisted of mesh independency, sensitivity and uncertainty analyses. According to sensitivity analysis, alteration in the measurement distance results in higher deviation than alteration in mass of the explosive in terms of peak over-pressure. The peak over-

pressure and time of arrivals obtained from numerical simulations showed very good agreement with the experimental results. Speed demonstrates that the hydrocode has the ability to model a closed volume application where superposed reflections occur continuously.

The filtering of experimental results was also carried out for explosive P-4. Low-pass 6^{th} order Butterworth filtering technique was utilized to reduce high frequency noise. The reasons of the experimental noise could be due to the cables, utilization of data acquisition system, mounting details of pressure sensors and material type of mechanical equipment. The comparison of raw and filtered data showed that this type of signal processing shall not affect the positive impulse results since alterations in peak values do not contribute to the total impulse generated. Additionally, it can be concluded that peak values were not altered significantly between experimental raw and filtered data.

Based on the explosive formulation, optimization of internal detonation performance can be enhanced using metallized charges in warhead systems. The explosives P-2 and P-4 were newly designed compositions consisting of metallic fuel additives where the main energetic components are HMX and RDX, respectively. P-1, namely TNT and P-3 were available explosives in the literature with qualified compositions. The performances of P-1, P-2, P-3 and P-4 explosives were compared with each other for both experimental and numerical results. According to both numerical and experimental results, explosive P-4 has the highest impulse. Therefore, it can be concluded from the experimental results that as the mass percentage of metallic fuel additive increases in explosive compositions, positive impulse increases due to the after-burning of these additives. Hence, to have an optimum blast performance, explosive formulation should be altered by the metallic fuel additive. However, peak over-pressure highly depends on energetic component of explosive. A meaningful comparison in terms of peak over-pressure can be evaluated between P-4 and P-2 due to the fact that detonation pressure of HMX is higher than RDX as given in Table 1-1 [1]. These results show an excellent understanding of effectiveness of high explosives between pressure and impulsive damage characteristics.

Additional metallic fuel additive lengthens the duration of positive blast which directly affects the impulse generated within closed areas such as tunnels, underground facilities, bunkers and shelters since these closed structures are composed of many confinements in which blast wave interacts continuously. Since P-4 has the highest impulse among other tested explosive, it is the most effective explosive type against structures that are heavy but relatively weak such as concrete, brick wall and soil. So-called enhanced blast warhead systems which contain enhanced blast explosive compositions such as P-2, P-3 and P-4, deliver lethality to the target in terms of demolition.

The utilization of Speed hydrocode brings many advantages over commercial softwares such as Autodyn. In addition to the user-friendly interface of Speed code with respect to Autodyn, Speed can solve problems that have relatively high meshed systems in very short times thanks to its Eulerian approach. These advantages are observed during analyzing the numerical studies of P-1, P-2, P-3 and P-4 explosives. The utilized case scenario was attempted to be solved by Autodyn but due to the complexity of the mesh grid for the Euler-Lagrange solvers, with the same mesh domain compared to Speed code, Autodyn can not handle the 32 ms run time. Total of 0.1 ms of analysis run was accomplished during 2 months of computational time. The related shock wave propagation obtained from Autodyn is presented in Figure 6-1 for 0.1 ms.

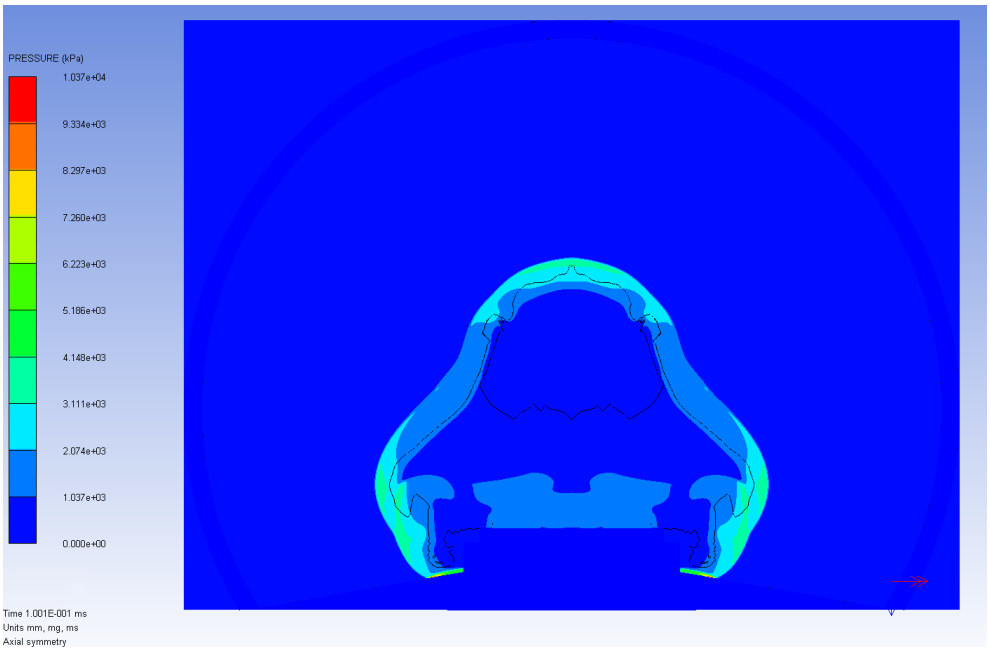

Figure 6-1 Shock Wave Propagation in Autodyn

6.2 Suggestions for Future Work

For the future study, there are recommendations about the topics including both experimental and numerical study. The experimental equipment can be improved in terms of sampling frequencies in order to reduce high frequency noise. Additionally, heat flux and thermocouples can be adapted to chamber body to measure the temperature and heat flux. Mechanical parts can be improved for the cost and easy handling.

In addition to the 2D analyses, the numerical study can be performed by 3D models that are initiated by remap sub-models.

REFERENCES

[1] Carleone J., "Tactical Missile Warheads", Vol. 155, 1993.

[2] Department of the Army Technical Manual, Military Explosives, 1984.

[3] Elek M.P., Dzingalasevic V.V., Jaramaz S.S. and Mickovic M.D., "Determination of Detonation Products Equation of State from Cylinder Test: Analytical Model and Numerical Analysis", Thermal Science, Vol.19, pp. 35-48, 2015.

[4] Speed User's Manual

[5] Togashi F., Baum J.D., Soto O.A., Löhner R. and Zhang F., "Numerical Simulation of TNT-Al Explosives in Explosion Chamber", Seventh International Conference on Computational Fluid Dynamics, 2012.

[6] Snyman, I.M., Mostert F.J. and Olivier M., "Measuring Pressure in a Confined Space", 27th International Symposium on Ballistics, 2012.

[7] Moster F.J. and .Ce D. T., "Measuring the Blast Output of Aluminized Explosive Charges in a Semi-Confined Environment", Insensitive Munitions & Energetic Materials Technology Symposium, 2010.

[8] Arnold W. and Rottenkolber E., "Combustion of an Aluminized Explosive in a Detonatio n Chamber", 39th International Annual Conference of ICT, 2008.

[9] Davison D. and Pratt D., "Measuring Pressure and Blast Impulse in a Closed Chamber", 27th International Symposium on Ballistics, 2013.

[10] Cullis I.G. and Huntington-Thresher W., "Blast Structure Interaction and the Role of Secondary Combustion", 23th International Symposium on Ballistics, 2007.

[11] Togashi F., Baum D.J. and Mestreau E., "Numerical Simulation of Long-Duration Blast Wave Evolution in Confined Facilities", 47th AIAA Aerospace Sciences Meeting Including the New Horizons Forum and Aerospace Exposition, 2009.

[12] Yu, Q. J., and Fan, S. C., "Effect of Blast and Gas Pressure on Debris Launching Velocity under Internal Detonation", Design and Analysis of Protective Structures Conference, 2010

[13] Rodriguez E.A. and Romero C. F., "Hydrodynamic Modeling of Detonations for Structural Design of Containment Vessels", ASME Pressure Vessels and Piping Division Conference, 2006.

[14] Vagsaether K., "Modelling of Gas Explosions", PhD Dissertation, Norwegian University of Science and Technology, pp. 64-66, 2010.

[15] Ludwig C., "Verifying Performance of Thermobaric Materials for Small to Medium Caliber Rocket Warheads", Talley Defense Systems.

[16] Simic D., Popovic M., Sirovatka R. and Andelic U.., "Influence of Cast Composite Thermobaric Explosive Compositions on Air Shock Wave Parameters", Scientific Technical Review, Vol. 63, 2013.

[17] Simoens B. and Lefebvre M.H. "Influence of Different Parameters on the TNT-Equivalent of an Explosion", Central European Journal of Energetic Materials, 2011.

[18] İncekürk T., Dilekliođlu E.A. "Açık Alan Patlayici Performans Testleri Test Sonuç Raporu", Roketsan A.Ş., 2014.

[19] "User's Manual for Installation, operation, Maintenance and Troubleshooting", 2012.

[20] Pappu, S., "Hydrocode and Microstrustural Analysis of Explosively Formed Penetrators", PhD Dissertation, University of Texas at El Paso, 2000

[21] Birnbaum N.K., Francis N.J. and Gerber, B. I., "Coupled Techniques for the Simulation of Fluid-Structure and Impact Problems", Computer Assisted Mechanics and Engineering Sciences, Vol. 6, pp. 295-311, 1999.

[22] Gürel E., "Modeling and Simulation of Shaped Charges", Ms. Thesis, Mechanical Engineering Department, Middle East Technical University, 2009.

[23] Hirt C.W., Amsden A.A. and Cook J.L. "An Arbitrary Lagrangian-Eulerian Computing Method for All Flow Speeds", Journal of Computational Physics, 1997.

[24] Autodyn Manual

[25] More about Speed, http://www.numerics-gmbh.de/en/speed.html, Last accessed on February 12, 2016

[26] Speed Theory Manual

[27] Brown B.W., "Critical Review of Theories of Steady Non-Ideal Two-Dimensional Detonation of Condensed Explosives", UK, 2002.

[28] Reichenbach H. and Kuhl A. L. "Characterization of Blasts from Laboratory-Scale Composite Explosive Charges", PhD Dissertation, The Pennsylvania State University The Graduate School College of Engineering, pp. 13-14, 2009.

[29] Esen S., Nyberg U., Arai H. and Ouchterlony F., "Determination of the Energetic Characteristics of Commercial Explosives with the Cylinder Expansion Test Technique", Swebrec, Sweden, 2005.

[30] Itoh S. and Hamashima H., "Determination of JWL Parameters from Underwater Explosion Test", Kumamoto University.

[31] Topkaraoğlu E. "Design and Development of a Cylinder Expansion Test Setup for Determination of Equation of State Parameters of Various Explosives" Ms. Thesis, Mechanical Engineering Department, Middle East Technical University, 2014.

[32] LLNL Explosives Handbook, University of California, 1985.

[33] Yılmaz M.Y. "Dent Test Konfigürasyonları", Roketsan A.Ş., 2014.

[34] Butterworth S. "On the Theory of Filter Amplifiers", Wireless Engineer, Vol. 7, pp. 536–541, 1930.

[35] Henisey A.T. "Comparing the Effects of Protective Plate Shape on Leg Injuries During Finite Element Blast Simulations with the Hybrid III Atd", Senior Thesis, University of Notre Dame, 2010.

[36] Eide H.O.S. and Melby E.A. "Blast Loaded Aluminium Plates", Norwegian University of Science and Technology, 2013.

[37] Lacanette K. "A Basic Introduction to Filters-Active, Passive, and Switched-Capacitor, National Semiconductor Application Note 779, 1991.

APPENDIX A

PRESSURE CONTOURS FOR EXPLOSIVE P-2, P-3 AND P-4

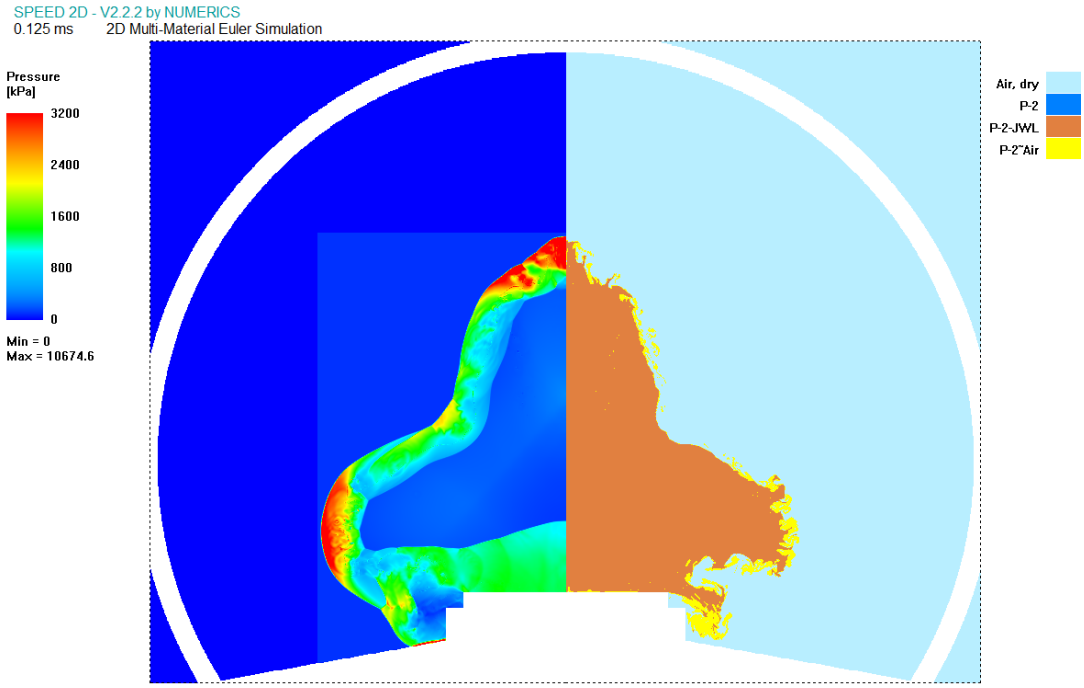

(a)

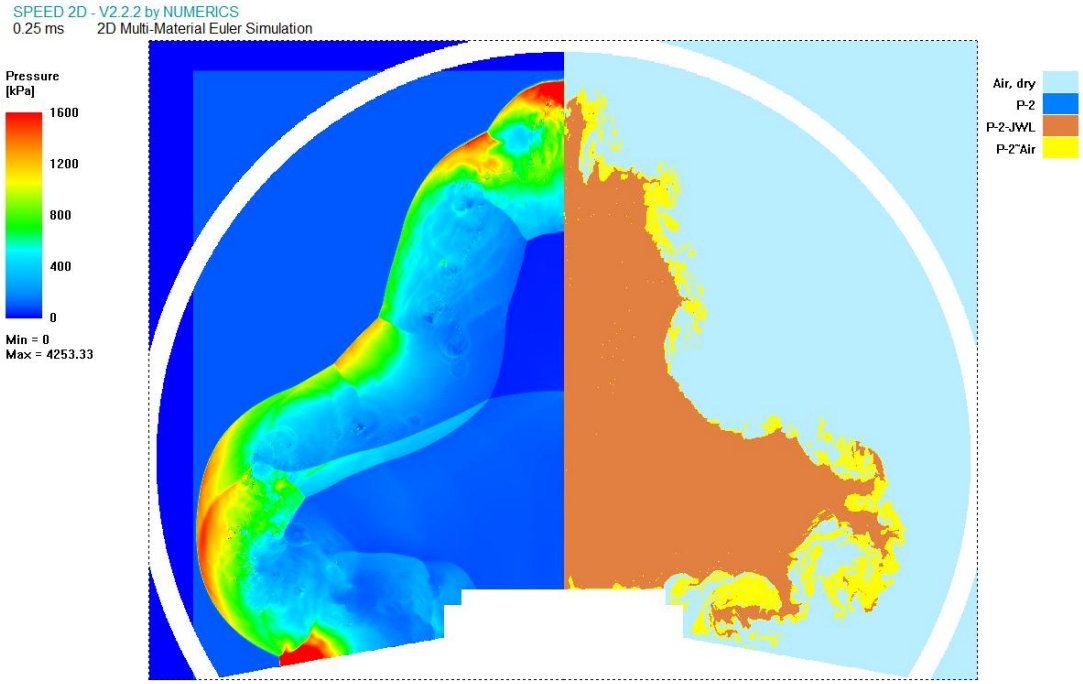
SPEED 2D - V2.2.2 by NUMERICS
0.25 ms 2D Multi-Material Euler Simulation
Pressure
[kPa]
1600
1200
800
400
0
Min = 0
Max = 4253.33
Air, dry
P-2
P-2-JWL
P-2"Air

(b)

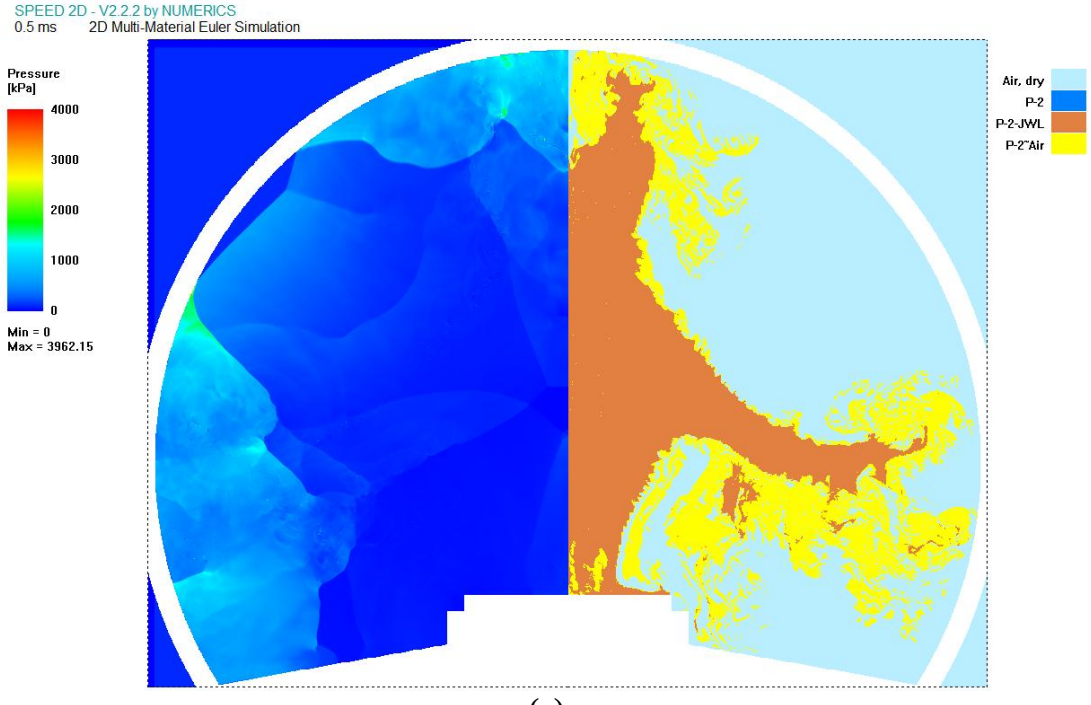
SPEED 2D - V2.2.2 by NUMERICS
0.5 ms 2D Multi-Material Euler Simulation
Pressure
[kPa]
4000
3000
2000
1000
0
Min = 0
Max = 3962.15
Air, dry
P-2
P-2-JWL
P-2"Air

(c)

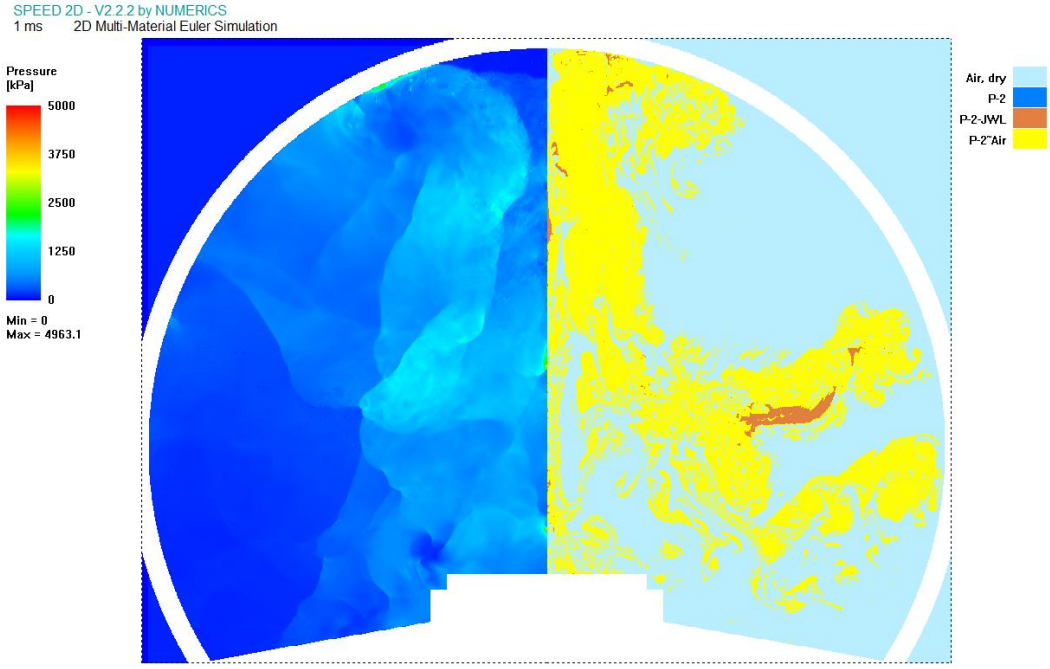
SPEED 2D - V2.2.2 by NUMERICS
1 ms 2D Multi-Material Euler Simulation
Pressure
[kPa]
5000
3750
2500
1250
0
Min = 0
Max = 4963.1
Air, dry
P-2
P-2-JWL
P-2~Air

(d)

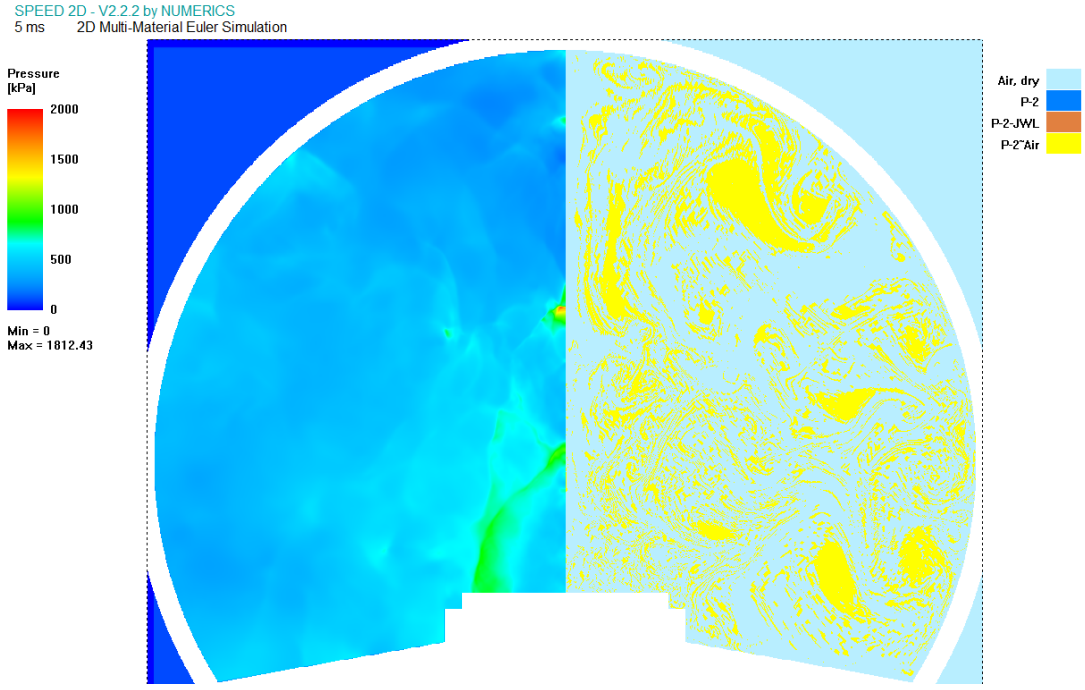
SPEED 2D - V2.2.2 by NUMERICS
5 ms 2D Multi-Material Euler Simulation
Pressure
[kPa]
2000
1500
1000
500
0
Min = 0
Max = 1812.43
Air, dry
P-2
P-2-JWL
P-2~Air

(e)

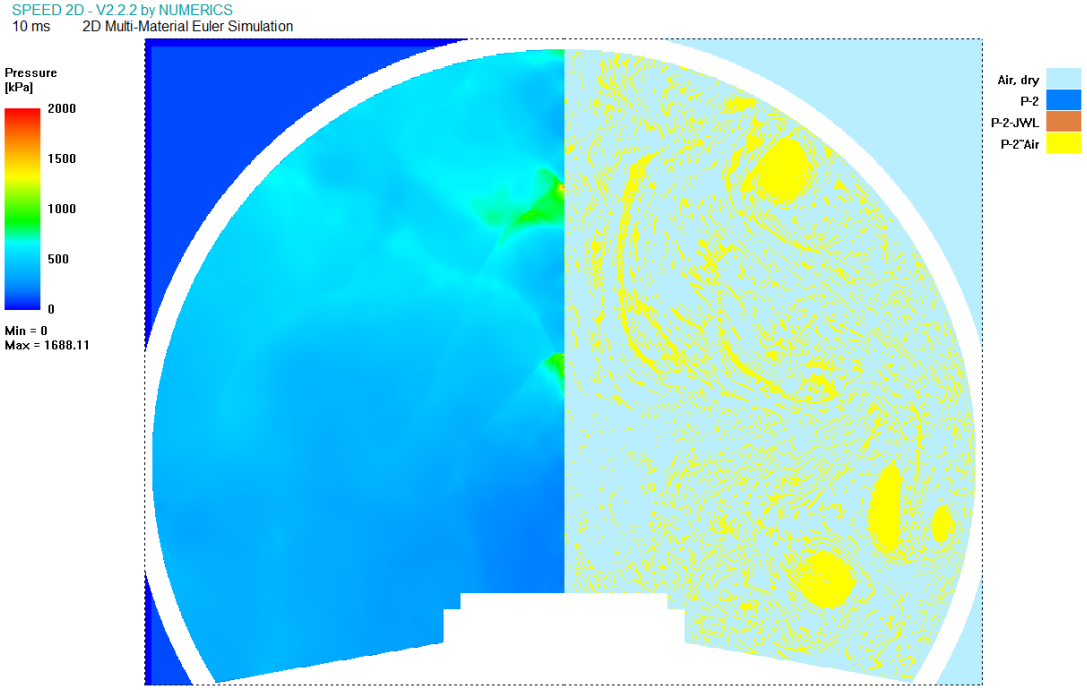
SPEED 2D - V2.2.2 by NUMERICS
10 ms 2D Multi-Material Euler Simulation
Pressure
[kPa]
2000
1500
1000
500
0
Min = 0
Max = 1688.11
Air, dry
P-2
P-2-JWL
P-2~Air

(f)

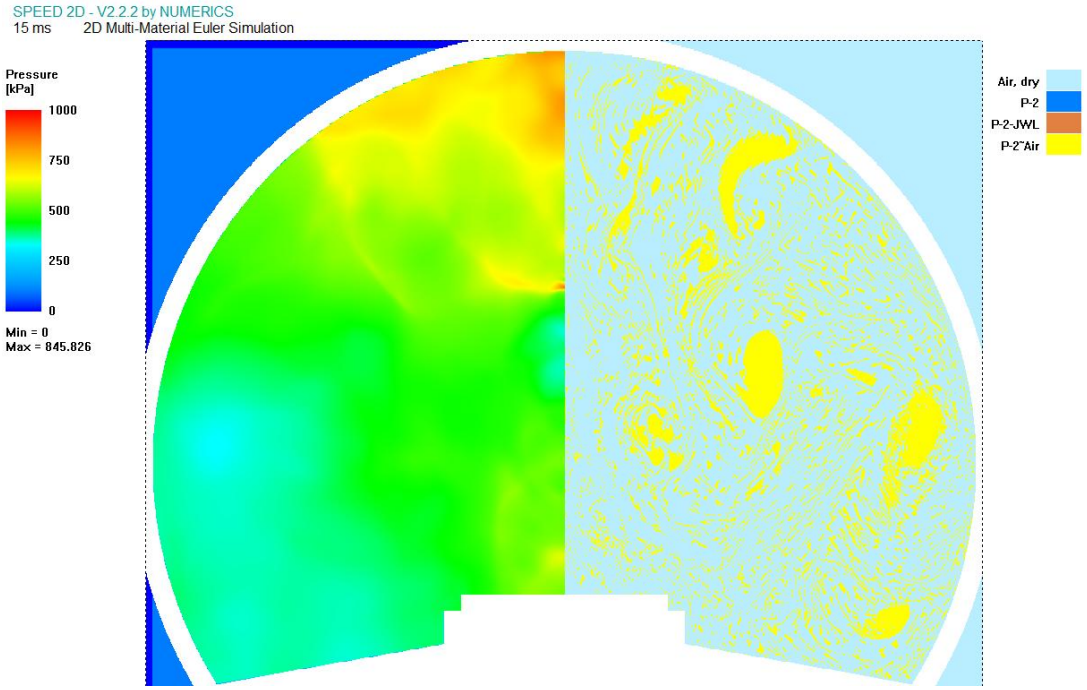
SPEED 2D - V2.2.2 by NUMERICS
15 ms 2D Multi-Material Euler Simulation
Pressure
[kPa]
1000
750
500
250
0
Min = 0
Max = 845.826
Air, dry
P-2
P-2-JWL
P-2~Air

(g)

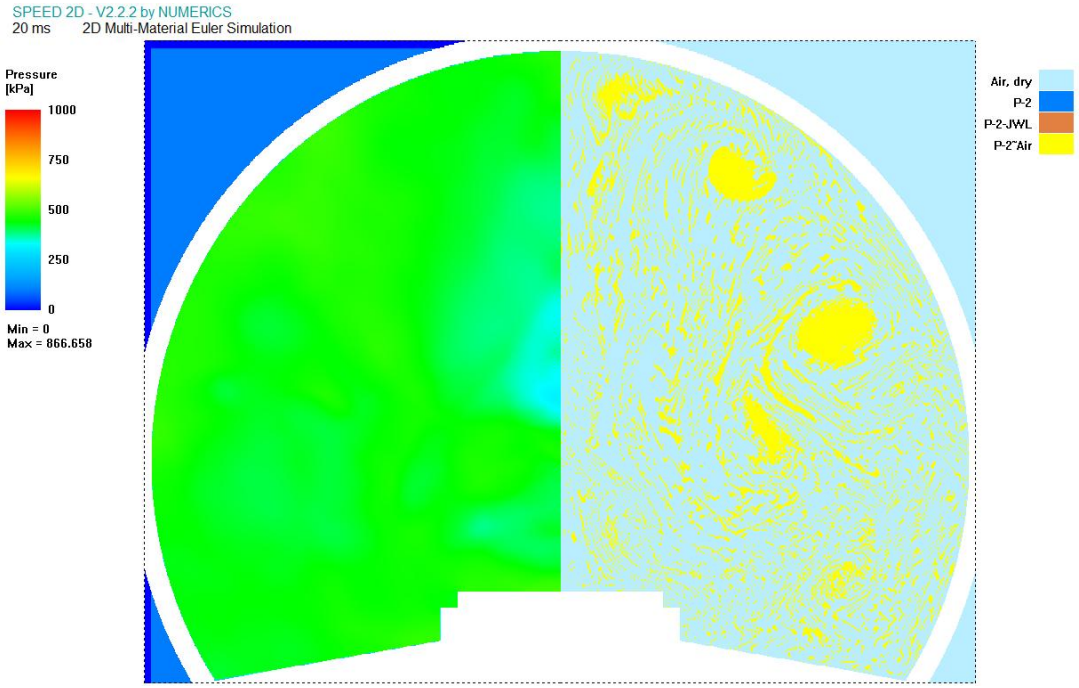
SPEED 2D - V2.2.2 by NUMERICS
20 ms 2D Multi-Material Euler Simulation
Pressure
[kPa]
1000
750
500
250
0
Min = 0
Max = 866.658
Air, dry
P-2
P-2-JWL
P-2~Air

(h)

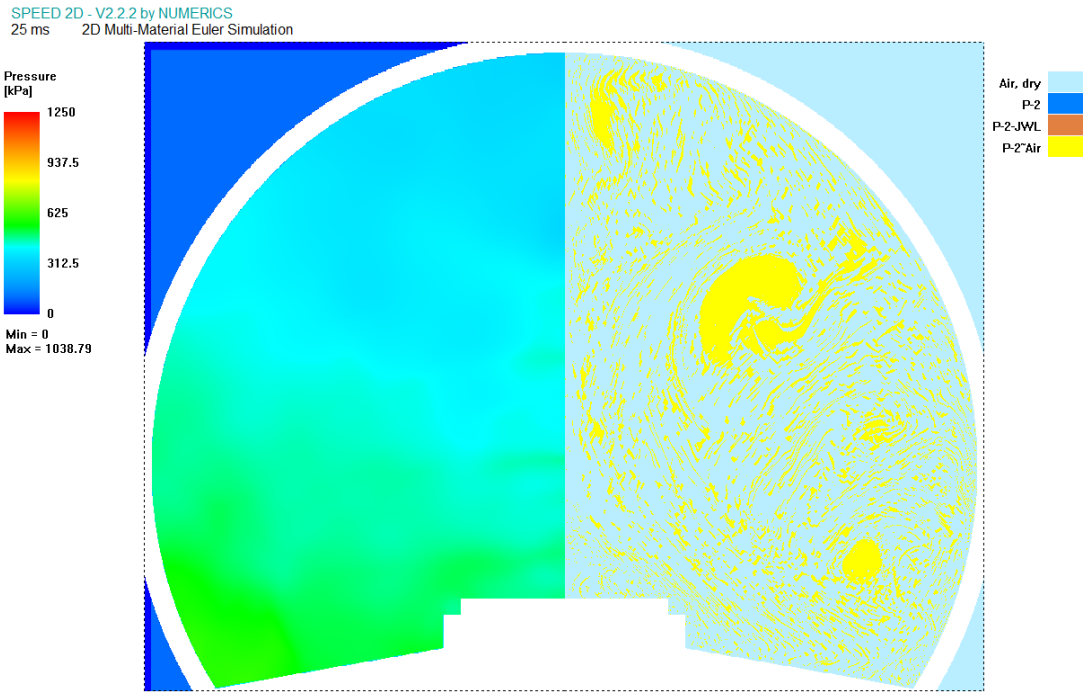
SPEED 2D - V2.2.2 by NUMERICS
25 ms 2D Multi-Material Euler Simulation
Pressure
[kPa]
1250
937.5
625
312.5
0
Min = 0
Max = 1038.79
Air, dry
P-2
P-2-JWL
P-2~Air

(i)

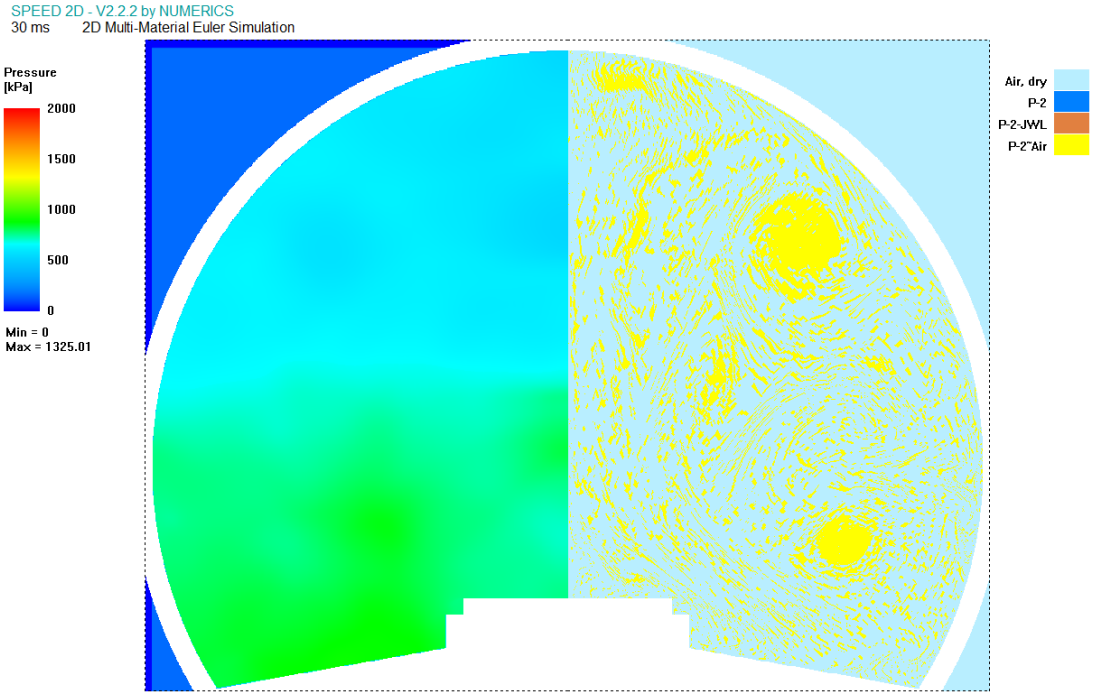

(j)

Figure A-1 Pressure and Material Distribution after Detonation of Explosive P-2 at Different Times:

(a) 0.125 ms (b) 0.25 ms (c) 0.5 ms (d) 1 ms (e) 5 ms (f) 10 ms (g) 15 ms (h) 20 ms (i) 25 ms (j) 30 ms

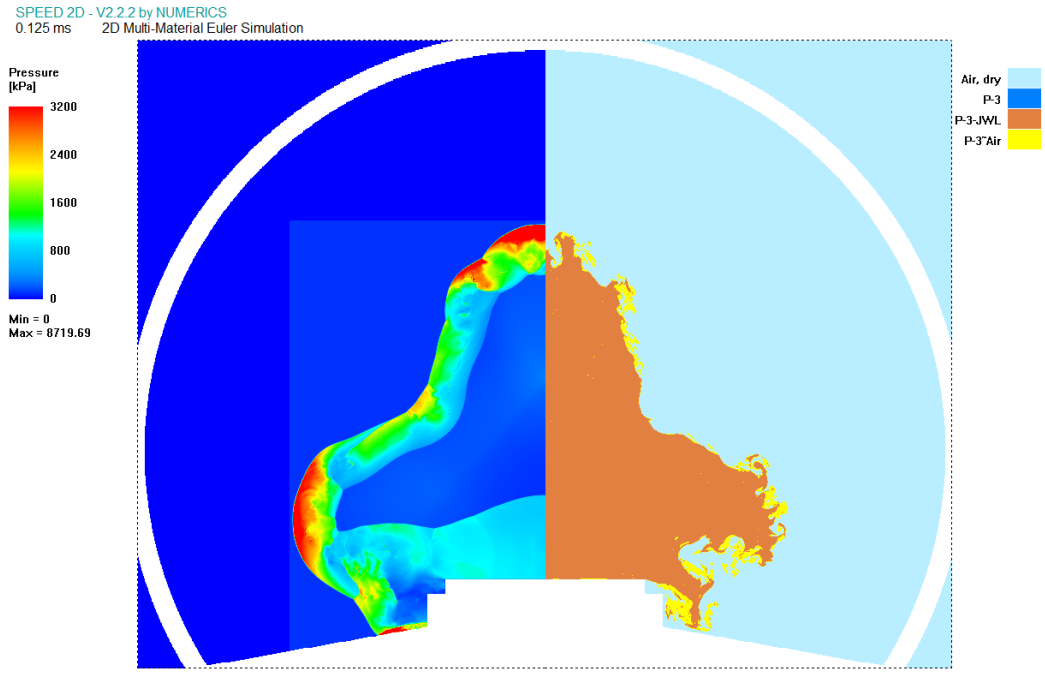
SPEED 2D - V2.2.2 by NUMERICS
0.125 ms
2D Multi-Material Euler Simulation
Pressure
[kPa]
3200
2400
1600
800
0
Min = 0
Max = 8719.69
Air, dry
P-3
P-3-JWL
P-3~Air

(a)

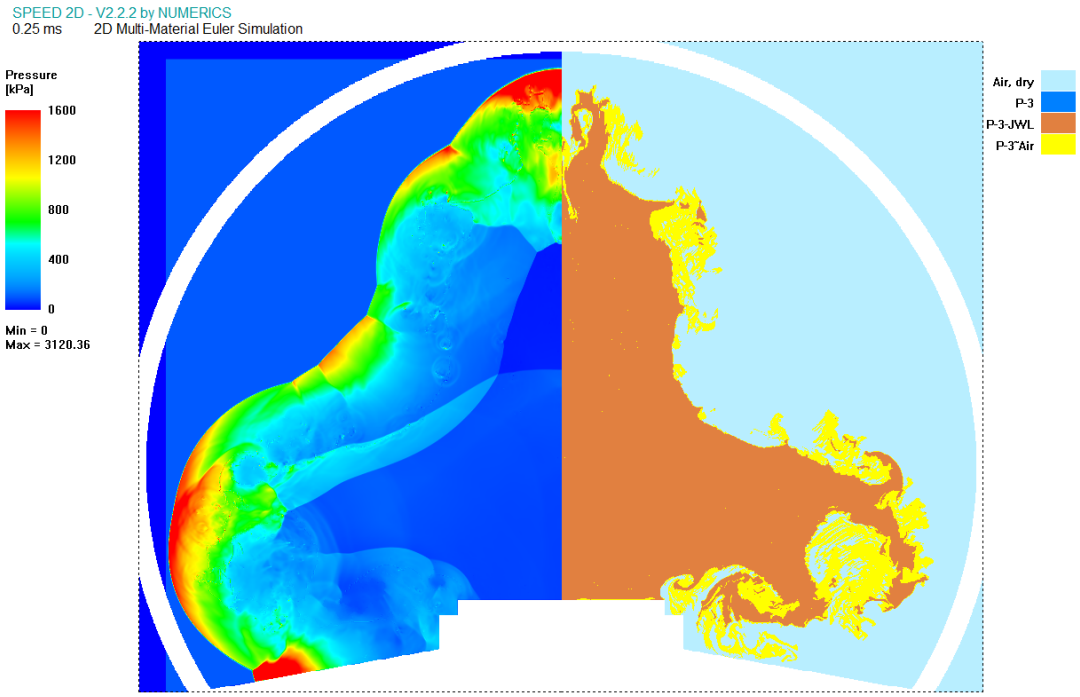
SPEED 2D - V2.2.2 by NUMERICS
0.25 ms
2D Multi-Material Euler Simulation
Pressure
[kPa]
1600
1200
800
400
0
Min = 0
Max = 3120.36
Air, dry
P-3
P-3-JWL
P-3~Air

(b)

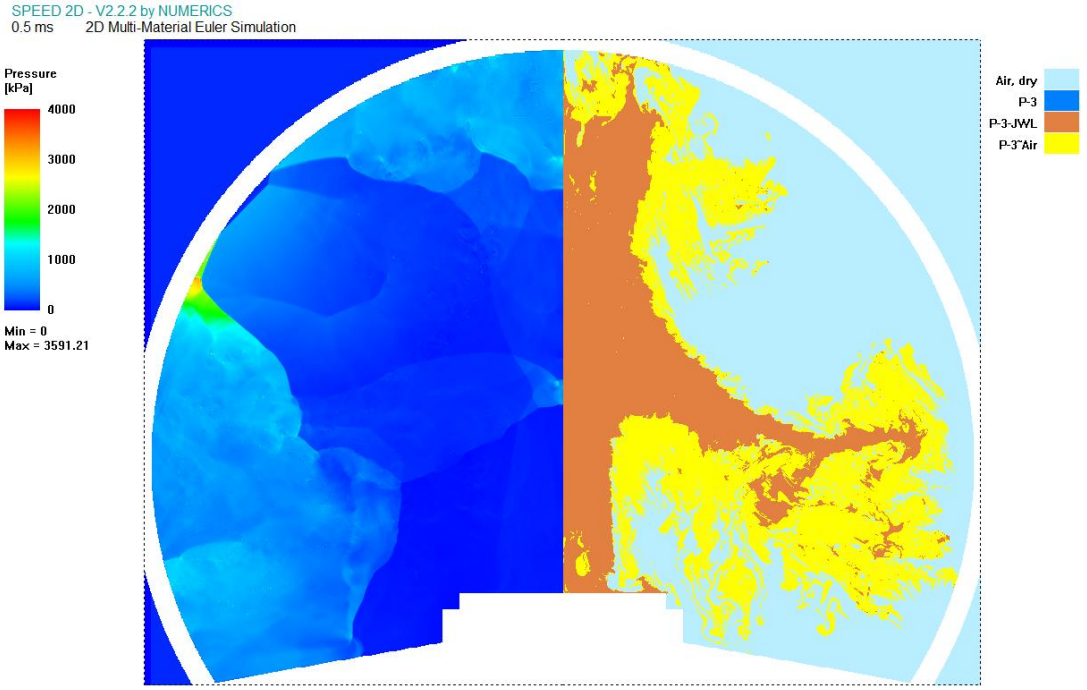
SPEED 2D - V2.2.2 by NUMERICS
0.5 ms 2D Multi-Material Euler Simulation
Pressure
[kPa]
4000
3000
2000
1000
0
Min = 0
Max = 3591.21
Air, dry
P-3
P-3-JWL
P-3^Air

(c)

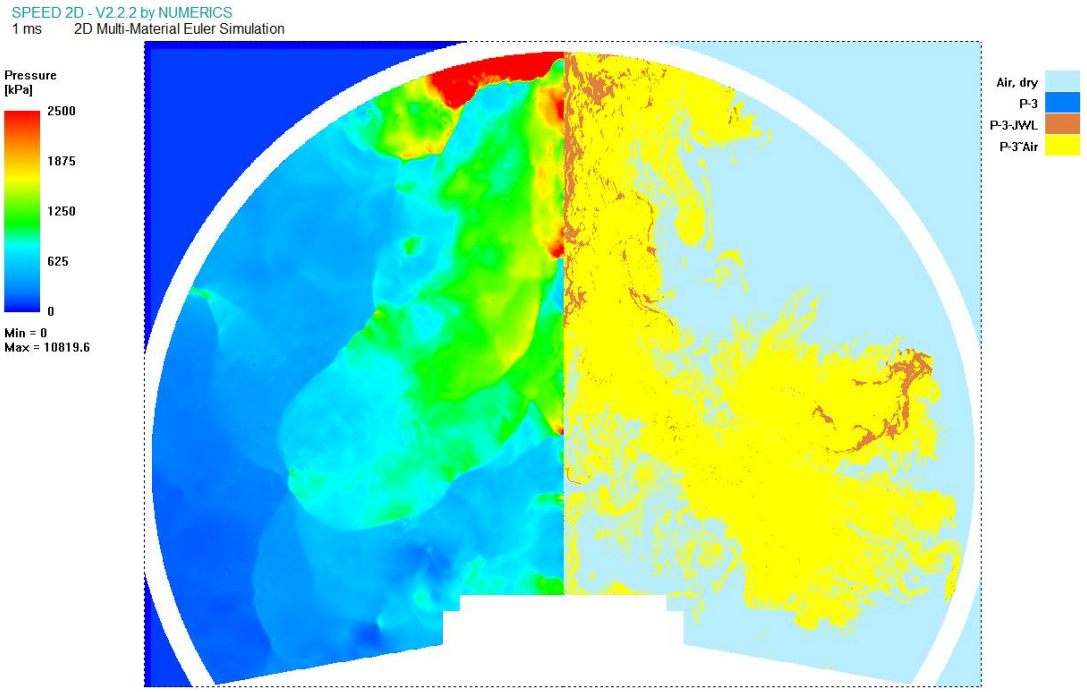
SPEED 2D - V2.2.2 by NUMERICS
1 ms 2D Multi-Material Euler Simulation
Pressure
[kPa]
2500
1875
1250
625
0
Min = 0
Max = 10819.6
Air, dry
P-3
P-3-JWL
P-3^Air

(d)

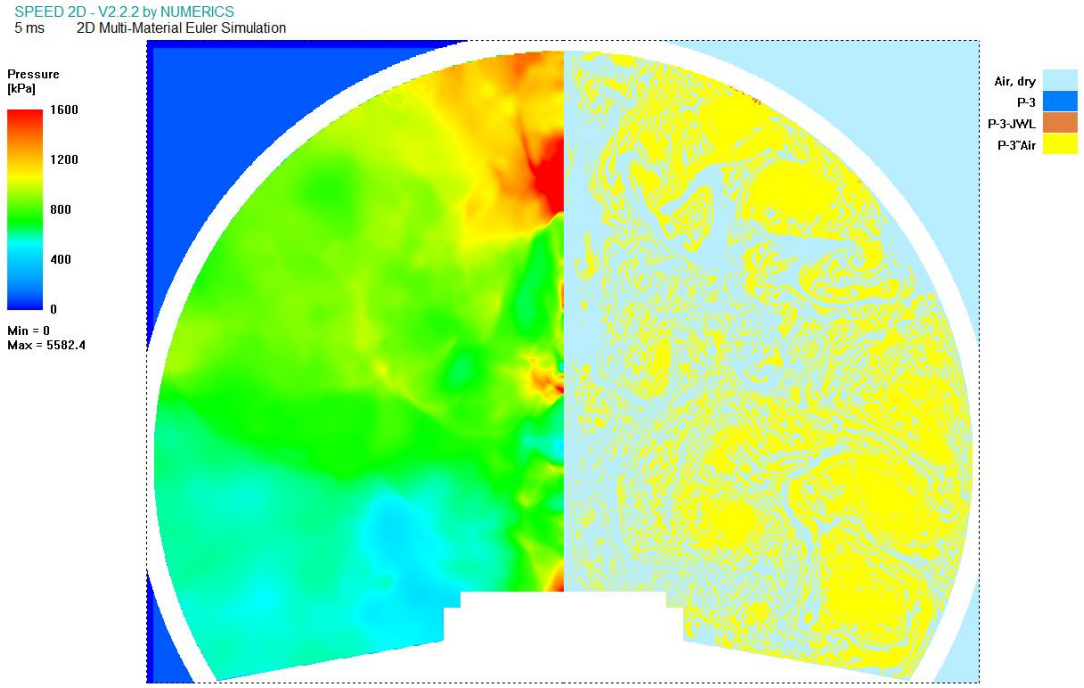
SPEED 2D - V2.2.2 by NUMERICS
5 ms 2D Multi-Material Euler Simulation
Pressure
[kPa]
1600
1200
800
400
0
Min = 0
Max = 5582.4
Air, dry
P-3
P-3-JWL
P-3~Air

(e)

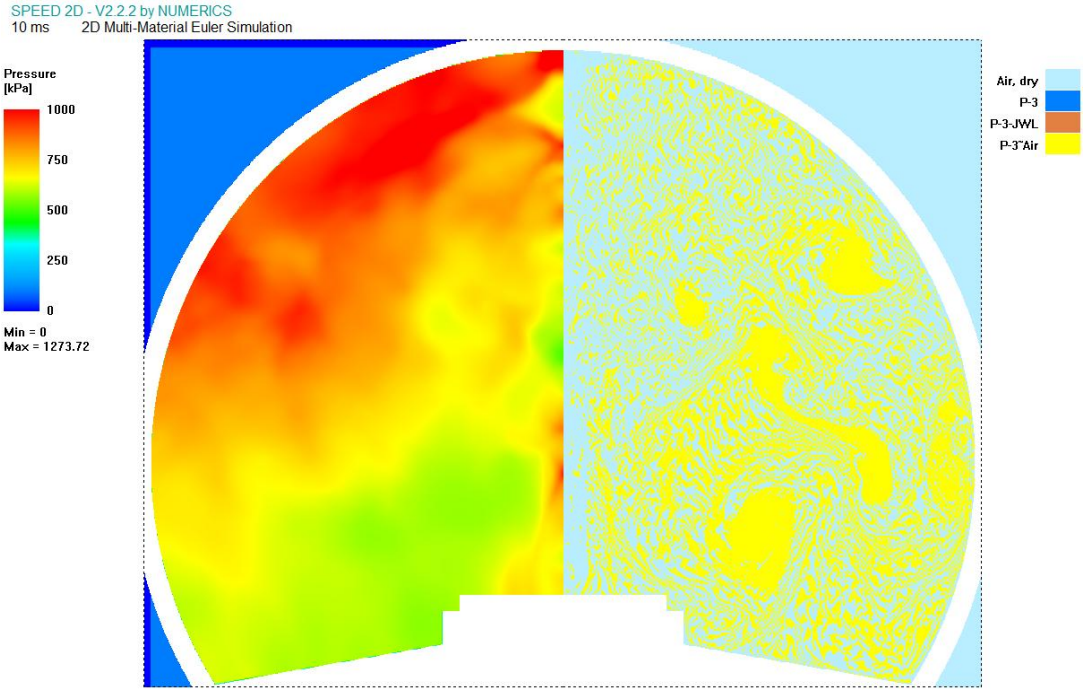
SPEED 2D - V2.2.2 by NUMERICS
10 ms 2D Multi-Material Euler Simulation
Pressure
[kPa]
1000
750
500
250
0
Min = 0
Max = 1273.72
Air, dry
P-3
P-3-JWL
P-3~Air

(f)

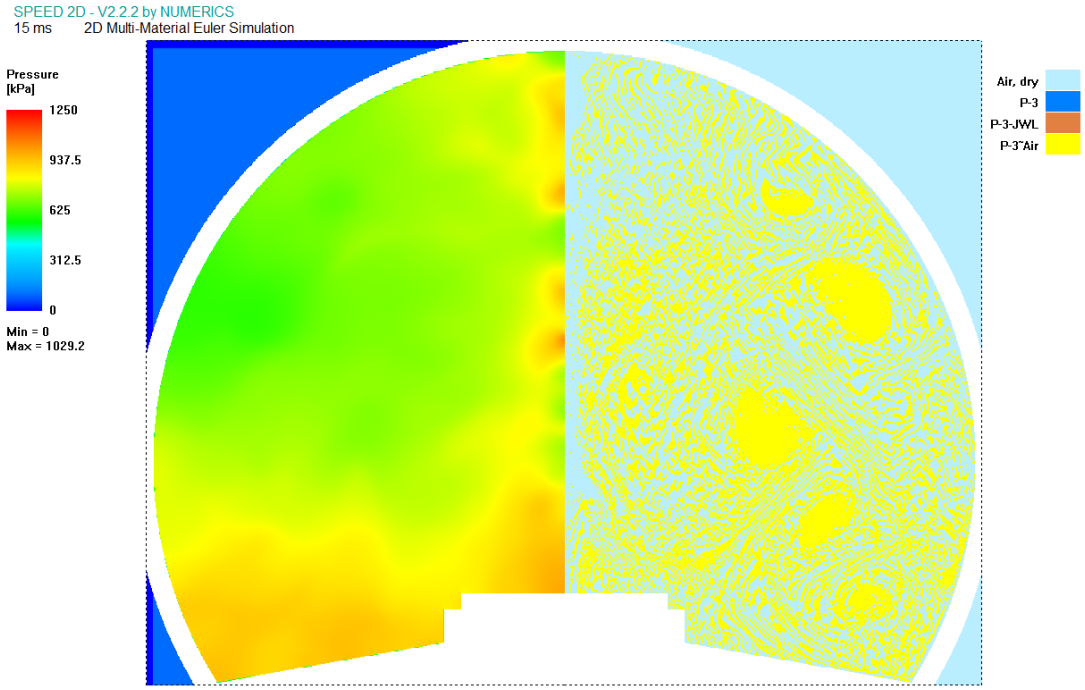
SPEED 2D - V2.2.2 by NUMERICS
15 ms 2D Multi-Material Euler Simulation
Pressure
[kPa]
1250
937.5
625
312.5
0
Min = 0
Max = 1029.2
Air, dry
P-3
P-3-JWL
P-3~Air

(g)

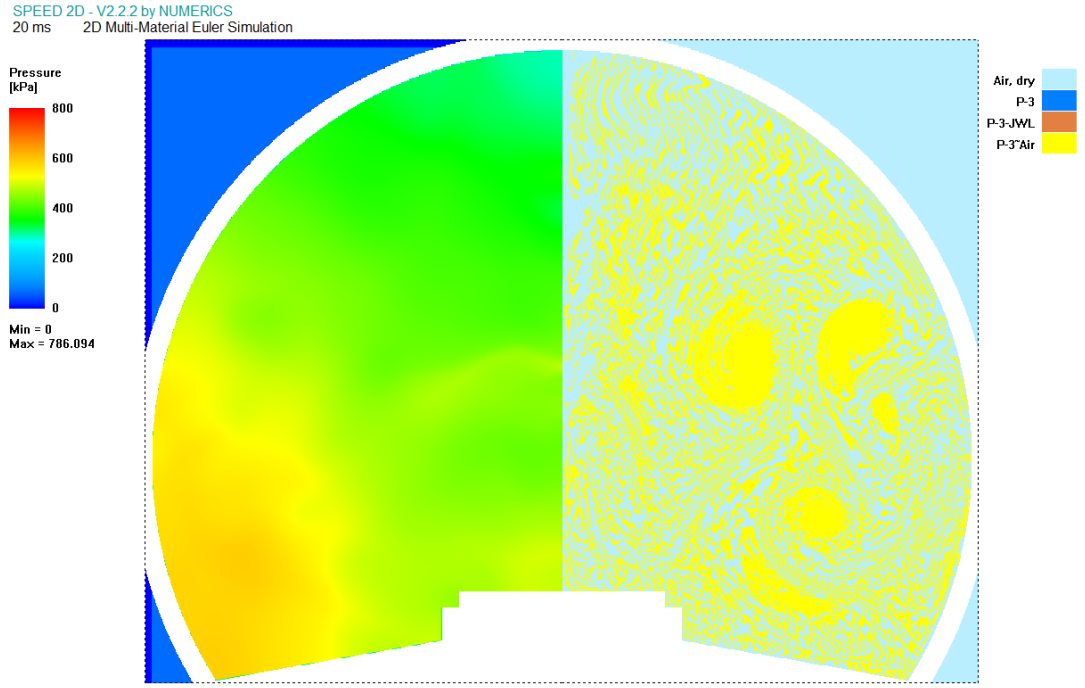
SPEED 2D - V2.2.2 by NUMERICS
20 ms 2D Multi-Material Euler Simulation
Pressure
[kPa]
800
600
400
200
0
Min = 0
Max = 786.094
Air, dry
P-3
P-3-JWL
P-3~Air

(h)

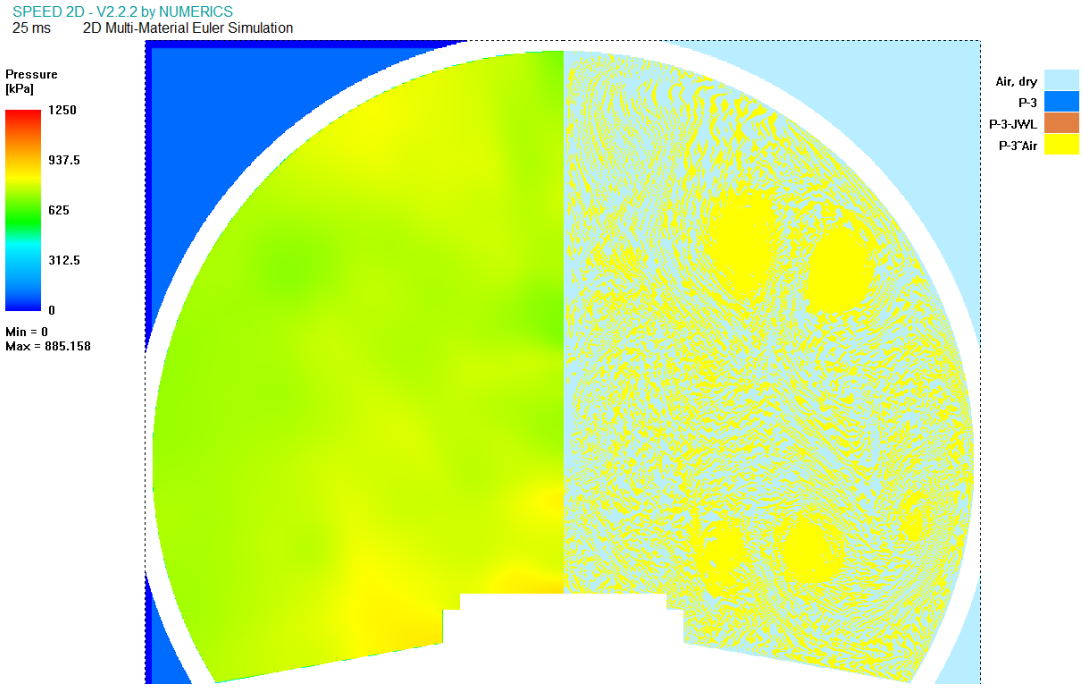
SPEED 2D - V2.2.2 by NUMERICS
25 ms 2D Multi-Material Euler Simulation
Pressure
[kPa]
1250
937.5
625
312.5
0
Min = 0
Max = 885.158
Air, dry
P-3
P-3-JWL
P-3^Air

(i)

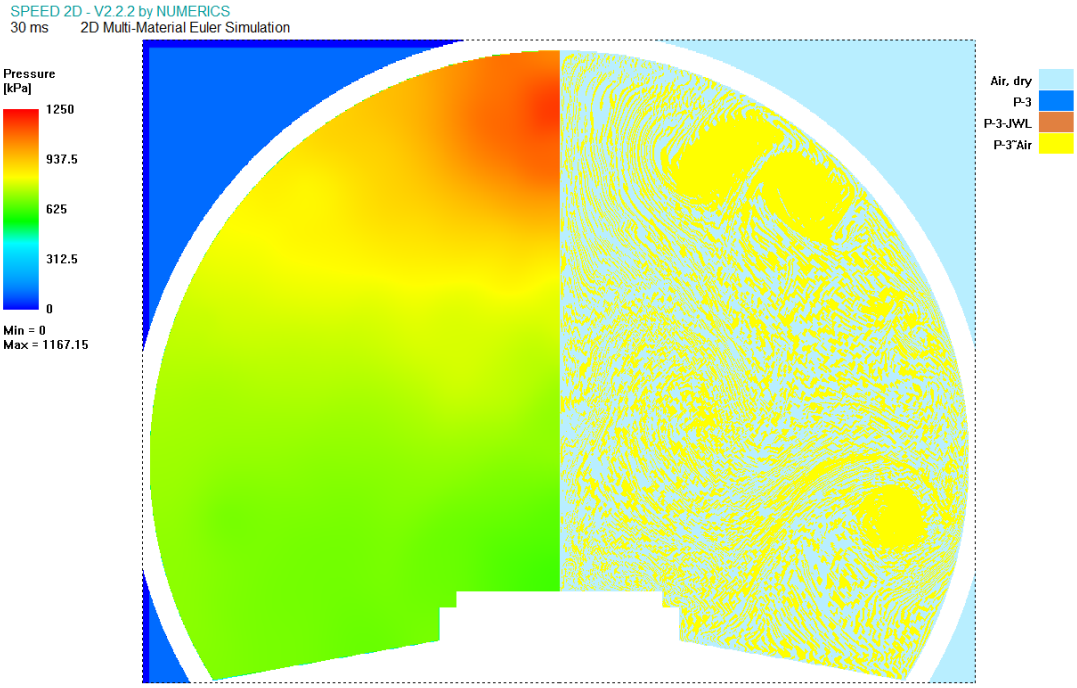

(j)

Figure A-2 Pressure and Material Distribution after Detonation of Explosive P-3 at Different Times:

(a) 0.125 ms (b) 0.25 ms (c) 0.5 ms (d) 1 ms (e) 5 ms (f) 10 ms (g) 15 ms (h) 20 ms (i) 25 ms (j) 30 ms

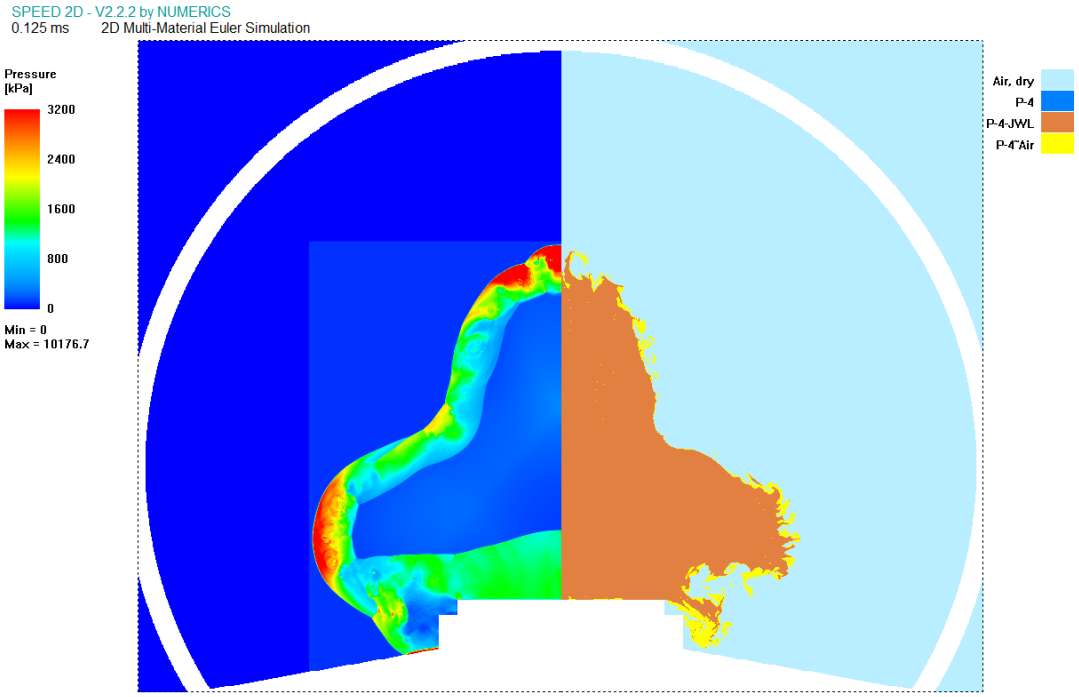
SPEED 2D - V2.2.2 by NUMERICS
0.125 ms 2D Multi-Material Euler Simulation
Pressure
[kPa]
3200
2400
1600
800
0
Min = 0
Max = 10176.7
Air, dry
P-4
P-4-JWL
P-4~Air

(a)

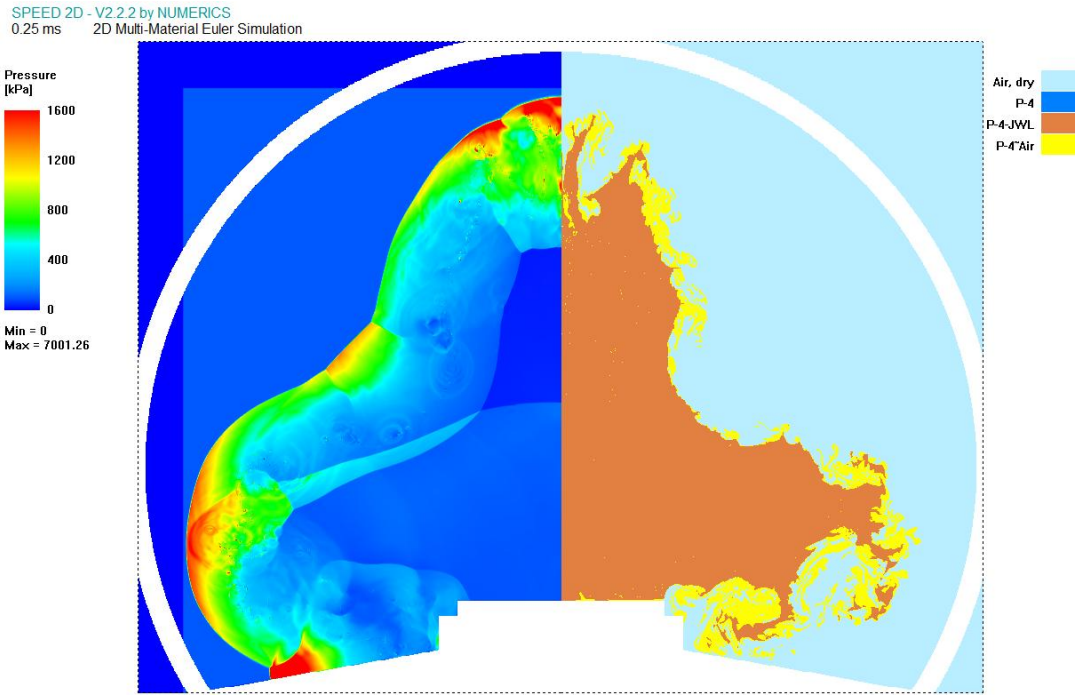
SPEED 2D - V2.2.2 by NUMERICS
0.25 ms 2D Multi-Material Euler Simulation
Pressure
[kPa]
1600
1200
800
400
0
Min = 0
Max = 7001.26
Air, dry
P-4
P-4-JWL
P-4~Air

(b)

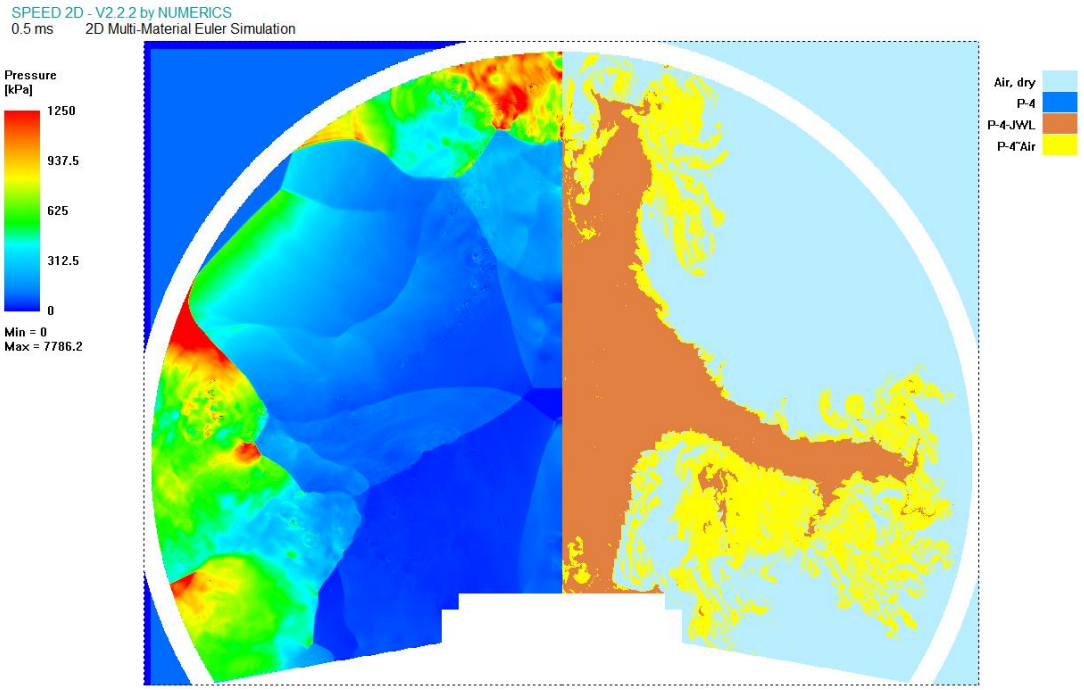
SPEED 2D - V2.2.2 by NUMERICS
0.5 ms 2D Multi-Material Euler Simulation
Pressure
[kPa]
1250
937.5
625
312.5
0
Min = 0
Max = 7786.2
Air, dry
P-4
P-4-JWL
P-4-Air

(c)

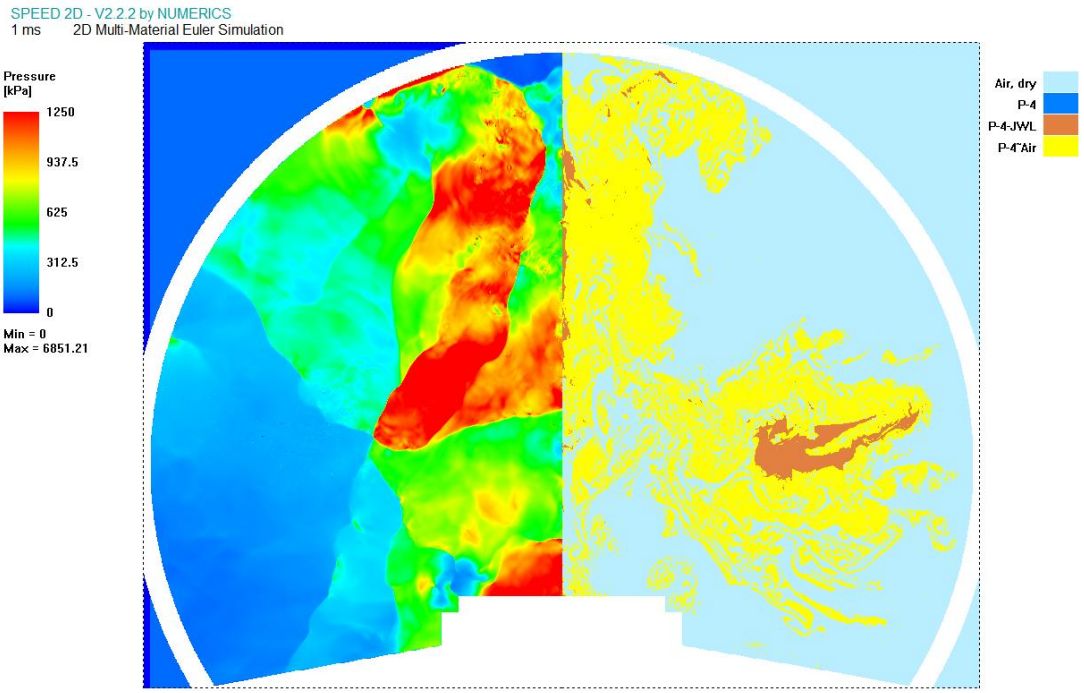
SPEED 2D - V2.2.2 by NUMERICS
1 ms 2D Multi-Material Euler Simulation
Pressure
[kPa]
1250
937.5
625
312.5
0
Min = 0
Max = 6851.21
Air, dry
P-4
P-4-JWL
P-4-Air

(d)

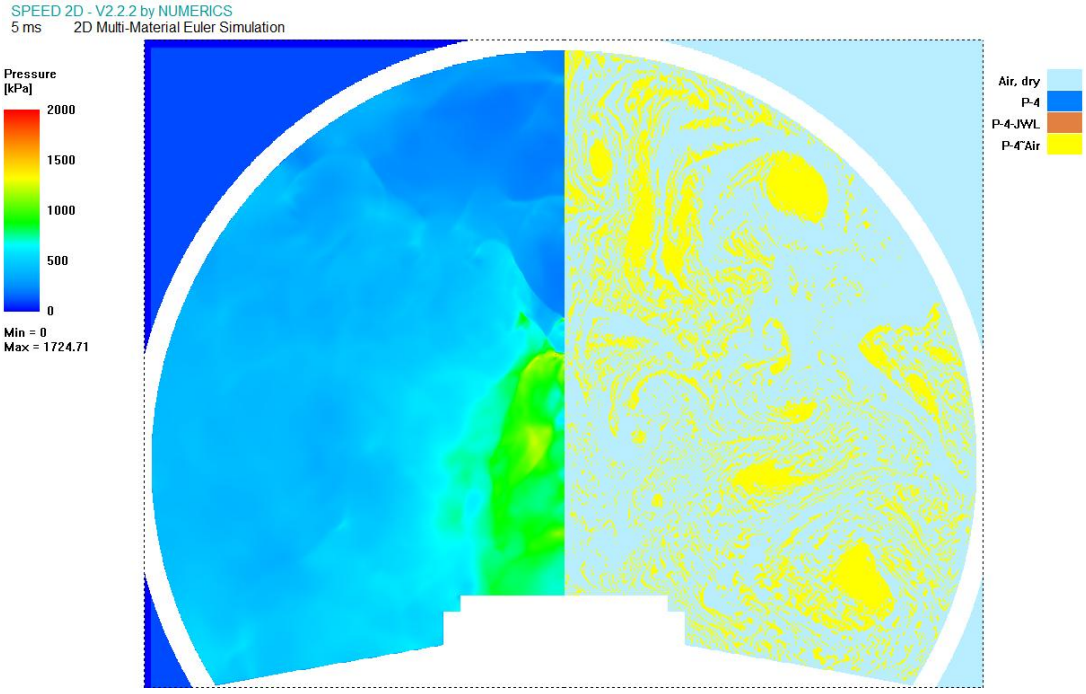
SPEED 2D - V2.2.2 by NUMERICS
5 ms 2D Multi-Material Euler Simulation
Pressure
[kPa]
2000
1500
1000
500
0
Min = 0
Max = 1724.71
Air, dry
P-4
P-4-JWL
P-4~Air

(e)

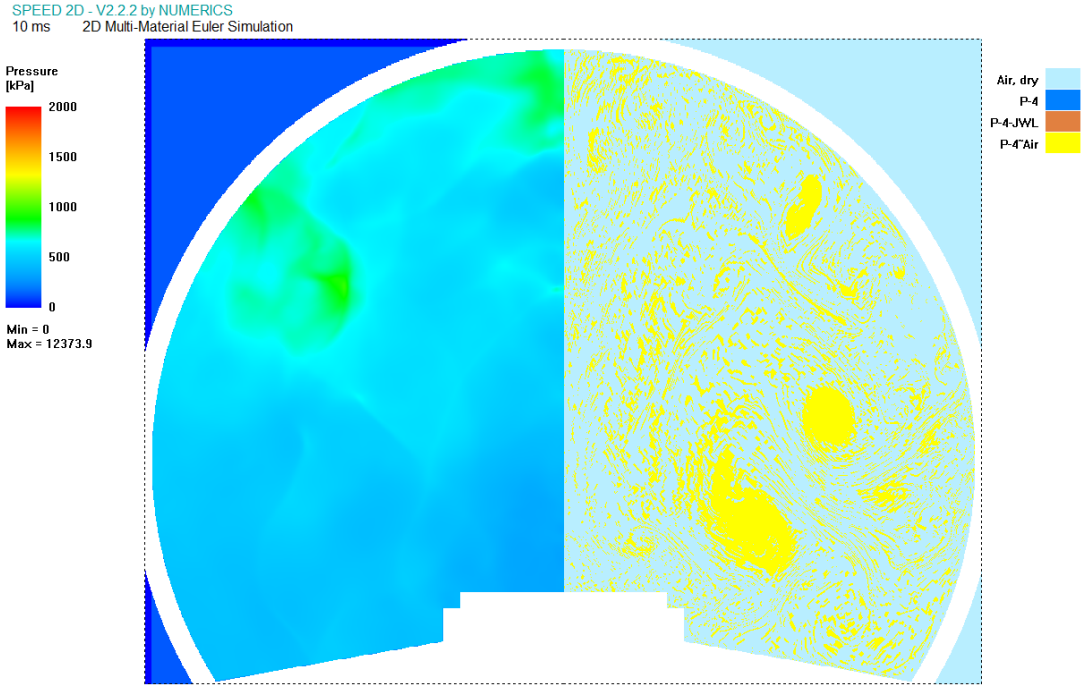
SPEED 2D - V2.2.2 by NUMERICS
10 ms 2D Multi-Material Euler Simulation
Pressure
[kPa]
2000
1500
1000
500
0
Min = 0
Max = 12373.9
Air, dry
P-4
P-4-JWL
P-4~Air

(f)

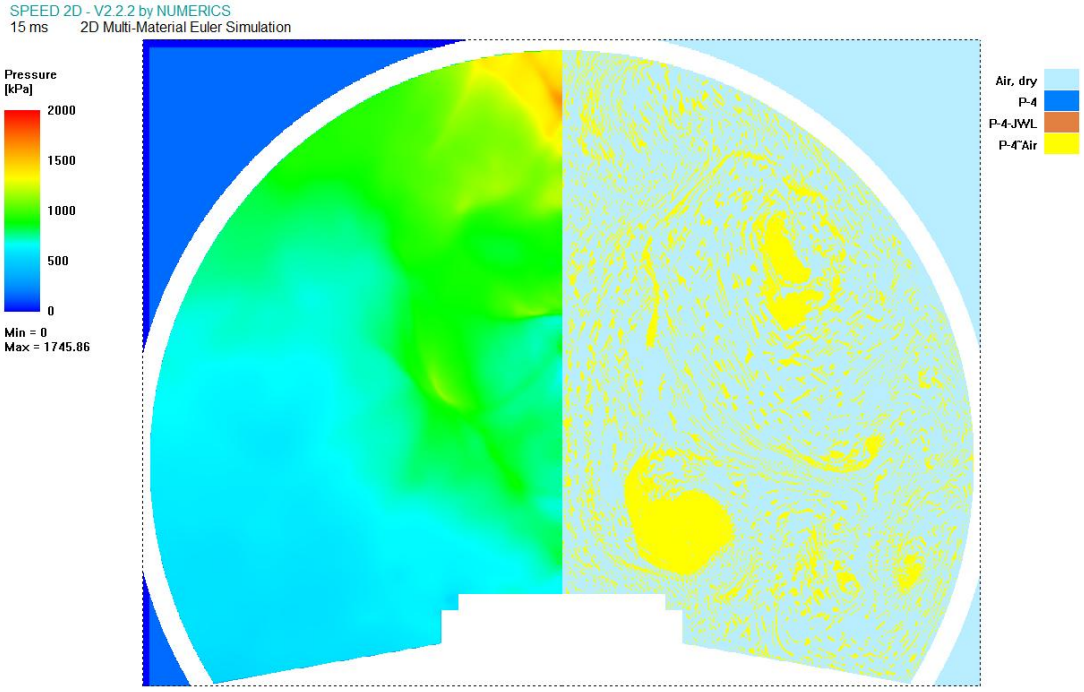
SPEED 2D - V2.2.2 by NUMERICS
15 ms 2D Multi-Material Euler Simulation
Pressure
[kPa]
2000
1500
1000
500
0
Min = 0
Max = 1745.86
Air, dry
P-4
P-4-JWL
P-4-Air

(g)

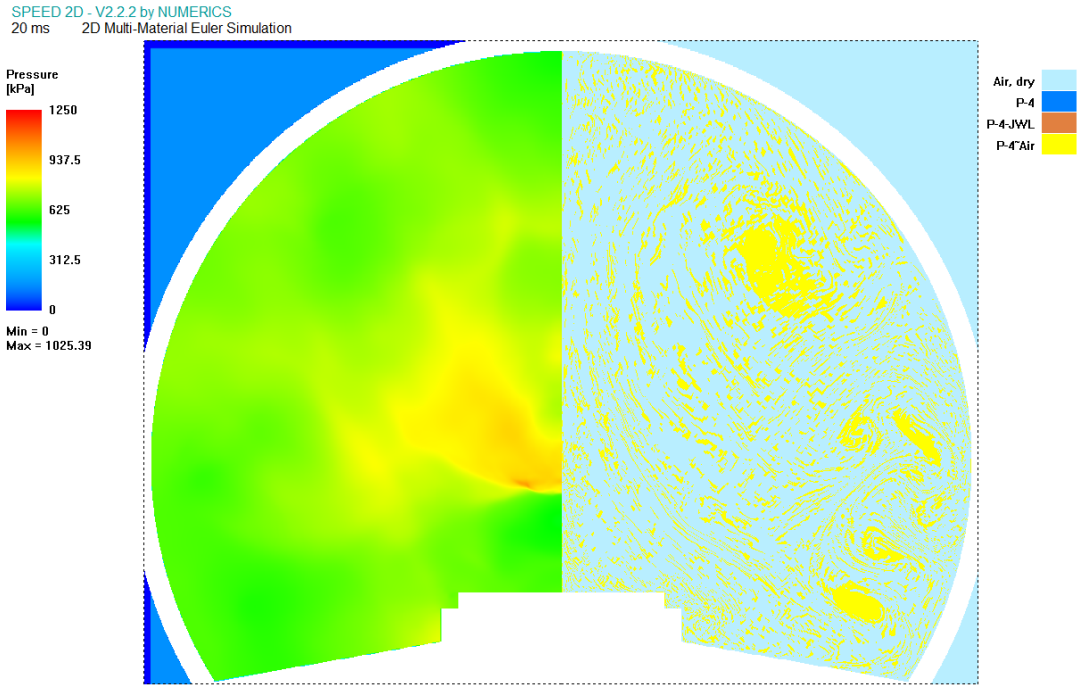
SPEED 2D - V2.2.2 by NUMERICS
20 ms 2D Multi-Material Euler Simulation
Pressure
[kPa]
1250
937.5
625
312.5
0
Min = 0
Max = 1025.39
Air, dry
P-4
P-4-JWL
P-4-Air

(h)

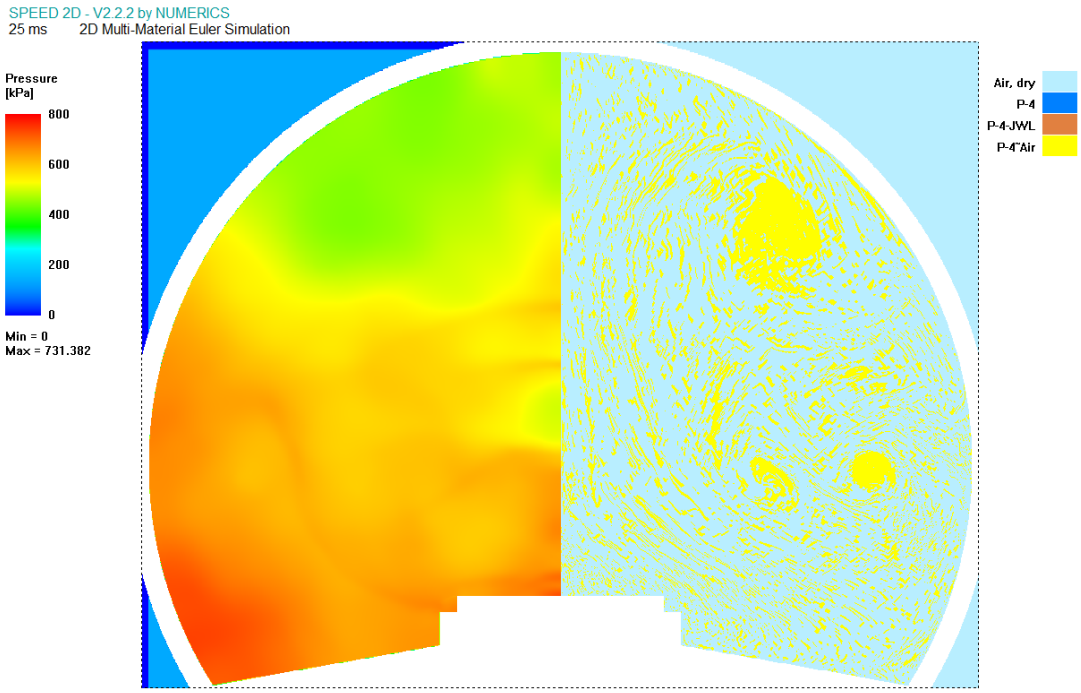
SPEED 2D - V2.2.2 by NUMERICS
25 ms
2D Multi-Material Euler Simulation
Pressure
[kPa]
800
600
400
200
0
Min = 0
Max = 731.382
Air, dry
P-4
P-4-JWL
P-4*Air

(i)

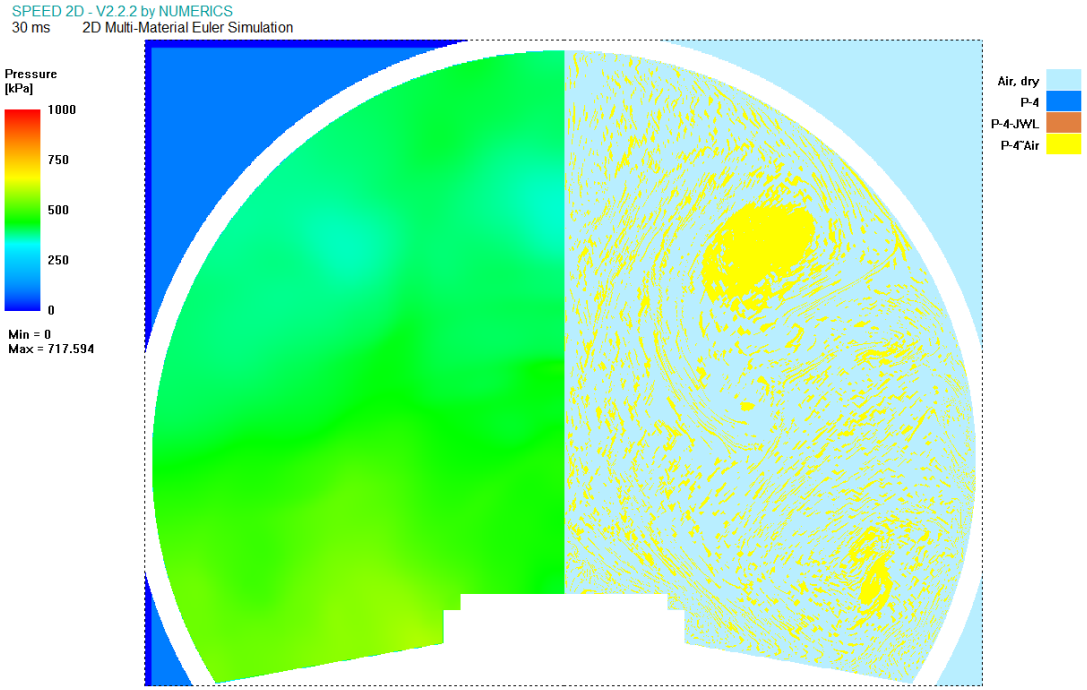

(j)

Figure A-3 Pressure and Material Distribution after Detonation of Explosive P-4 at Different Times:

(a) 0.125 ms (b) 0.25 ms (c) 0.5 ms (d) 1 ms (e) 5 ms (f) 10 ms (g) 15 ms (h) 20 ms (i) 25 ms (j) 30 ms

APPENDIX B

STRENGTH AND EOS MODELS OF STEEL 4340 AND CU (OFHC)

Table B-1 EOS Model of Cu (OFHC) [24]

Parameter	Value	Unit
Density	8.93	g/cm^3
Gruneisen Coefficient	2.02	-
Parameter C1	3940	m/s
Parameter S2	0	-
Reference Temperature	300.0	K
Specific Heat	383.0	J/kg-K

Table B-2 Strength Model of Cu (OFHC) [24]

Parameter	Value	Unit
Shear Modulus (G)	4.441×10^7	kPa
Yield Stress (Y)	0.9×10^5	kPa
Hardening Constant (B)	2.92×10^5	kPa
Strain Rate Constant (C)	0.025	-
Melting Temperature	1356	K

Table B-3 EOS Model of Steel 4340 [24]

Parameter	Value	Unit
Density	7.83	g/cm^3
Gruneisen Coefficient	1.67	-
Parameter C1	4578	m/s
Parameter S2	0	-
Reference Temperature	300.0	K
Specific Heat	477.0	J/kg-K

Table B-4 Strength Model of Steel 4340 [24]

Parameter	Value	Unit
Shear Modulus (G)	8.01×10^7	kPa
Yield Stress (Y)	7.92×10^5	kPa
Hardening Constant (B)	5.10×10^5	kPa
Strain Rate Constant (C)	0.014	-
Melting Temperature	1793	K